ENGINEERING LIBRARY

JAN 25 1950

JOURNAL OF THE AERONAUTICAL SCIENCES

VOLUME 17 JANUARY, 1950 NUMBER 1

CONTENTS

Predictions of Supersonic Airplane Performance.....HAROLD LUSKIN 5

The Calculation of Supersonic Downwash Using Line Vortex Theory.....
.....HAROLD MIRELS AND RUDOLPH C. HAEFELI 13

The Pulse Method for the Determination of Aircraft Dynamic Performance.....
.....R. C. SEAMANS, JR., B. P. BLASINGAME, AND G. C. CLEMENTSON 22

The Theoretical Lateral-Stability Derivatives for Wings at Supersonic Speeds.....
.....ARTHUR L. JONES 39

Influence of Acceleration on Aerodynamic Characteristics of Thin Airfoils in Supersonic and Transonic Flight.....C. S. GARDNER AND H. F. LUDLOFF 47

Readers' Forum: "Supersonic Airfoils Simplified," by James E. Broadwell; "Unsteady Flow Theory in Dynamic Stability," by John W. Miles; "Stability of Sandwich Plates in Combined Shear and Compression," by P. P. Bijlaard; "On the Reduction of Unsteady Supersonic Flow Problems to Steady Flow Problems," by John W. Miles.....61–64

Published by the

INSTITUTE OF THE AERONAUTICAL SCIENCES, INC.

JOURNAL OF THE AERONAUTICAL SCIENCES

ENGINEERING LIBRARY
TL
501
.J86

Editor: HUGH L. DRYDEN, *Director, N.A.C.A.*

Associate Editor: ROBERT R. DEXTER *Associate Editor:* BERNEICE H. JARCK

The Institute of the Aeronautical Sciences publishes monthly the JOURNAL OF THE AERONAUTICAL SCIENCES AND THE AERONAUTICAL ENGINEERING REVIEW.

The JOURNAL OF THE AERONAUTICAL SCIENCES prints papers of scientific and technical interest to Institute members and subscribers. In general, it provides an opportunity for specialists to publish articles disclosing new knowledge and new applications in the field of the aeronautical sciences. The JOURNAL restricts itself to the aeronautical aspects of advances in science and engineering, and papers printed have either been submitted directly to the JOURNAL or have been previously presented at a meeting of the Institute.

The AERONAUTICAL ENGINEERING REVIEW keeps members and subscribers informed regarding the contents of new books and current periodicals in the field of aeronautics. It reviews new developments in the aircraft industry and reports on progress from house organs and catalogs published by aircraft and engine manufacturers and other companies engaged in aeronautical activities. It publishes papers on applied engineering and aircraft production. News of Institute activities is published in the REVIEW.

Statements and opinions expressed in the JOURNAL are to be understood as individual expressions of the authors and not those of the Institute.

W. M.

SUBSCRIPTION RATES

Journal of the Aeronautical Sciences
Published Monthly

United States and Possessions		Foreign Countries Including Canada (American Currency Rate)	
1 Year	$12.00	1 Year	$13.00
Single Copies	1.50	Single Copies	1.50

Aeronautical Engineering Review
Published Monthly

United States and Possessions		Foreign Countries Including Canada (American Currency Rates)	
1 Year	$3.00	1 Year	$3.50
Single Copies	0.50	Single Copies	0.50

Notices of change of address should be sent to the Institute at least 30 days prior to actual change of address.

Manuscripts for publication, proofs, and all correspondence should be addressed to the Editorial Office of the JOURNAL.

Correspondence regarding subscriptions may be addressed to Publication Office, 20th and Northampton Sts., Easton, Pa., or to the Editorial Office of the JOURNAL OF THE AERONAUTICAL SCIENCES, 2 East 64th Street, New York 21, New York.

Copyright, 1950, by the Institute of the Aeronautical Sciences, Inc.

Entered as Second Class Matter at the Post Office, Easton, Pa., May 1, 1937. Acceptance for mailing at a special rate of Postage provided for in the Act of August 24, 1912. Authorized April 29, 1937.

INSTITUTE of the AERONAUTICAL SCIENCES

President
W. A. M. BURDEN

Vice-Presidents
J. L. ATWOOD
C. J. McCARTHY
G. S. SCHAIRER
ELMER A. SPERRY, JR.

Director
S. PAUL JOHNSTON

Assistant Director
JAMES L. STRAIGHT

Past-Presidents
J. C. HUNSAKER
CHARLES L. LAWRENCE
DONALD W. DOUGLAS
GLENN L. MARTIN
CLARK B. MILLIKAN
T. P. WRIGHT
GEORGE W. LEWIS (Deceased)
JAMES H. DOOLITTLE
FRANK W. CALDWELL
HALL L. HIBBARD
HUGH L. DRYDEN
R. H. FLEET
CHARLES H. COLVIN
ARTHUR E. RAYMOND
P. R. BASSETT
JOHN K. NORTHROP

Secretary
ROBERT R. DEXTER

Treasurer
EARL D. OSBORN

Controller
JOSEPH J. MAITAN

Counsel
ALLAN D. EMIL

COUNCIL

P. R. BASSETT
REX B. BEISEL
WILLIAM BOLLAY
VICTOR E. CARBONARA
CHARLES H. COLVIN
SHERMAN M. FAIRCHILD
LUIS DE FLOREZ
R. G. FOLSOM
C. C. FURNAS
LEROY R. GRUMMAN
WILLIS M. HAWKINS
J. A. HERLIHY
WILLSON H. HUNTER
JOHN C. LESLIE
J. S. McDONNELL
JOHN K. NORTHROP
L. B. RICHARDSON
RUSSELL G. ROBINSON
D. R. SHOULTS
ERNEST G. STOUT
GEORGE H. TWENEY
H. RUSSELL YOUNG

ADVISORY COMMITTEE

WALTER BEECH
FRANK W. CALDWELL
RALPH S. DAMON
KENNETH S. M. DAVIDSON
R. H. FLEET
R. PAUL HARRINGTON
R. M. HAZEN
HALL L. HIBBARD
J. C. HUNSAKER
TH. von KÁRMÁN
THOMAS A. KNOWLES
WILLIAM LITTLEWOOD
GROVER LOENING
GLENN L. MARTIN
CLARK B. MILLKAN
THOMAS A. MORGAN
ARTHUR E. RAYMOND
F. W. REICHELDERFER
LAURANCE S. ROCKEFELLER
W. C. ROCKEFELLER
T. CLAUDE RYAN
EDWARD P. WARNER
BURDETTE S. WRIGHT
T. P. WRIGHT

HONORARY MEMBERS

CALVIN M. BOLSTER
FRANK O. CARROLL
E. U. CONDON
HARRY F. GUGGENHEIM
LOUIS A. JOHNSON
MARION M. KALEZ
D. A. KIMBALL
THEODORE LONNQUEST
JOSEPH J. O'CONNELL, JR.
HOWARD T. ORVILLE
GEORGE B. PEGRAM
ALFRED M PRIDE
DONALD L. PUTT
F. W. RHICHELDERFER
DELOS W. RENTZEL
W. STUART SYMINGTON
HOYT S VANDENBERG

HONORARY FELLOWS

H. H. ARNOLD
FRANK W. CALDWELL
SIR GEOFFREY DE HAVILLAND
JAMES H. DOOLITTLE
DONALD W. DOUGLAS
HUGH L. DRYDEN
W. F. DURAND
SIR RICHARD FAIREY
SIR ROY FEDDEN
SIR FREDERICK HANDLEY PAGE
J. C HUNSAKER
SIR MELVILL JONES
GLENN L. MARTIN
CLARK B MILLIKAN
J. LAURENCE PRITCHARD
D. R. PYE
IGOR I. SIKORSKY
SIR GEOFFREY TAYLOR
TH. von KÁRMÁN
EDWARD P. WARNER
T. P. WRIGHT

BENEFACTORS

E. E. ALDRIN
HART O. BERG (Deceased)
W. A. M. BURDEN
E. L. CORD
DONALD W. DOUGLAS
ALLAN D. EMIL
SHERMAN M. FAIRCHILD
SIR RICHARD FAIREY
R. H. FLEET
LESTER D. GARDNER
FLORENCE GUGGENHEIM (Deceased)
C. D. HANSCOM
JOHN P. V. HEINMULLER
ALEXANDER KLEMIN
PAUL KOLLSMAN
BELLA C. LANDAUER
WILLIAM LANDAUER
GROVER LOENING
EDMUND C. LYNCH (Deceased)
F. W. MAGIN
GLENN L. MARTIN
GEORGE J. MEAD (Deceased)
S. A. REED (Deceased)
LAURANCE S. ROCKEFELLER
EDWARD P. WARNER

AMERICAN FELLOWS

IRA H. ABBOTT
JOHN D. AKERMAN
E. E. ALDRIN
H. JULIAN ALLEN
HARRY G. ARMSTRONG
KARL ARNSTEIN
J. L. ATWOOD
PAUL S. BAKER
RALPH S. BARNABY
P. R. BASSETT
WELLWOOD E. BEALL
REX B. BEISEL
G. M. BELLANCA
DON R. BERLIN
HENRY A. BERLINER
MAURICE A. BIOT
WILLIAM BOLLAY
GEORGE W. BRADY
LYMAN J. BRIGGS
W. G. BROMBACHER
WILLIAM G. BROWN
CHARLES P. BURGESS
KENNETH CAMPBELL
CHARLES H. CHATFIELD
ALLAN CHILTON
FRANCIS H CLAUSER
FRANKLIN R. COLLBOHM
CHARLES H. COLVIN
KARL T. COMPTON
EMERSON W. CONLON
JOHN W. CROWLEY, JR.
RALPH S. DAMON
LUIS DE FLOREZ
SMITH J. DE FRANCE
J. P. DEN HARTOG
WALTER S. DIEHL
C. S. DRAPER
IVAN H. DRIGGS
WILLIAM K. EBEL
OLIVER P. ECHOLS
C. L. EGTVEDT
FREDERIC FLADER
CHARLES FROESCH
JACK FRYE
GARLAND FULTON
C. C. FURNAS
LESTER D. GARDNER
RICHARD C. GAZLEY
MICHAEL E. GLUHAREFF
MELVIN N. GOUGH
LEROY R. GRUMMAN
HAROLD R. HARRIS
R. M. HAZEN
EDWARD H. HEINEMANN
S. D. HERON
HALL L. HIBBARD
L. S. HOBBS
PAUL E. HOVGAARD
WILLIAM HOVGAARD
ROBERT INSLEY
EASTMAN N. JACOBS
C. L. JOHNSON
S. PAUL JOHNSTON
CARL KAPLAN
ALEXANDER KARTVELI
PAUL H. KEMMER
CARLETON KEMPER
J. H. KINDELBERGER
OTTO E. KIRCHNER
ARTHUR L. KLEIN
ALEXANDER KLEMIN
W. B. KLEMPERER
PAUL KOLLSMAN
OTTO C. KOPPEN
B. V. KORVEN-KROUKOVSKY
S. M. KRAUS
ARNOLD M. KURTHE
I. M. LADDON
E. S. LAND
CHARLES L. LAWRENCE
JEROME LEDERER
JOHN G. LEE
JOHN C. LESLIE
CHARLES A. LINDBERGH
WILLIAM LITTLEWOOD
GROVER LOENING
ALBERT E. LOMBARD
F. A. LOUDEN
W. RANDOLPH LOVELACE, II
EUGENE E. LUNDQUIST
R. D. MACCART
JOHN R. MARKHAM
ERLE MARTIN
WM. H. McAVOY
C. J. McCARTHY
J. S. McDONNELL
ROBERT J. MINSHALL
JOSEPH S. NEWELL
ALFRED S. NILES
JOHN K. NORTHROP
ARTHUR NUTT
SHATSWELL OBER
ROBERT R. OSBORN
W. BAILEY OSWALD
GEORGE A. PAGE, JR.
F. W. PAWLOWSKI
F. W. PENNOYER, JR.
A. A. PRIESTER
ARTHUR E. RAYMOND
F. W. REICHELDERFER
ELLIOTT G. REID
H. J. E. REID
H. C. RICHARDSON
L. B. RICHARDSON
RUSSELL G. ROBINSON
LEONARD E. ROOT
C. E. ROSENDAHL
ADDISON M. ROTHROCK
W. R. SEARS
GALEN B. SCHUBAUER
WILLIAM T. SCHWENDLER
FRANCIS R. SHANLEY
JAMES M. SHOEMAKER
IGOR ALEXIS SIKORSKY
ABE SILVERSTEIN
C. RICHARD SODERBERG
SELDEN B. SPANGLER
ELMER A. SPERRY, JR.
JOHN STACK
ROBERT M. STANLEY
WILLIAM B. STOUT
HARRY A. SUTTON
C. FAYETTE TAYLOR
EDWARD S. TAYLOR
PHILIP B. TAYLOR
TH. THEODORSEN
T. E. TILLINGHAST
S. TIMOSHENKO
F. L. THOMPSON
L. B. TUCKERMAN
RALPH H. UPSON
J. PARKER VAN ZANDT
J. G. VINCENT
RICHARD von MISES
FRANK L. WATTENDORF
P. V. H. WEEMS
FRED E. WEICK
R. D. WEYERBACHER
JOHN B. WHEATLEY
DONALD H. WOOD
ROBERT J. WOODS
JOHN E. YOUNGER
ALBERT F. ZAHM
STEPHEN J. ZAND

Corporate Members

of the

Institute of the Aeronautical Sciences

Academy of Aeronautics, Inc.
Casey Jones School of Aeronautics
Alvin P. Adams and Associates
Adams Rite Manufacturing Company
Aerojet Engineering Corporation
Aerolab Development Company
Aeroproducts Division, General Motors Corporation
Aeroquip Corporation
Agawam Aircraft Products, Inc.
Airborne Accessories Corporation
Airborne Instruments Laboratory, Inc.
Aircraft Radio Corporation
AiResearch Manufacturing Company, Division of The Garrett Corporation
Allis-Chalmers Manufacturing Company
Allison Division, General Motors Corporation
Aluminum Company of America
American Airlines System
American Bosch Corporation
American Overseas Airlines, Inc.
Iceland Airport Corporation (Subsidiary)
American Phenolic Corporation
Associated Aviation Underwriters
Atlas Supply Company
Baker Steel & Tube Company
Beech Aircraft Corporation
Bell Aircraft Corporation
Bendix Aviation Corporation
Bendix International Division
Bendix Products Division
Bendix Radio Corporation
Eclipse-Pioneer Division
Friez Instrument Division
Pacific Division
Scintilla Magneto Division
The BG Corporation
Boeing Airplane Company
Seattle Division
Wichita Division
Breeze Corporations, Inc.
Aircraft Standard Parts Company, Inc.
Aldrich Company
Anderson Stove Company, Inc.
Federal Laboratories, Inc.
Foundry Service, Inc.
Brooks and Perkins, Inc.
Cal-Aero Technical Institute, A Division of Grand Central Airport Company
Canadair, Ltd.
Cessna Aircraft Company
Chandler-Evans Division, Niles-Bement-Pond Company
Chase Aircraft Company, Inc.
Chase National Bank of the City of New York
The Cleveland Pneumatic Tool Company
Automatic-Aircraft Division
Clifford Manufacturing Company, Division of Standard-Thomson Corporation
Consolidated Vultee Aircraft Corporation
Fort Worth Division
Stinson Aircraft Division
Continental Motors Corporation
Curtiss-Wright Corporation
Airplane Division
Propeller Division
Wright Aeronautical Corporation Division
Dayton Aircraft Products, Inc.
Doak Aircraft Company, Inc.
Doelcam Corporation
Douglas Aircraft Company, Inc.
El Segundo Plant
Long Beach Plant
Santa Monica Plant
The Dow Chemical Company
Dzus Fastener Company, Inc.
Eastern Air Lines, Inc.
Eaton Manufacturing Company
Dynamatic Corporation (Subsidiary)
Eaton-Wilcox-Rich Ltd. (Subsidiary)
Edo Corporation
Elastic Stop Nut Corporation of America
Electrol Incorporated
Esso Standard Oil Company
Ethyl Corporation
Fairchild Camera & Instrument Corporation
Fairchild Aerial Surveys, Inc.
Fairchild Engine and Airplane Corporation
Al-Fin Division
Fairchild Aircraft Division
Fairchild Personal Planes Division
Fairchild Pilotless Plane Division
NEPA Division
Ranger Aircraft Engines Division
Stratos Corporation (Subsidiary)

Federal Telephone and Radio Corporation
Federal Electric Manufacturing Company, Ltd.
Federal Telecommunication Laboratories, Inc. (Partial Subsidiary)
The Firestone Tire & Rubber Company of California
Fletcher Aviation Corporation
General Electric Company
Aircraft Gas Turbine Division
Aviation Divisions
Globe Corporation, Aircraft Division
The B. F. Goodrich Company
The Goodyear Tire & Rubber Company
Goodyear Aircraft Corporation
Grumman Aircraft Engineering Corporation
W. & L. E. Gurley
Harvey Machine Company, Inc.
Industrial Sound Control
Insurance Company of North America Companies
The Alliance Insurance Company of Philadelphia
Indemnity Insurance Company of North America
Insurance Company of North America
Philadelphia Fire and Marine Insurance Company
The International Nickel Company, Inc.
Irving Air Chute Company, Inc.
Jack & Heintz Precision Industries, Inc.
Johns-Manville Sales Corporation
Earle M. Jorgensen Company
Walter Kidde & Company, Inc.
Kollsman Instrument Division, Square D Company
Lavelle Aircraft Corporation
Lear Incorporated
Link Aviation, Inc.
The Liquidometer Corporation
Lockheed Aircraft Corporation
Airquipment Company (Subsidiary)
Lockheed Air Terminal (Subsidiary)
Lockheed Aircraft Overseas Corporation (Subsidiary)
Lockheed Aircraft Service, Inc. (Subsidiary)
Longines-Wittnauer Watch Company, Inc.
Marman Products Company, Inc.
The Glenn L. Martin Company
GLM Chemical Division
Rotawings Division
McDonnell Aircraft Corporation
Meletron Corporation
Minneapolis-Honeywell Regulator Company
Brown Instrument Company (Subsidiary)
National Credit Office, Inc.
North American Aviation, Inc.
North American Aviation, Inc., of Texas
Northrop Aircraft, Inc.
Northwest Airlines, Inc.
Pan American World Airways System
The Parker Appliance Company
Pesco Products Division, Borg-Warner Corporation
Phillips Petroleum Company
Pure Oil Company
Radioplane Company
Republic Aviation Corporation
Rheem Manufacturing Company
E. V. Roberts and Associates
A. V. Roe Canada Limited
John A. Roebling's Sons Company
Rohr Aircraft Corporation
Ryan Aeronautical Company
Saval, Inc.
Schrillo Aero Tool Engineering Company
Servomechanisms, Inc.
Shell Oil Company, Inc.
Simmonds Aerocessories, Inc.
A. O. Smith Electrical Manufacturing Company
Socony-Vacuum Oil Company, Inc.
Solar Aircraft Company
Sperry Gyroscope Company Division of The Sperry Corporation
Square D Company
Standard Oil Company of California
Standard Oil Company (Indiana)
The Steel Products Engineering Company
Stewart-Warner Corporation, South Wind Division
Sturgess, Inc.
Summers Gyroscope Company
Telecomputing Corporation
H. I. Thompson Company
Thompson Products, Inc.
Tinnerman Products, Inc.
Toolko Engineering Company
Union Carbide and Carbon Corporation
Bakelite Corporation
Electro Metallurgical Company
Haynes Stellite Company
The Linde Air Products Company
National Carbon Company, Inc.
United Air Lines, Inc.
United Aircraft Corporation
Chance Vought Aircraft Division
Hamilton Standard Propellers Division
Pratt & Whitney Aircraft Division
Sikorsky Aircraft Division
United Aircraft Export Corporation
United Aircraft Service Corporation
United States Aviation Underwriters, Inc.
Vard Inc.
Vickers, Inc.
Western Gear Works
Westinghouse Electric Corporation
Aviation Gas Turbine Division
Industrial Electronics Division
Marine & Aviation Sales Department
Small Motor Division, Aviation Sales
Weston Electrical Instrument Corporation
Wyman-Gordon Company
Young Radiator Company

EDITORIAL COMMITTEE

HUGH L. DRYDEN, *Chairman*

Aerodynamics
Francis Clauser
Howard Emmons
R. Paul Harrington
R. T. Jones
Carl Kaplan
W. B. Klemperer
Otto C. Koppen
John G. Lee
H. W. Liepmann
C. C. Lin
H. F. Ludloff
John R. Markham
Clark B. Millikan
Shatswell Ober
W. Bailey Oswald
Allen E. Puckett
Elliott G. Reid
H. J. F. Reid
Russell Robinson
G. B. Schubauer
W. R. Sears
John Stack
Th. von Kármán
Richard von Mises

Air Transport
Charles Froesch
J. A. Herlihy
Otto E. Kirchner
John C. Leslie

Aircraft Design
W. E. Beall
Rex B. Beisel
W. K. Ebel
Hall L. Hibbard
C. L. Johnson
I. M. Laddon
C. J. McCarthy
Fred E. Weick
Robert J. Woods

Physiologic Problems

H. G. Armstrong
Louis H. Bauer
Eugene Du Bois
W. Randolph Lovelace, II
Ross A. MacFarland
A. D. Tuttle

Aircraft Propulsion

George W. Brady
Frank W. Caldwell
L. S. Hobbs
E. E. Johnson
Joseph Keenan
R. P. Kroon
Arthur Nutt
Hans Reissner
Abe Silverstein
C. Fayette Taylor
E. S. Taylor
P. Taylor

Structures and Materials

W. B. Bleakney
E. W. Conlon
J. P. Den Hartog
L. H. Donnell
E. C. Hartmann
N. J. Hoff
E. E. Lundquist
C. F. Nagel, Jr.
J. S. Newell
Alfred S. Niles
W. Ramberg
E. Reissner
F. R. Shanley
H. W. Sibert
C. R. Strang
S. Timoshenko
H. S. Tsien
Chi-Teh Wang

Meteorology
C. F. Brooks
D. M. Little
E. J. Minser
F. W. Reichelderfer
H. C. Willett

Fuels and Oils
A. L. Beall
J. H. Doolittle
Graham Edgar
R. T. Goodwin
S. D. Heron
A. M. Rothrock

Instruments
Allan G. Binnie
W. G. Brombacher
Charles H. Colvin
B. M. Craig
B. Del Mar
C. S. Draper
O. E. Esval
W. L. Howland
J. E. Lindberg
David W. Moore
George H. Purcell
W. A. Reichel
C. F. Savage
O. Hugo Schuck
C. L. Seward, Jr.
R. Sylvander
D. K. Warner
P. F. Weber

Rotating Wing Aircraft
Robert Coleman
K. H. Hohenemser
Alexander Klemin
Ralph McClarren
R. H. Miller
R. H. Prewitt
Igor I. Sikorsky
Robert A. Wolf

Vibration and Flutter
Lee Arnold
M. A. Biot
William Bollay
Chieh-Chien Chang
Martin Goland
J. P. Den Hartog
Manfred Rauscher

Flight Testing
W. K. Ebel
R. R. Gilruth
Melvin N. Gough
Robert Stanley
E. G. Stout

I.A.S. REPRESENTATIVES TO OTHER ORGANIZATIONS

Aircraft Industries Association of America, Inc.—CHARLES MARCUS

American Association for the Advancement of Science—J. C. HUNSAKER

American Society of Mechanical Engineers—CHARLES H. COLVIN

American Standards Association—P. R. BASSETT

Engineering Society of Detroit—DONALD C. HUNT, GEORGE TWENEY

Greater New York Safety Council—WILLIAM LITTLEWOOD

Daniel Guggenheim Medal Board of Award—PRESTON R. BASSETT, W. A. M. BURDEN, S. PAUL JOHNSTON

Institute of Radio Engineers—L. M. HULL

Manufacturers Aircraft Association—ARTHUR E. RAYMOND

National Aeronautic Association—WILLIAM R. ENYART

National Fire Protection Association—E. E. ALDRIN

National Research Council Engineering Division—HUGH L. DRYDEN

National Safety Council—JEROME LEDERER

Society of Automotive Engineers—STEPHEN J. ZAND

JOURNAL OF THE AERONAUTICAL SCIENCES

VOLUME 17 JANUARY, 1950 NUMBER 1

Predictions of Supersonic Airplane Performance

HAROLD LUSKIN*

Douglas Aircraft Company, Inc.

ABSTRACT

Previous writers on the history and prediction of the trend in airplane maximum speeds have sometimes represented the trend as being linear with time. This paper discusses the more general type of growth curve in relation to airplane speeds. Limiting factors in airplane performance are studied, and a prediction is made for supersonic developments expected to be possible by 1960. It is pointed out that increases in speed and improvements in the safety record have been obtained simultaneously, in spite of increasing wing loadings. This trend is expected to continue.

THE GROWTH CURVE

THE NATURE OF THE GROWTH of things is in many cases[1] given by a curve of a well-known type. Fig. 1, showing the history of steam railroad road mileage in the United States,[2, 3] is an example of such a curve. It is seen that progress begins at roughly a constant percentage rate; then tapers off; reaches an upper limit; and, finally, begins a decline. In some cases additional characteristics are found. Fig. 2, from a competing industry, shows a curve of growth and greater eventual decline,[1] the high L/D of horse-drawn vehicles notwithstanding! Fig. 3 shows a growth in two segments, the break corresponding to a revolutionary change in the nature of the growing thing.[1] The last two of these figures are plotted on semilogarithmic coordinates, on which the initial curvature to be noted on Fig. 1 is removed.

Progress in aeronautics also has its growth curve. The aeronautical engineer, however, is likely to spend several years working on a design at *one fixed level* of the growth curve. This has the result of dulling the perception to the time derivative of the curve existing at that level. The failure of past predictions of even our most brilliant engineers will later be discussed in proof of this point. It is believed to be important that the sense of change, the awareness of growth, be developed.[9]

To establish an appreciation for the long-term growth trend, a few examples thought to be of special interest will be drawn from fields of transportation other than the aeronautical.

The real beginning of our railroad system took place in 1830. To provide transportation for the rapidly growing nation, there had been, in the decades just previous to this, considerable development of travel on our rivers and in man-made barge canals. Water travel was not, however, a perfect method of transportation, and in its heyday "500 people annually lost their lives in river boat accidents, and Charles Dickens was able to say that the high-pressure river boats 'conveyed that kind of feeling to me which I should be likely to experience, I think, if I had lodgings on the first floor of a powder mill.' "[4] Considering the population size, and the low speed of the river boats, the fatalities per passenger-mile for river boats must have been enormous compared to those for modern air travel. The gradual ascendency of the railroads over river boats and barges was not accomplished without difficulty, however. An amusing editorial view of the competition offered by the upstart rail industry can be gained from the following item from the *Ploughman's Gazette Courier*, Canton, Ohio, August 15, 1830:†

"Returning Travellers report that the people of the East are still suffering from the Railroad mania. Disregarding the warnings of Providence, they have extended the line of the Railroad thirteen miles to Elliott's Mills west of Baltimore.

"One traveller recently told of having seen with his own eyes a single horse drawing two waggons containing 41 persons at a speed of 11 miles per hour on the portion of track which is completed. He heard, however, of several serious accidents caused by the horse stumbling and being run over by the heavy waggons, which were derailed and upset.

Presented at the Aerodynamics Session, Annual Summer Meeting, I.A.S., Los Angeles, July 21–22, 1949.

* Aerodynamics Research Engineer, Santa Monica Plant.

† Furnished by courtesy of the Association of American Railroads.

FIGURE 1

THOUSANDS OF MILES OF ROAD OWNED BY AMERICAN STEAM RAILROADS

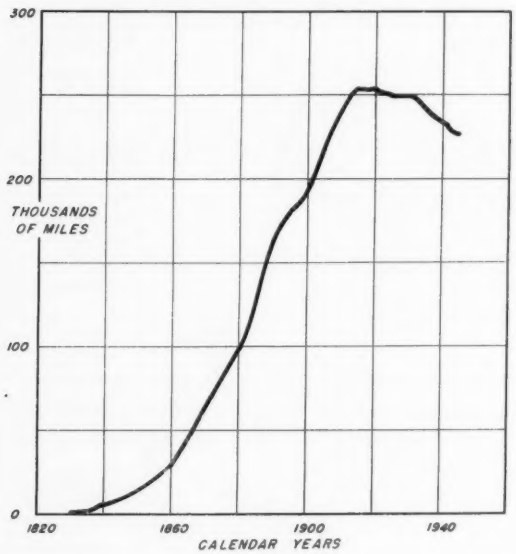

FIGURE 2

VALUE OF U.S. HORSE-DRAWN VEHICLE PRODUCTION MILLIONS OF 1926 DOLLARS

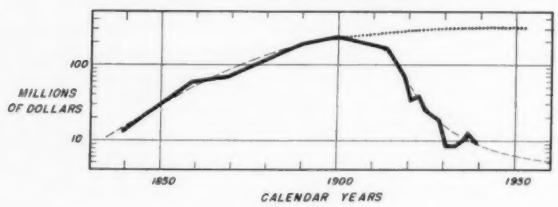

FIGURE 3

U.S. SMELTER COPPER PRODUCTION MILLIONS OF POUNDS

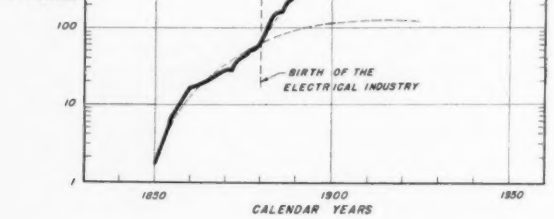

FIGURE 4

HISTORY OF AIRPLANE SPEED RECORDS AND A COMPARISON WITH SEVERAL PREDICTIONS

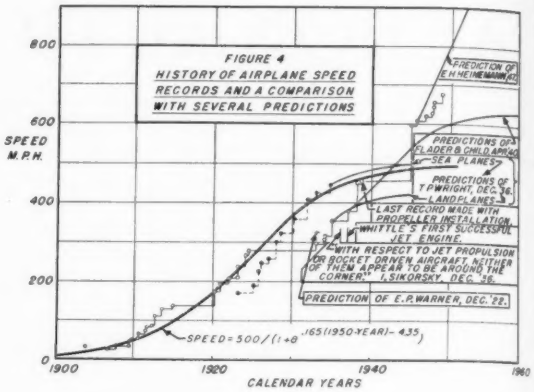

FIGURE 5

MAXIMUM SPEED OF AMERICAN TRANSPORT LANDPLANES

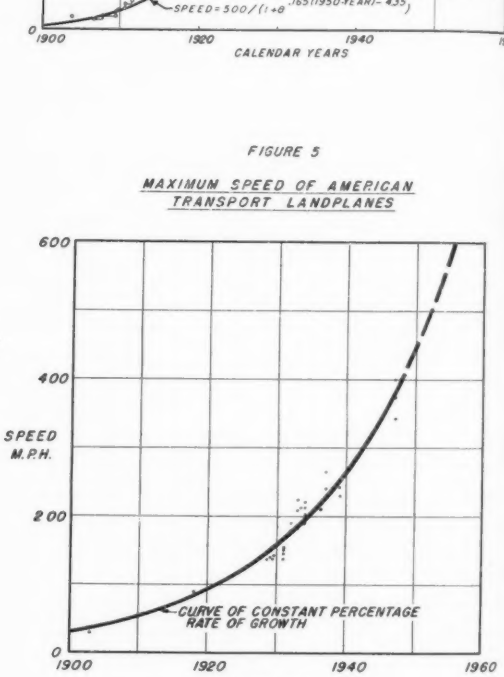

FIGURE 6

DRAG AND THRUST CURVES FOR SEVERAL AIRCRAFT

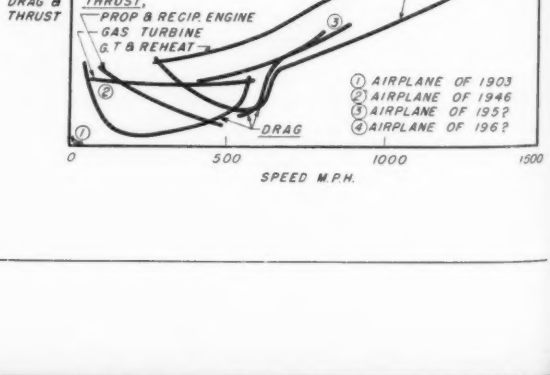

"Little confidency is now felt in Mr. Peter Cooper's plan for propelling the carriages by means of a steam engine.

"Except as a novelty, however, Railroads will never take the place of canals. Railroads are untried for long distances in any country, and for short distances they are still in the experimental stage. The longest in existence is the London and Manchester which is but 40 miles in length.

"Any farmer can build a canal boat of 25 tons capacity from materials growing on his own land. To carry this amount on a Railroad would require eight waggons and a locomotive costing $4,000 at the least, and no farmer could afford this equipment.

"His canal boat would carry livestock, hay, firewood, large trees for ship buildings, boards, planks and grain. Railroads can not do this. Imagine a load of hay coming along a Railroad. The sparks would set it afire before it started.

"The farmer who is watchful of his interest will not be misled by talk about Railroads, which would be of no service to him and destroy his crops and his stock—but will endeavor in all possible ways to promote the building of canals."

In the first example, we saw that an economically valuable means of transportation successfully grew through a period of bad safety. In the second, we saw lack of vision.

The Growth of Airplane Speeds

The 45 years that have elapsed since the first powered airplane flight have provided a wealth of statistical aviation information for study purposes. Certain of these data were used in a recent paper by Clauser,[5] in which an analysis of the history of aircraft power plants was made. The history of aircraft maximum speeds, measured in formal fashion over a course at sea level, has also been frequently discussed, and the data are again reproduced in Fig. 4. A typical growth curve has been faired through the data on propeller-reciprocating power-plant powered airplanes. Various predictions[6–8, 11, 12] by skillful engineers are shown, the rule being that the predictions are conservative. There is no intent here to belittle these predictions. The point can be made, on the other hand, that these men were so familiar with the difficulties facing designers of the day that further rapid advances must have seemed hardly likely. The prediction of Heinemann made in 1947 has yet to be thoroughly put to test. Developments in the next few years' flights will begin to provide the desired comparison. A change in the method of determining the speed record is also needed, particularly in allowing higher altitudes to be used. The maximum speed of transport airplanes has followed a regular trend and is shown on Fig. 5.

No attempt will be made to predict the future growth curve of airplane maximum speeds in the present paper. It is felt that the increases will be more rapid, however, than the average rate for the past 45 years and that a new segment of the growth curve—that for jet airplanes—is beginning. This would produce a speed-growth curve similar in shape to that of Fig. 3. The first portion of such a curve is faired through the data of Fig. 4, using the standard form for the growth curve. There are insufficient data available at this time on jet speed records to attempt to fit the new portion of the growth curve.

A more fundamental reason for a new trend in the growth curve than the empirical data of Fig. 4 is the new type of thrust and resistance variations to be expected from modern jet units and supersonic air frames. The point was made in connection with Fig. 3 that a great change in the nature of the growing thing being studied could lead to a new growth period. That such a change is now taking place in airplane design is certain. For the space of time given by the data of Fig. 4 to which the growth curve is fitted, the speed of each and every airplane was determined by the subsonic intersection of drag and thrust curves of a similar nature. Gradual advances changed the constants determining the high speed but did not have the effect of changing the nature of the laws governing the performance. Design improvements were the cause of these gains. They include the transition from biplanes to externally braced monoplanes to cantilever monoplanes (a reduction in structural thickness to span ratio considerably more drastic than any proposed today for supersonic flight); elimination of open cockpits; retractable landing gear; cowling and cowl flaps for engines; variable-pitch propellers; and, probably more important, a steady increase in specific ratings and maximum ratings of the reciprocating engine. Fig. 6 has been prepared to show several aspects of this process of improvement. The curves for the subsonic aircraft have similar shapes but cannot be clearly compared on the same scales because of the minute thrust and resistance of the Wright brothers' first airplane. Also shown in Fig. 6 are the types of thrust and drag variations to be expected from future supersonic airplanes. The great values of thrust and the increase in thrust due to ram for jet engines compensate for the increase in drag with speed. The subsonic intersection of the thrust and drag curves is eliminated, thus opening up an extensive new speed region, heretofore beyond reach. This completely new speed régime will be the cause of the new rapid development of the speed growth curve. It is interesting to note that the first period of growth was preceded by a period in which the thrust required for flight had to be obtained from means other than the installed power plant. A component of the weight obtained by gliding downward or energy taken from the atmosphere was used to provide power. The supersonic era is also being ushered in by "simple" means of obtaining power, including rocket motors and dives. Supersonic aircraft of economic and military usefulness will result from the development of suitable air-

FIGURE 7

HISTORY OF SPEED RECORDS

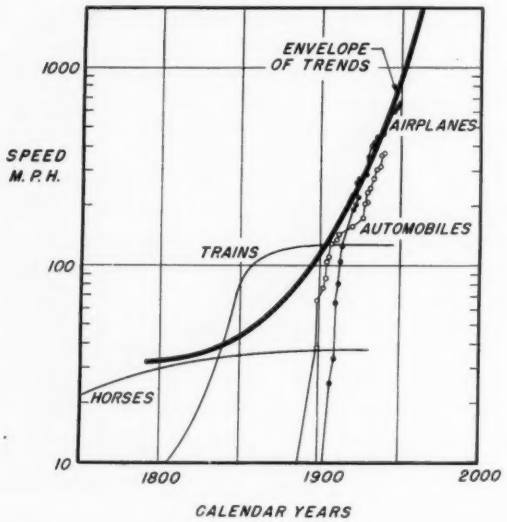

breathing engines, just as in the case of subsonic airplanes.

An unusual speed prediction was recently made using data collected by Prof. Hornell Hart, of Duke University.[10] His data, shown in Fig. 7, were faired by Time Artist R. M. Chapin, Jr., to show a speed of 1,700 m.p.h. by 1960. The growing things studied by Hart were not just airplane speeds but were velocities of several man-carrying vehicles. Such an approach is novel in the literature studied during the preparation of this paper. Hart states that the airplane speed curve appears to have several subcurves. The jet airplanes, as pointed out above, may well make an additional subcurve. An appreciation of the growth of airplane speeds is obtained by noting that the airplane speed record curve does not cross the horse curve until 1909 and the railroad curve until 1913.

Speed, Ceiling, Wing Loading, and Safety

It has just been pointed out that a new speed growth curve for jet-propelled aircraft is starting. This new period of growth will carry speeds well into the supersonic-speed régime. The airplanes of this future era will certainly fall into design and performance patterns, much as has been the case with subsonic aircraft. Rough calculations will be made in an attempt to predict the simpler of these patterns. The performance characteristics, speed and altitude, will be studied first.

Before examining the supersonic case, however, the reasoning will be applied to subsonic airplanes. These will be assumed to have conventional characteristics. There is, therefore, a limit to maximum speed set by the drag rise occurring in the transonic region, to overcome which sufficient power cannot be obtained. There is also a lower bound to the minimum speed arising from the limiting lifting area which can be fabricated from a given weight of structural material. This is a consequence of the strength of materials. Stated differently, the lower speed limit is a result of the fact that the lowest possible wing loading is of necessity greater than the minimum unit wing weight.

It will be of some interest to calculate, for the subsonic region, the wing loading for maximum lift to drag ratio. Assuming a parabolic drag polar, the maximum lift to drag ratio corresponds to a condition where the induced and parasite drags are equal.[16]

$$C_{D_P} = C_{L^2_{L/D}}/\pi \text{A.R.}_e \tag{1}$$

in which

C_{D_P} = parasite drag coefficient
$C_{L_{L/D}}$ = lift coefficient for maximum lift to drag ratio
A.R.$_e$ = effective aspect ratio

To obtain the desired rough approximations for the performance limits, we shall assume that the values of C_{D_P} and A.R.$_e$ are constant for all subsonic airplanes. Then, the variables remaining are speed, altitude, and wing loading. For horizontal unaccelerated flight the lift will equal the weight, and Eq. (1) is equivalent to a relation between the speed, atmospheric density, and wing loading for maximum L/D.

$$(W/S)_{L/D} = (\rho V^2/2)\sqrt{\pi C_{D_P} \text{A.R.}_e} \tag{2}$$

While it is not necessary that an airplane operate according to Eq. (2), the penalties for great deviations may be large, since the parabolic drag polar has the property

$$\frac{(D/L)}{(D/L)_{min.}} = \frac{1}{2}\left[\frac{C_{L_{L/D}}}{C_L} + \frac{C_L}{C_{L_{L/D}}}\right] \tag{3}$$

Since

$$\frac{C_L}{C_{L_{L/D}}} = \frac{(W/S)/(\rho V^2/2)}{[(W/S)/(\rho V^2/2)]_{L/D}} \tag{4}$$

it is possible to easily compute the penalty in lift to drag ratio which results from deviating from Eq. (2). At a given speed and altitude the variation of minimum drag to lift ratio with wing loading is given in Table 1.

Table 1

$(W/S)/(W/S)_{L/D}$	$(D/L)/(D/L)_{min.}$
1.0; 1.000	1.000
0.8; 1.250	1.025
0.6; 1.667	1.133
0.4; 2.500	1.480
0.2; 5.000	2.600
0.1; 10.000	5.050

FIGURE 8

AIRPLANE PERFORMANCE LIMITS

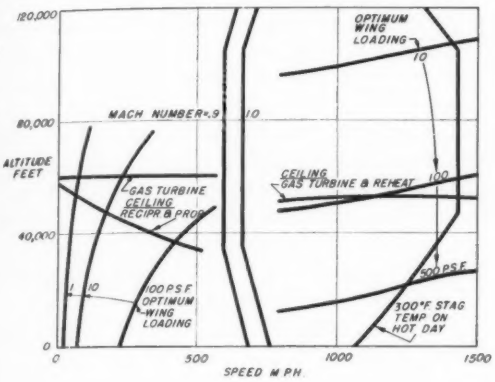

Fig. 8 has been prepared to show the performance limits under discussion. Optimum wing loading lines according to Eq. (2) are shown, that for 1 lb. per sq.ft. being used to indicate the approximate minimum speed limit. For these curves, A.R.$_e$ = 10 and C_{DP} = 0.02 have been used.

The ceiling is determined by the fact that the maximum power-plant output falls off with increasing height at a different and greater rate than the minimum power required. It is well known that at full throttle the altitude variation of power output for a reciprocating type aircraft engine approximately follows the empirical relation

$$P/P'_{SL} = (\sigma - 0.1)/0.9 \tag{5}$$

in which P'_{SL} is the full throttle output that would be obtained at sea level. If the engine is restricted to part throttle at sea level, with an output P_{SL}, then

$$\frac{P}{P_{SL}} = \frac{P}{P'_{SL}}\frac{P'_{SL}}{P_{SL}} = \frac{\sigma - 0.1}{\sigma_{CR} - 0.1} \tag{6}$$

will hold above the critical altitude. σ is the atmospheric density ratio. P_{SL} is taken here to be the constant power rating that holds below the critical altitude, at which $\sigma = \sigma_{CR}$. The weight of the complete power-plant installation will be assumed to be

$$W_{PP} = KP_{SL} \tag{7}$$

which will further be assumed to be some fraction λ of the total airplane weight W. Then,

$$W = \left(\frac{K}{\lambda}\right)P_{SL} = \left(\frac{K}{\lambda}\right)P\left(\frac{\sigma_{CR} - 0.1}{\sigma - 0.1}\right) \tag{8}$$

For a given weight of airplane and for some values of the constants K and λ, Eq. (8) gives the altitude variation of maximum brake horsepower above the critical altitude.

Since the drag-weight ratio for minimum power required is

$$D/W_{mp} = \sqrt{16C_{DP}/3\pi\text{A.R.}_e} \tag{9}$$

the power to weight ratio for minimum power is

$$P/W = (V/375\eta)\sqrt{16C_{DP}/3\pi\text{A.R.}_e} \tag{10}$$

and at the ceiling,

$$\frac{V_{s\,p}}{375\eta}\sqrt{\frac{16C_{DP}}{3\pi\text{ A.R.}_e}} = \frac{\lambda}{K}\frac{\sigma - 0.1}{\sigma_{CR} - 0.1} \tag{11}$$

This ceiling limitation has been plotted on Fig. 8, using η = 0.85, C_{DP} = 0.02, A.R.$_e$ = 10, λ/K = 0.13, and σ_{CR} = 0.4. The wing loadings for the points on this curve are $\sqrt{3}$ times greater than those shown for maximum L/D.

For a jet-propelled subsonic airplane, the ceiling will approximately correspond to the condition that the minimum drag to lift ratio will equal the ratio of maximum thrust to gross weight. For that condition

$$(D/W)_{min.} = (D/L)_{min.} = 2\sqrt{C_{DP}/\pi\text{A.R.}_e} \tag{12}$$

The thrust output of a gas turbine, above about 35,000 ft., follows the approximate relation

$$T/T_{SL} = 1.2\sigma \tag{13}$$

If c is the gas-turbine installed weight per unit of sea-level thrust and λ is the fraction of the gross weight allotted to the power plant,

$$T/W = 1.2\,(\lambda/c)\sigma \tag{14}$$

Equating to the minimum D/L,

$$1.2\,(\lambda/c)\sigma = (2/\eta)\sqrt{C_{DP}/\pi\text{A.R.}_e} \tag{15}$$

Here η represents the installation efficiency factor and takes into account duct losses and, in addition, the variation of thrust with speed. The fact that Eq. (15) does not depend on speed, as did Eq. (11), is a result of the assumption of constant thrust for the gas turbine.

Eq. (15), defining the ceiling of subsonic jet airplanes, is plotted on Fig. 8, using λ/c = 0.5, η = 0.90, C_{DP} = 0.02, and A.R.$_e$ = 10. Both of the relations, Eqs. (11) and (15), are unusual because they define ceilings in terms of the main aerodynamic, power plant, and weight parameters in general fashion.

Simple considerations have now shown that subsonic airplanes operate in a limited region of the speed-altitude diagram. The minimum speed is determined by structural weights; the maximum speed, by the drag associated with compressibility; and the ceiling, by the drop-off in power-plant output with altitude. It must be kept in mind that the limits shown are not those for any single airplane but rather are those of various airplanes whose wing loadings vary with speed and altitude. Since the regions bounded by these limits are reasonably close to the performances actually obtained by subsonic airplanes, the same approach will now be used in the supersonic régime. Some characteristics of the supersonic drag polar will be discussed in addi-

tion, since no textbooks have yet appeared giving the information needed here.

Subsonic airplane performance calculations are based on the type of drag variation of the elliptic plan-form wing. This gives a constant drag coefficient plus one varying with the square of the life coefficient. Drags other than that of the wing are included in the two wing terms. For supersonic performance calculations, the two-dimensional wing will serve as the basis. Its drag coefficient[17] is

$$C_D = K_{PR}\frac{(t/c)^2}{\sqrt{M^2-1}} + \frac{C_L^2}{4}\sqrt{M^2-1} + C_{Df} \quad (16)$$

The first term is the profile drag associated with the distribution of normal pressure at zero lift. Its magnitude depends on the airfoil profile shape. The second term represents the drag associated with normal pressures at an angle of attack, independent of profile shape. The third term is the skin friction. The variation of profile drag with the plan-form variables can be introduced into the first term, since such drags are also dependent on the factor $(t/c)^2/\sqrt{M^2-1}$. By combining this term with the skin friction term, a profile drag coefficient is obtained similar to the subsonic one. The second term can also be corrected for plan form and other effects to give a coefficient depending on C_L^2 just as in subsonic performance calculations. The induced drag corrections can be grouped to form an induced drag efficiency factor, e.

Because of the rearward shift of the wing center of pressure at transonic speeds, the effect of tail loads on induced drag can have an important effect on e. Simple calculations show this factor to be

$$e_t = \frac{1-2(d/l_t)+(d/l_t)^2}{1-(d\epsilon/d\alpha)(d/l_t)+(S_w/S_t)(d/l_t)^2} \cong 1 - 2\left(\frac{d}{l_t}\right) \quad (17)$$

Here, e has the definition

$$C_{Di} = (C_L^2/4e\sqrt{M^2-1};\quad C_L = W/qS \quad (18)$$

and e_t is the portion of e resulting from the trimming tail load. d/l_t is the distance from the center of gravity to the wing-fuselage center of pressure, measured in tail lengths with both dimensions positive when the center of pressure and the tail are behind the c.g. $d\epsilon/d\alpha$ is the wing downwash derivative at the tail. S_t/S_w is the ratio of horizontal tail area to wing area. The importance of this effect can be seen by noting that values of $d/l_t = 0.1$ are not only possible but are probable. The trimming tail load thus can add 25 per cent to the induced drag.

The effect of the wing plan form on e is obtained for sharp leading-edge wings from the slope of the lift curve, since then

$$C_{Di} = C_L\alpha \quad (19)$$

The plan-form contribution to e is

$$e_p = (dC_L/d\alpha)_{3\text{-dimensional}}/(dC_L/d\alpha)_{2\text{-dimensional}} \quad (20)$$

The final value of e is the product of e_p, e_t, and some other factors that take into account the variation of fuselage drag with attitude, etc., just as in the subsonic case.

It is suggested that, as a consequence of the natural division of the supersonic drag into terms independent of lift and dependent on lift squared, the terminology of subsonic performance analysis be retained. The first term may thus be called the parasite drag; the second can be called induced drag. This is believed to be more practical than adaptation of new terms having to do with wave drag. It is obvious that, with the parabolic drag polar, not only the subsonic terminology can be retained but also all the formulas having to do with maximum lift-drag ratio, minimum power, etc., as discussed in reference 16.

Using suitable values in the relations just developed, the ceiling characteristics of supersonic aircraft have been calculated and are shown in Fig. 8. It is seen that ceilings of over 50,000 ft. can be obtained and the optimum wing loadings tend to be high. There is also shown in this figure the variation of speed and altitude for which, on an Air Force hot day, a stagnation temperature of 300°F. will be reached. There can be no doubt of the serious nature of this temperature effect. It will force structural weight increases and make necessary the provision of huge refrigerators for cooling the crew, communicating equipment, instruments, engine accessories, batteries, tires, and all sorts of other equipment. It is estimated that a penalty of 10 per cent of weight-empty will be required to design for continuous operation with a 300°F. stagnation temperature. Further increases in speed will rapidly increase this penalty because of the fact that increase in temperature depends on the square of the velocity.

Developments beyond those just discussed are certainly going to take place. A crude estimate for these has been obtained in the following way. First, the subsonic airplanes were assumed to have afterburners installed, and, second, the power-plant thrust-to-weight ratio has been doubled. The doubled thrust was shown by Clauser[5] to be possible over a 7-year period. Fig. 9 shows the results of these calculations, together with peak performances of 1903 and 1949. Rocket-powered aircraft, of course, should be able to achieve much higher speeds and higher ceilings than those shown on Fig. 9. The calculations made here are confined solely to airplanes using air-breathing engines, since only these vehicles will have usable endurance, at least with presently foreseeable rocket fuels.

The calculations also show some of the other characteristics of the supersonic airplanes. On Fig. 10, for example, are plotted the maximum lift-drag ratios and lift coefficients for maximum lift-drag ratios which will be properties of these airplanes. While the magnitude

of the lift-drag ratio is small compared with those for conventional aircraft, it should be remembered that range depends on the product of lift-drag ratio and velocity, so that the great speed of a supersonic airplane in some measure compensates for the reduced aerodynamic efficiency. Increases in size will also lead to better aerodynamic efficiency. In addition, the normal rate of engineering improvement will provide better performance than that predicted here.

The wing loading for best lift-drag ratio for these small supersonic airplanes is shown in Fig. 11. It can be seen that enormous wing loadings are required to achieve maximum lift-drag ratios at sea level. Requirements for maneuverability, take-off, and landing will prohibit the use of such high wing loading. Penalties as shown in Table 1 will then reduce the performance at sea level, so that actual lift-drag ratios will no doubt be in the order of magnitude of one-half. The possibility of obtaining great endurance at supersonic speeds at low altitudes thus appears to be remote.

The general trends of the wing loadings shown are in the direction of higher loadings than those now in use. While it would be desirable to have efficient fast aircraft with low wing loadings, it is nevertheless true that the trends in aircraft design have indicated that higher performance, improved safety, and higher wing loading can go hand in hand. On Fig. 12, for example, is shown the wing loading and speed of fighter airplanes. To aid in

FIGURE 9

AIRPLANE PERFORMANCE HISTORY

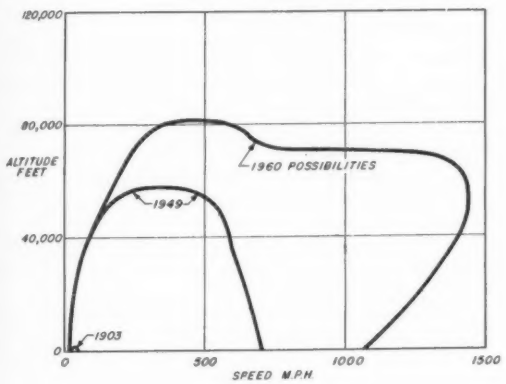

FIGURE 10

MAXIMUM LIFT-DRAG RATIO AND CORRESPONDING LIFT COEFFICIENT

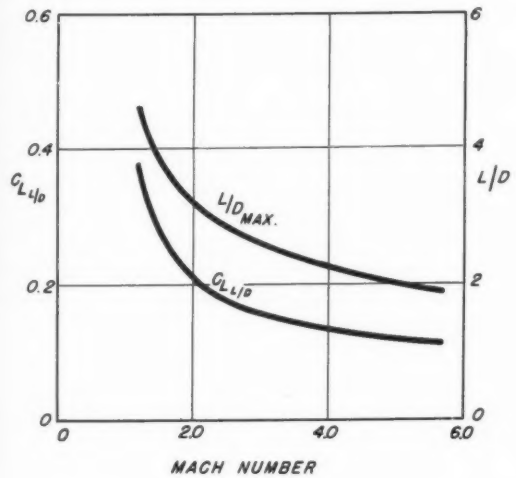

FIGURE 11

WING LOADING FOR BEST LIFT-DRAG RATIO

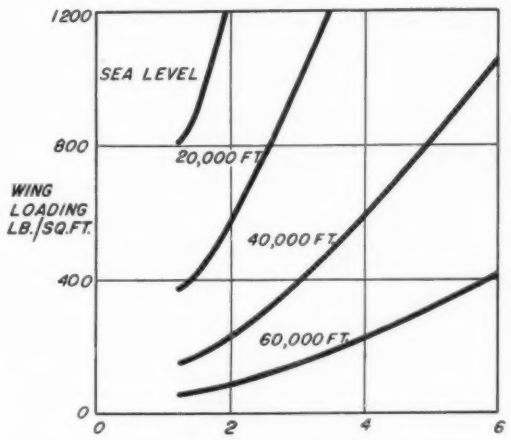

FIGURE 12

WING LOADING AND SPEED OF FIGHTER AIRPLANES

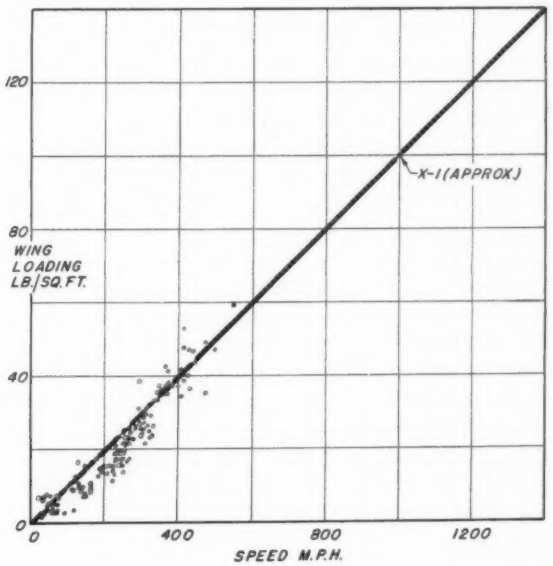

FIGURE 13
U.S. DOMESTIC AIRLINE OPERATIONS
MILLIONS OF PASSENGER MILES
FLOWN PER PASSENGER FATALITY

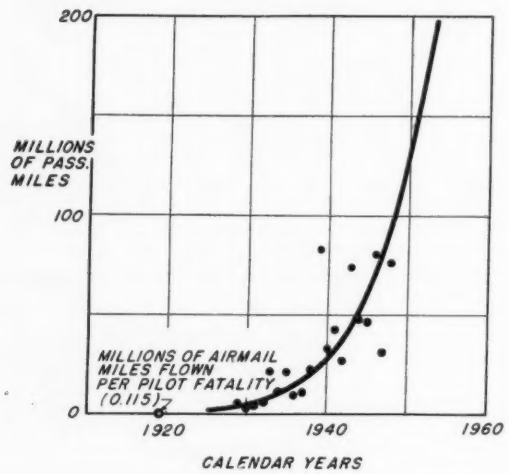

the extrapolation, a value for the X-1 airplane has also been shown, based on data given by *Aviation Week*.[18] A steady increase in wing loading can be seen to have taken place and certainly will continue to take place, but it will be accompanied by higher speeds.

Much the same sort of wing-loading trend can be shown for transport aircraft. Tremendous improvements in their safety record have nevertheless been achieved. On Fig. 13 are plotted the data that show the safety record of the United States domestic scheduled air-line operators. I predict that, in spite of the fact that airlines are now operating aircraft with unprecedentedly high wing loadings, the safety record will continue to show great improvement. There may be, in the next decade, several years in which there will be no passenger fatalities on the domestic scheduled air lines. The curve on Fig. 13 has been extended into the future, using a constant percentage rate of improvement. A tendency to level off may begin to appear but cannot be predicted by any means known to the author.

Conclusions

Progress in the aeronautical sciences has been continuous and rapid since the flights of the Wright Brothers in 1903. The engineering technologies, including jet propulsion and high-speed aerodynamics, are sufficiently advanced to allow soon the exploitation of the supersonic region, first with military aircraft and later with passenger-carrying vehicles. Top speeds, cruising speeds, and ceilings will be increased greatly, and there will also be a continuation in the improvement of flying safety. These goals are a challenge to those working in the aeronautical sciences, a challenge that will surely be met.

References

[1] Dewey and Dakin, *Cycles—The Science of Prediction;* Henry Holt and Company, New York, 1947.

[2] National Industrial Conference Board, *The Economic Almanac for 1948;* N.I.C.B., 1948.

[3] Holbrook, S. H., *The Story of American Railroads;* Crown Publishers, 1947.

[4] Healy, *The Economics of Transportation;* The Ronald Press Company, New York, 1940.

[5] Clauser, M. U., *Trends in Aircraft Power Plants,* Aeronautical Engineering Review, Vol. 6, No. 11, November, 1947.

[6] Warner, E. P., *Airplane Speeds of the Future,* N.A.C.A. T.M. No. 178, 1923.

[7] Wright, T. P., *Speed and Airplane Possibilities,* Journal of the Aeronautical Sciences, Vol. 4, No. 3, January, 1937.

[8] Flader, F., and Child, E. R., *Studies of High Speed Airplanes,* Journal of the Aeronautical Sciences, Vol. 7, No. 6, April, 1949.

[9] Stout, W. B., *Planes of Yesterday,* Aviation, April, 1932.

[10] Hart, H., *Logistic Social Trends,* American Journal of Sociology, Vol. L., pp. 337–352, 1945. (Reported in *Time,* July 8, 1946, p. 77.)

[11] Heinemann, E. H., *High Speed Aircraft Developments,* paper presented before the A.S.M.E. National Aviation Meeting, 1947.

[12] Sikorsky, I. I., *The Next Five Years in Aviation,* Journal of the Aeronautical Sciences, Vol. 4, No. 2, December, 1936.

[13] Warner, E. P., *Is There a Limit on Speed,* Aviation, November, 1932.

[14] Warner, E. P., *The Early History of Air Transportation;* Norwich University, 1937.

[15] Eyston, G. E. T., *Fastest on Earth;* Clymer, Los Angeles, 1946.

[16] Millikan, C. B., *Aerodynamics of the Airplane;* John Wiley and Sons, Inc., New York, 1941.

[17] Liepmann, H. W., and Puckett, A. E., *Introduction to Aerodynamics of a Compressible Fluid;* John Wiley and Sons, Inc., New York, 1947.

[18] Anon., Aviation Week, p. 11, February 7, 1949.

The Calculation of Supersonic Downwash Using Line Vortex Theory

HAROLD MIRELS* AND RUDOLPH C. HAEFELI*

Lewis Flight Propulsion Laboratory, N.A.C.A.

ABSTRACT

A straightforward procedure, based on lifting-line theory, is presented for obtaining the downwash behind lifting surfaces at supersonic speeds. The customary assumptions of an inviscid fluid and small perturbation velocities are made.

In particular, the vortex field associated with a supersonic lifting surface is examined; the vertical perturbation velocity field due to a line vortex segment of constant slope is presented in explicit form and is utilized to discuss some of the properties of line vortices in a supersonic free stream; and a bent lifting-line method and an unbent lifting-line method (horseshoe vortex system) are proposed for determining the downwash field behind swept and unswept wings, respectively. The lifting-line methods are applied to triangular and rectangular wings and give results that are in close agreement with the exact linearized solutions.

This paper is an abbreviated version of reference 1.

INTRODUCTION

SEVERAL METHODS, based on linearized theory, have been presented for obtaining the downwash behind supersonic wings. These employ conical superposition,[2] doublet distributions,[3,4] and vortex distributions.[5] Each method provides integral expressions for downwash which are generally tedious to evaluate. The complexity of these expressions indicates the need for a straightforward procedure for obtaining reasonably accurate, if not exact, downwash solutions.

A logical approach to the development of a simplified supersonic downwash theory is to derive the supersonic analogues of the line vortex procedures that have proved valuable in incompressible flow theory. Certain differences exist, however, between the properties of vortices in an incompressible flow field and vortices in a supersonic flow field. These differences must be investigated before an extension of subsonic techniques is possible. The present paper has two main objectives: (1) The downwash field induced by a line vortex segment of constant slope, obtained from an integral expression provided by Robinson,[6] is presented in explicit form and is utilized to discuss some of the properties of line vortices in a supersonic free stream;† (2) lifting-line methods for computing supersonic downwash are presented, and several calculations, based on these methods, are compared with the exact linearized solutions.

Zero thickness wings (lifting surfaces) are considered throughout. The wings are assumed to induce small perturbation velocities in an inviscid fluid so that the linearized equations of motion are applicable.

SYMBOLS

Only important symbols are defined here.

x, y, z / x_o, y_o, z_o	=	Cartesian coordinate system (Fig. 1)
u, v, w	=	perturbation velocities
ξ, η, ζ	=	components of vortex vector (three-dimensional field)
ξ', η', ζ'	=	components of vortex vector (vortex sheet)
b	=	wing span
C_p	=	pressure coefficient
$G_i(m)$	=	$\dfrac{(Y_i - m_iX_i)(\beta^2 m_i Y_i - X_i)}{r_i[(Y_i - m_iX_i)^2 + (1 - \beta^2 m_i^2)Z_i^2]}$
$G_i(0)$	=	$-X_iY_i/r_i(Y_i^2 + Z_i^2)$
M	=	free-stream Mach Number
m	=	slope of line vortex or lifting line (dy/dx)
r_i	=	$\sqrt{X_i^2 - \beta^2 Y_i^2 - \beta^2 Z_i^2}$
X_i	=	$x - x_i$
Y_i	=	$y - y_i$
Z_i	=	$z - z_i$
α	=	angle of attack
β	=	$\sqrt{M^2 - 1}$
ϵ	=	integration interval
K	=	circulation
φ	=	perturbation velocity potential
$\Delta\varphi$	=	$\varphi_T - \varphi_B$
ρ	=	free-stream density
Γ	=	bound circulation
Γ_m	=	bound circulation at midspan

COORDINATE SYSTEM

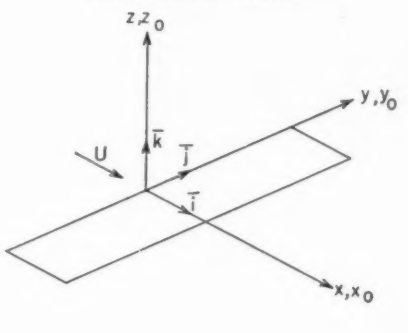

FIG. 1

Presented at the Aerodynamics Session, Annual Summer Meeting, I.A.S., Los Angeles, July 21–22, 1949.

* Wind Tunnel and Flight Division.

† An alternate approach is to derive the velocity field due to the line vortex by using an equivalent surface distribution of doublets. Schlichting[2] obtained the flow field about a horseshoe vortex in a supersonic stream in this manner.

Subscripts

a, b	= points of intersection of forward Mach cone with lifting line (or edge of vortex sheet)
B	= bottom surface of $z = 0$ plane
i	= 1, 2, 3 . . . points on line vortex
l	= plan-form leading edge
T	= top surface of $z = 0$ plane
t	= plan-form trailing edge
o	= variable of integration

Superscripts

m^-	= slope at bend in line vortex when approaching from negative y-direction
m^+	= slope at bend in line vortex when approaching from positive y-direction

Vortex Field Relations

The definitions of vorticity and circulation apply equally to subsonic and supersonic flow fields. Several defining relations for a volume distribution of vorticity, a surface distribution of vorticity, and a line vortex are presented in the following section.

The velocity field is assumed to consist of a supersonic free-stream velocity U plus small perturbation velocities u, v, and w. In vector form

$$\bar{q} = (U + u)\bar{i} + v\bar{j} + w\bar{k} \tag{1}$$

The coordinate system is illustrated in Fig. 1. The vortex vector field $\bar{\omega}$ is defined as the curl of the velocity vector. Thus,

$$\bar{\omega} = \nabla \times \bar{q} = \xi\bar{i} + \eta\bar{j} + \zeta\bar{k} \tag{2}$$

where

$$\xi = \frac{\partial w}{\partial y} - \frac{\partial v}{\partial z}, \quad \eta = \frac{\partial u}{\partial z} - \frac{\partial w}{\partial x}, \quad \zeta = \frac{\partial v}{\partial x} - \frac{\partial u}{\partial y}$$

The magnitude of $\bar{\omega}$ is referred to as vorticity. Vortex lines are lines that are tangent at all points to the local vortex vector and are determined from

$$dx/\xi = dy/\eta = dz/\zeta \tag{3}$$

Vortex lines cannot terminate within a flow field but must either form a closed curve or extend to infinity or a boundary of the field. Circulation is the line integral about a closed curve

$$K = \oint u\,dx + v\,dy + w\,dz \tag{4}$$

If vorticity exists as a surface of velocity discontinuity in the $z = 0$ plane, then outside this plane ξ, η, and ζ are all zero. In the $z = 0$ plane, $\zeta = 0$, whereas ξ and η are infinite. However, the limits

$$\xi' = \lim_{dz \to 0} \xi dz, \qquad \eta' = \lim_{dz \to 0} \eta dz$$

are finite and equal[5]

$$\xi' = v_B - v_T, \qquad \eta' = u_T - u_B \tag{5}$$

The subscripts T and B designate velocities on the top and bottom surface of the $z = 0$ plane, respectively.

The vortex lines through all points on an infinitely small closed curve bound a vortex "tube." The circulation about any path encircling the tube is constant and equals $K = \omega\sigma$, where ω is the vorticity and σ is the normal cross-sectional area at any point along the tube. A line vortex is generated by allowing the cross section of the vortex tube to approach zero while maintaining $\omega\sigma$ constant. Thus, the distinction between a line vortex and a vortex line is that the line vortex has an assigned constant circulation K, whereas the vortex line indicates the direction of the local vortex vector at each point along its length.

Linearized Supersonic Wing Theory Relations

The vortex field generated by a lifting surface in a supersonic stream will now be considered.

Velocity Potential

If the boundary conditions for a lifting surface are specified in the $z = 0$ plane, the u and v velocities are antisymmetric and the w velocities are symmetric about this plane.[5] Thus, the velocities on the top and bottom surface of the $z = 0$ plane (considering each surface separately) are related by $u_T = -u_B$, $v_T = -v_B$, and $w_T = w_B$. The discontinuities in u and v constitute a vortex sheet. If it is assumed that the field, excluding the vortex sheet, is everywhere irrotational, a perturbation-velocity potential φ can be so defined that

$$\left.\begin{aligned} d\varphi &= \frac{\partial \varphi}{\partial x}dx + \frac{\partial \varphi}{\partial y}dy + \frac{\partial \varphi}{\partial z}dz \\ &= u\,dx + v\,dy + w\,dz \end{aligned}\right\} \tag{6}$$

When the undisturbed flow field upstream of the wing is considered to be of zero potential and the boundary condition requiring $u_T = u_B = 0$ off the wing ($u_T = -u_B \neq 0$ implies lift) is applied, the potential in the $z = 0$ plane may be obtained by integrating, along lines of constant y,

$$\varphi_T = \int_{x_l}^{x} u_T\,dx, \qquad \varphi_B = \int_{x_l}^{x} u_B\,dx \tag{7}$$

where x_l is the equation of the leading edge as a function of y. From Eq. (7) it may be concluded that:

(1) $\varphi_T = \varphi_B = 0$ everywhere in the $z = 0$ plane except behind the wing leading edge.

LINES OF CONSTANT POTENTIAL FOR RECTANGULAR WING

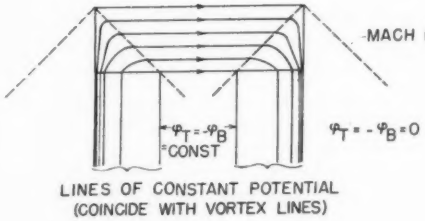

LINES OF CONSTANT POTENTIAL (COINCIDE WITH VORTEX LINES)

FIG. 2.

(2) At a given span station, φ_T and φ_B remain constant for all values of x downstream of the trailing edge. Lines of constant potential for a rectangular wing are shown in Fig. 2.

Vortex Lines

The equation for the vortex lines, from Eq. (3), is

$$\eta'\,dx - \xi'\,dy = 0$$

Substituting,

$$\xi' = -(v_T - v_B) = -2\frac{\partial \varphi_T}{\partial y} = 2\frac{\partial \varphi_B}{\partial y}$$

$$\eta' = u_T - u_B = 2\frac{\partial \varphi_T}{\partial x} = -2\frac{\partial \varphi_B}{\partial x}$$

The equation for the vortex lines becomes

$$\frac{\partial \varphi_T}{\partial x}\,dx + \frac{\partial \varphi_T}{\partial y}\,dy = \frac{\partial \varphi_B}{\partial x}\,dx + \frac{\partial \varphi_B}{\partial y}\,dy = 0 \qquad (8)$$

Comparison with Eq. (6) shows that Eq. (8) represents lines of constant potential. Thus, vortex lines coincide with the lines of constant potential in the $z = 0$ plane (Fig. 2).

Circulation

The circulation included between two points x_1,y_1 and x_2,y_2 on a wing can be obtained by the integration indicated in Eq. (4). The path of integration is arbitrary, except that the path should cross the $z = 0$ plane only at the two specified points. Taking the integral along the top and bottom surface of the $z = 0$ plane,

$$\begin{aligned} K &= \int_{x_1,y_1}^{x_2,y_2} (u_T\,dx + v_T\,dy) + \int_{x_2,y_2}^{x_1,y_1} (u_B\,dx + v_B\,dy) \\ &= (\varphi_{T,2} - \varphi_{T,1}) + (\varphi_{B,1} - \varphi_{B,2}) \\ &= \Delta\varphi_2 - \Delta\varphi_1 \end{aligned} \qquad (9)$$

where $\Delta\varphi$ equals $\varphi_T - \varphi_B$ and represents the jump in potential at the point. The quantity $\Delta\varphi$ is, in fact, the doublet strength[8] so that *the net circulation between two points in the $z = 0$ plane equals the difference between the doublet strengths at these points* [*Eq. (9)*]. The equivalence of a doublet distribution and a vortex distribution indicates that the flow about a lifting surface can be calculated on either basis. Schlichting[7] computed the velocity field due to a supersonic horseshoe vortex by using an equivalent surface distribution of doublets.

Circulation and Lift

The wing lift per unit span is given by the chordwise integration

$$L(y) = \frac{1}{2}\,\rho U^2 \int_{x_L}^{x_t} (C_{p,\,B} - C_{p,\,T})\,dx \qquad (10)$$

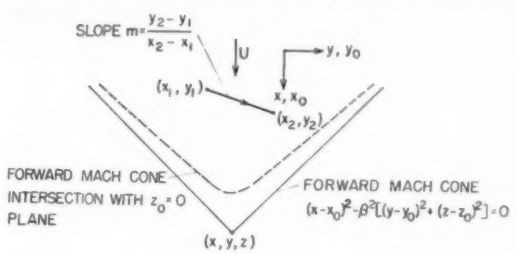

FIG. 3

Substituting the linearized expressions for pressure coefficient

$$C_{p,\,T} = -\frac{2}{U}\frac{\partial \varphi_T}{\partial x}, \qquad C_{p,\,B} = -\frac{2}{U}\frac{\partial \varphi_B}{\partial x}$$

and integrating, Eq. (10) becomes

$$\left.\begin{aligned} L(y) &= \rho U\,\Delta\varphi_t \\ &= \rho U \Gamma \end{aligned}\right\} \qquad (11)$$

where $\Delta\varphi_t$ is the doublet strength at the trailing edge and Γ is the bound circulation. Also,

$$d\Gamma/dy = d(\Delta\varphi_t)/dy = -(\xi')_t \qquad (12)$$

Eq. (12) relates the shed vorticity to the bound circulation. Eqs. (11) and (12) are familiar incompressible flow relations.

Upwash Due to Supersonic Line Vortex

Line Vortex Segment

Complicated velocity fields can be generated by the linear superposition of relatively simple fields. It will therefore prove useful to examine the upwash field due to a line vortex segment of constant slope m which extends from x_1,y_1 to x_2,y_2 in the $z = 0$ plane.

The upwash at x,y,z, a point whose forward Mach cone contains the entire line vortex segment (Fig. 3), is

$$w = (K/2\pi)[G_2(m) - G_1(m)] \qquad (13)$$

where

$$G_i(m) = \frac{(Y_i - m_i X_i)(\beta^2 m_i Y_i - X_i)}{r_i[(Y_i - m_i X_i)^2 + (1 - \beta^2 m_i^2) Z_i^2]}$$

$$X_i = x - x_i, \quad Y_i = y - y_i, \quad Z_i = z - z_i$$

$$r_i = \sqrt{X_i^2 - \beta^2(Y_i^2 + Z_i^2)}$$

$$i = 1, 2$$

The limits are chosen so that $y_2 \geq y_1$. The strength K is positive when the vortex vector (applying right-hand rule) has a component in the positive y-direction. For a line vortex parallel to the x-axis, the strength is positive when the vortex vector is in the positive x-direction.

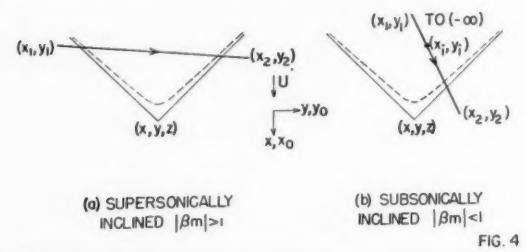

FIG. 4

Eq. (13) applies for any line vortex segment of constant slope. If the line vortex segment terminates on, or is outside of, the forward Mach cone from x,y,z, the corresponding limit [$G_i(m)$ term] in Eq. (13) is neglected.[1]

Infinite Line Vortex

Supersonically Inclined ($|\beta m| > 1$).*—An infinite line vortex inclined supersonically to the free stream is indicated in Fig. 4a. Both limits in Eq. (13) are outside the forward Mach cone and therefore neglected. Thus, the upwash and, in fact, all the perturbation velocities induced by this line vortex are zero. This result agrees with oblique airfoil theory, since the perturbation velocities are zero downstream of the two Mach waves from the trailing edge of a two-dimensional airfoil inclined supersonically to the free stream. (The line vortex may be considered as the limit of a two-dimensional airfoil whose chord goes to zero at constant lift.)

It may appear that the circulation integral [Eq. (4)] taken about the supersonically inclined line vortex will yield zero and thus violate the statement that the circulation is equal to the strength of the line vortex. However, the proper value of circulation will be obtained if the necessary precautions are taken when the path of integration crosses the Mach waves from the line vortex (that is, take the line integral about a lifting surface whose chord goes to zero at constant lift). A value of $K/2$ is obtained when the path crosses a Mach wave.

Subsonically Inclined ($|\beta m| < 1$).—An infinite line vortex inclined subsonically has one limit that extends to infinity but remains within the forward Mach cone (Fig. 4b). From Eq. (13), the upwash for $0 \leq \beta m < 1$ is

$$w = -(K/2\pi) \lim_{x_1 \to -\infty} G_1(m)$$

$$= \frac{K}{2\pi} \frac{\sqrt{1-\beta^2 m^2}(Y_i - mX_i)}{(Y_i - mX_i)^2 + (1-\beta^2 m^2) z^2} \qquad (14)$$

where x_i,y_i is a point on the line vortex. The upwash is infinite along the line vortex, and the flow circulates about the vortex in a manner similar to that for a vortex in an incompressible field. For $m = 0$, Eq. (14) becomes

$$w = (K/2\pi)[Y_i/(Y_i^2 + z^2)]$$

which is identical with the expression for upwash due to an infinite line vortex parallel to the stream (along $y = y_i$) in an incompressible field.

These results indicate that the behavior of the infinite line vortex is completely different from that of the incompressible flow vortex when $|\beta m| > 1$. However, when $|\beta m| < 1$, both vortices have similar flow fields and are, in fact, identical for $m = 0$.

Bent-Line Vortex

A bent-line vortex can be considered as the superposition of two line vortex segments (Fig. 5). The upwash, utilizing Eq. (13), is

$$w = (K/2\pi)[G_1(m^-) - G_1(m^+)] \qquad (15)$$

where m_1^- and m_1^+ designate the slopes of the line vortex before and after the bend at x_1,y_1. The term r_1 appears as a factor in the denominator of Eq. (15), so that the upwash exists only in the downstream Mach cone from x_1,y_1 and is infinite on the cone surface (except in the $z = 0$ plane).

If $m^- = \infty$ and $m^+ = 0$, a horseshoe vortex results (Fig. 6a). The upwash is zero, except within the Mach cone from the bend. The stream-line pattern in a plane normal to the free stream (section AA) is shown in Fig. 6b.[7] At the cone surface, the stream lines are radial to the center. The perturbation velocities are infinite at the cone surface except in the $z = 0$ plane. The spanwise distribution of upwash in this plane is shown in Fig. 6c for $z = 0$ and $z = 0.3R$ (R is radius of Mach cone at section AA).

Lifting-Line Theory

The vertical perturbation velocity field due to a bent-line vortex is given by Eq. (15). The vortex distribution associated with a lifting surface has been discussed. These relations will be used to develop lifting-line methods for computing supersonic downwash assuming the load distribution for the lifting surface is known.

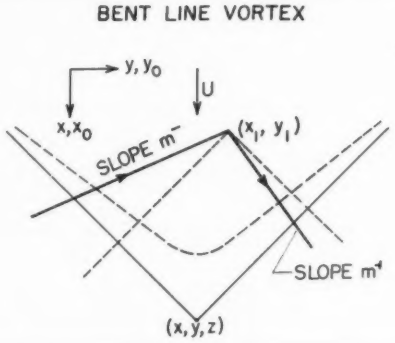

FIG. 5

* A line vortex is supersonically or subsonically inclined as the component of the free-stream velocity normal to the line is supersonic or subsonic, respectively.

PERTURBATION VELOCITIES DUE TO HORSESHOE VORTEX

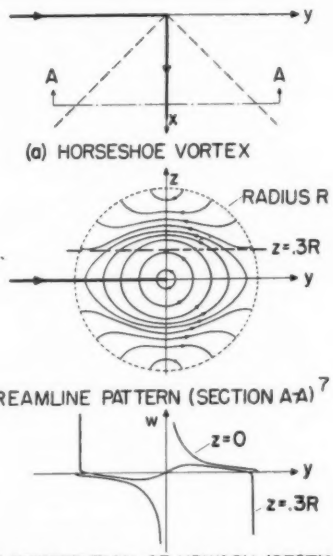

FIG. 6

The load distribution for a large variety of plan forms can be found by the methods of Evvard[9] and Heaslet and Lomax.[8]

A lifting line concentrates the chordwise loading into a line. Thus, the bound circulation is represented by a line vortex of variable strength ($\Gamma = \Delta\varphi_l$), whereas the trailing vortex sheet maintains the same vorticity but now originates at the line rather than the wing trailing edge.

Bent Lifting Line

A bent lifting line approximating the section centers of pressure (Fig. 7a) seems to be a reasonable representation of a swept wing. The vortex distribution associated with the bent lifting line can be represented by the superposition of bent-line vortices as indicated in Fig. 7b.* The vortex sheet is considered to consist of elemental bent-line vortices each of strength $dK = \pm(d\Gamma/dy_o)dy_o$. The contribution, to the downwash field, of each elemental bent line vortex is [from Eq. (15)]

$$dw = -\frac{1}{2\pi}\,[G_o(m) - G_o(0)]\,\frac{d\Gamma}{dy_o}\,dy_o$$

where the subscript o designates a variable of integration and refers to the coordinates at the bend. The vertical perturbation velocity field due to the bent lifting line of Fig. 7 is the sum of the contributions of the elemental vortices and the bent-line vortex of strength Γ_m (bound circulation at midspan) and equals

$$w = \frac{\Gamma_m}{2\pi}\,[G_o(m^-) - G_o(m^+)]_{x_o\,=\,y_o\,=\,0} - \frac{1}{2\pi}\int_{y_o}^{y_b}[G_o(m) - G_o(0)]\,\frac{d\Gamma}{dy_o}\,dy_o \qquad (16)$$

LINE VORTEX REPRESENTATION OF BENT LIFTING LINE

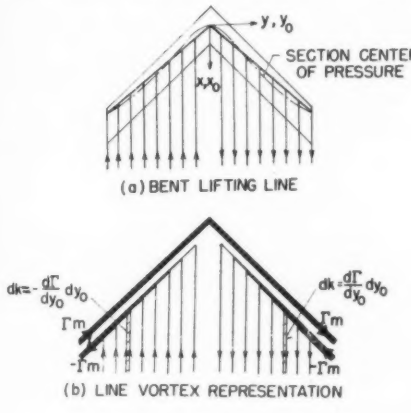

FIG. 7

IMPROPER INTERVALS OF DOWNWASH INTEGRAL

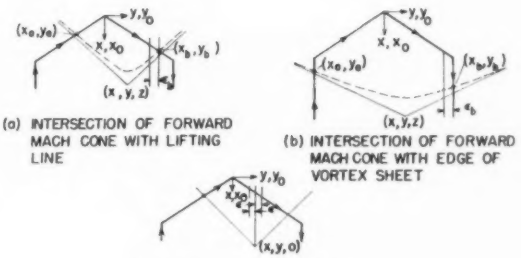
y, y_o
(x_o, y_o)
x, x_o
(x_b, y_b)
(x, y, z)
(a) INTERSECTION OF FORWARD MACH CONE WITH LIFTING LINE
(b) INTERSECTION OF FORWARD MACH CONE WITH EDGE OF VORTEX SHEET
(x, y, 0)
(c) POINT ON VORTEX SHEET

FIG. 8

The integration is conducted along the lifting line included in the forward Mach cone. The nonintegral term of Eq. (16) is readily evaluated. The integral term may be evaluated by analytical or mechanical means. When mechanical methods are used, the singularities in the integrand must be isolated. Suitable procedures for isolating the commonly encountered singularities are as follows:

(a) Singularity due to intersection of forward Mach cone with lifting line. The integrand of Eq. (16) is infinite at the intersection of the forward Mach cone and the lifting line (for $z \neq 0$). The contribution δw of the integral, for the interval $y_b - \epsilon_b \leq y_o \leq y_b$ (Fig. 8a), to the vertical perturbation field may be written

* Suggested by H. S. Ribner.

$$\delta w = -1/2\pi \int_{y-\epsilon_b}^{y_b} [G_o(m) - G_o(0)](d\Gamma/dy_o)dy_o \tag{17a}$$

$$\delta w = -\frac{1}{2\pi}\int_{y_b-\epsilon_b}^{y_b}\left([G_o(m) - G_o(0)]r_o\frac{d\Gamma}{dy_o} - \left\{[G_o(m) - G_o(0)]r_o\frac{d\Gamma}{dy_o}\right\}_{y_o=y_b}\right)\frac{dy_o}{r_o} - \frac{1}{2\pi}\left\{[G_o(m) - G_o(0)]r_o\frac{d\Gamma}{dy_o}\right\}_{y_o=y_b}\int_{y_b-\epsilon_b}^{y_b}\frac{dy_o}{r_o} \tag{17b}$$

where ϵ_b is a convenient length. The first integral in Eq. (17b) is proper and may be mechanically evaluated (the integrand is zero at $y_o = y_b$). The second integral is

$$\int_{y_b-\epsilon_b}^{y_b}\frac{dy_o}{r_o} = \frac{2m}{\sqrt{1-\beta^2m^2}}\sinh^{-1}\sqrt{\frac{(1-\beta^2m^2)\,\epsilon_b}{2[m(x-\beta^2my)-(1-\beta^2m^2)y_b]}}, \quad (0 < \beta m < 1)$$

$$= m\sqrt{2\epsilon_b/(mx-y)}, \quad (\beta m = 1)$$

$$= \int_{y_b-\epsilon_b}^{y_b}\frac{dy_o}{r_o}\frac{2m}{\sqrt{\beta^2m^2-1}}\sin^{-1}\sqrt{\frac{(\beta^2m^2-1)\epsilon_b}{2[m(x-\beta^2my)-(1-\beta^2m^2)y_b]}}, \quad (\beta m > 1)$$

where m is the slope of the lifting line at y_b. A similar procedure applies at y_a.

(b) Singularity in $d\Gamma/dy_o$ at wing tip. The vertical perturbation velocity at a point whose forward Mach cone intersects the edges of the trailing vortex sheet (Fig. 8b) is obtained by integrating between the limits $y_o = \pm b/2$. If $d\Gamma/dy_o$ is singular at these limits (a half order singularity is common), the singularity may be isolated by a procedure similar to that used in Eq. (17b). Thus, the integral in Eq. (16) may be written, for the interval $[(b/2) - \epsilon_b] \leq y_o \leq b/2$,

$$\delta w = -\frac{1}{2\pi}\int_{b/2-\epsilon_b}^{b/2}([G_o(m) - G_o(0)] - \{[G_o(m) - G_o(0)]\}_{y_o=b/2})\frac{d\Gamma}{dy_o}dy_o + \frac{1}{2\pi}\{[G_o(m) - G_o(0)]\}_{y_o=b/2}(\Gamma)_{y_o=(b/2)-\epsilon_b} \tag{18}$$

The integrand in Eq. (18) equals zero at $y_o = b/2$.

(c) Singularity at points on vortex sheet. The Cauchy principal value of the integral [Eq. (16)] is required for determining w at a point on the trailing vortex sheet. Consider the interval $y - \epsilon \leq y_o \leq y + \epsilon$ (Fig. 8c). The integral, in expanded form, is

$$\delta w = \frac{1}{2\pi}\int_{y-\epsilon}^{y+}\frac{m_o\sqrt{X_o^2-\beta^2Y_o^2}}{(Y_o - m_oX_o)\,Y_o}\frac{d\Gamma}{dy_o}\,dy_o \tag{19}$$

If $d\Gamma/dy_o$ can be approximated by the first two terms of the Taylor's expansion

$$\frac{d\Gamma}{dy_o} \cong (d\Gamma/dy_o)_{y_o=y} + (y_o - y)\,(d^2\Gamma/dy_o^2)_{y_o=y}$$

and ϵ is sufficiently small that

$$m_o\sqrt{X_o^2 - \beta^2Y_o^2}/(Y_o - m_oX_o) \cong -1$$

Eq. (19) may be approximated by

$$\delta w = -\frac{1}{2\pi}\int_{y-\epsilon}^{y+\epsilon}\left[\left(\frac{d\Gamma}{dy_o}\right)_{y_o=y} - Y_o\left(\frac{d^2\Gamma}{dy_o^2}\right)_{y_o=y}\right]\frac{dy_o}{Y_o} = \frac{\epsilon}{\pi}\left(\frac{d^2\Gamma}{dy_o^2}\right)_{y_o=y} \tag{20}$$

The value $\epsilon = 0.05b$ is satisfactory for most computations.

Unbent Lifting Line (Horseshoe Vortex System)

The unbent lifting line (Fig. 9) appears to be a reasonable representation for an unswept wing. The vertical perturbation velocities are obtained from Eq. (16) by setting $m = \infty$ and equal, in the expanded form,

$$w = -\frac{1}{2\pi}\int_{y_a}^{y_b}\frac{xY_o(r_o^2 - \beta^2z^2)}{r_o(x^2 - \beta^2z^2)(Y_o^2 + z^2)}\frac{d\Gamma}{dy_o}\,dy_o \tag{21}$$

The singularities are isolated as follows:

(a) Singularity due to intersection of forward Mach cone with lifting line.

$$\delta w = -\frac{1}{2\pi}\int_{y_b-\epsilon_b}^{y_b}\left[\frac{x Y_o(r_o^2-\beta^2z^2)}{(x^2-\beta^2z^2)(Y_o^2+z^2)}\frac{d\Gamma}{dy_o}+\left(\frac{\beta^2z^2}{xY_o}\frac{d\Gamma}{dy_o}\right)_{y_o=y_b}\right]\frac{dy_o}{r_o}+\frac{1}{\beta\pi}\left(\frac{\beta^2z^2}{xY_o}\frac{d\Gamma}{dy_o}\right)_{y_o=y_b}\sin^{-1}\sqrt{\frac{\epsilon_b}{2(y_b-y)}} \tag{17a}$$

(b) Singularity in $d\Gamma/dy_o$ at the tip.

$$\delta w = -\frac{1}{2\pi}\int_{b/2-\epsilon_b}^{b/2}\left\{\frac{x Y_o(r_o^2-\beta^2z^2)}{r_o(x^2-\beta^2z^2)(Y_o^2+z^2)}-\left[\frac{x Y_o(r_o^2-\beta^2z^2)}{r_o(x^2-\beta^2z^2)(Y_o^2+z^2)}\right]_{y_o=b/2}\right\}\frac{d\Gamma}{dy_o}dy_o+\frac{1}{2\pi}\left[\frac{x Y_o(r_o^2-\beta^2z^2)}{r_o(x^2-\beta^2z^2)(Y_o^2+z^2)}\right]_{y_o=b/2}(\Gamma)_{y_o=b/2-\epsilon_b} \tag{17b}$$

(c) Singularity at points on vortex sheet.

$$\delta w = (\epsilon/\pi)(d^2\Gamma/dy_o^2)_{y_o=y}$$

The chordwise location of the unbent lifting line yielding the best average agreement with the exact linearized solution is still to be determined. According to the techniques used in incompressible flow theory, an unbent lifting line at the wing center of pressure should be a good approximation. It may be possible to determine the best location for each general class of plan forms by comparing the lifting-line solution with the exact linearized solution for several representative plan forms.

Downwash at Infinity

The velocity field an infinite distance downstream of a lifting line is obtained by allowing x to become infinite in Eq. (16). The result is

$$w = -\frac{1}{2\pi}\int_{-b/2}^{b/2}\frac{Y_o}{Y_o^2+z^2}\frac{d\Gamma}{dy_o}dy_o \tag{18}$$

Eq. (22) is identical to that for the velocities an infinite distance behind a wing in an incompressible flow field. This result has been pointed out by others.[2,3] The evaluation of Eq. (22) is relatively simple and may be used to approximate the downwash several chords behind a supersonic wing.

Examples and Discussion

Examples

A bent lifting line and an unbent lifting line will be used to obtain solutions for the downwash in the $y = 0$ plane behind triangular wings having subsonic leading edges. The chordwise distribution of wing loading suggests the use of the bent lifting line. The unbent lifting line will be used for purposes of comparison. An unbent lifting line will be used to compute the downwash in the $y = 0$ plane behind rectangular wings. The unbent lifting line will be placed at the chordwise location giving the best average agreement with the exact linearized solution for each wing. In order to simplify the expressions, $M = \sqrt{2}$ (that is, $\beta = 1$) will be assumed.

LINE VORTEX REPRESENTATION OF UNBENT LIFTING LINE

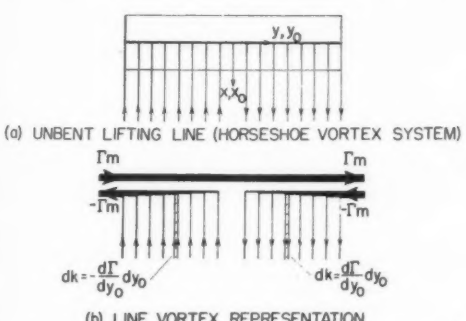

FIG. 9

Triangular Wings.—The spanwise distribution of circulation for a triangular wing of span b and root chord c_r, having subsonic $[(b/2c_r) < 1]$ leading edges, is [from Eq. (24), Heaslet and Lomax[2]]

$$\Gamma = \Delta\varphi_l = (\alpha U b/E)\sqrt{1-(4/b^2)y_o^2}$$

where E is the complete elliptic integral of the second kind with modulus $\sqrt{1-(b/2c_r)^2}$. The vertical perturbation velocities in the $y = 0$ plane, using the bent lifting line approximation of Fig. 10a, is

$$w = -\frac{\alpha U b}{\pi E}[G_o(m^+)]_{x_o=y_o=0}+\frac{4\alpha U}{\pi b E}\times\int_0^{y_b}\frac{[G_o(m^+)-G_o(0)]}{\sqrt{1-(4/b^2)y_o^2}}y_o\,dy_o \tag{23}$$

where $(m^+) = b/c_r$. Eq. (23) is obtained from Eq. (16) utilizing the properties of an even function. The vertical perturbation velocity field behind an unbent lifting line having the same loading (Fig. 10b), is [from Eq. (21)]

$$w = -\frac{4\alpha U}{\pi b E}\times\int_0^{y}\frac{x\,(r_o^2-z^2)\,y_o^2\,dy_o}{r_o(x^2-z^2)(y_o^2+z^2)\sqrt{1-(4/b^2)y_o^2}} \tag{24}$$

LIFTING LINE REPRESENTATIONS OF TRIANGULAR WING

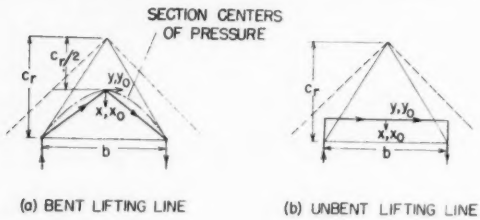

(a) BENT LIFTING LINE (b) UNBENT LIFTING LINE

FIG. 10

DOWNWASH ALONG LINE y=0, z=0 BEHIND TRIANGULAR WINGS USING BENT LIFTING LINE APPROXIMATION

M=$\sqrt{2}$

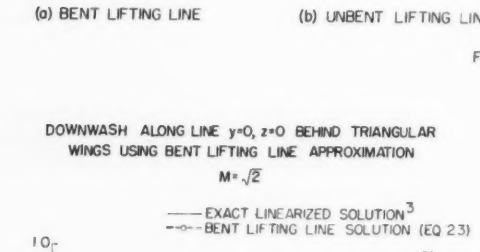

FIG. 11(a)

DOWNWASH ALONG LINE y=0, z=.1b BEHIND TRIANGULAR WINGS USING BENT LIFTING LINE APPROXIMATION

M=$\sqrt{2}$

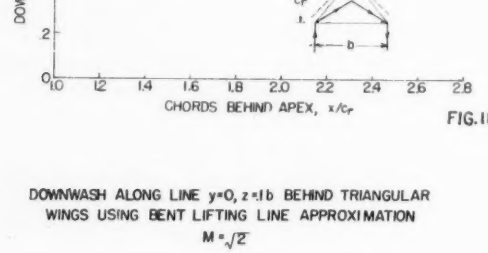

FIG. 11(b)

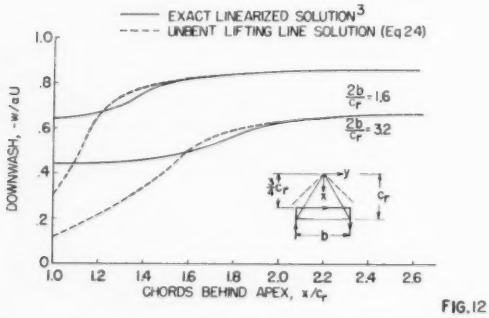

FIG. 12

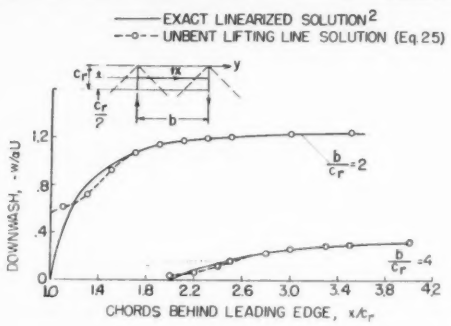

FIG 13

Rectangular Wings.—The spanwise distribution of circulation for a rectangular wing of aspect ratio $b/c_r \geq 2$ is [from Eq. (20), Evvard[9]], for $[(b/2) - c_r] \leq y_o \leq b/2$,

$$\Gamma = \Delta\varphi_l = \frac{4\alpha U}{\pi}\left[\sqrt{\left(y_o + c_r - \frac{b}{2}\right)\left(\frac{b}{2} - y_o\right)} + c_r \tan^{-1}\sqrt{\frac{(b/2) - y_o}{y_o + c_r - (b/2)}}\right]$$

and, for $0 \leq y_o \leq [(b/2) - c_r]$,

$$\Gamma = 2\alpha U c_r$$

The vertical perturbation velocities in the $y = 0$ plane behind an unbent lifting line having this loading is given by

$$w = -\frac{4\alpha U c_r}{\pi^2}\int_{(b/2)-c_r}^{b/2} \frac{x(r_o^2 - z^2)y_o}{r_o(x^2 - z^2)(y_o^2 + z^2)} \times \sqrt{\frac{y_o + c_r - (b/2)}{(b/2) - y_o}}\,dy_o \quad (25)$$

Computations.—Eq. (23) was evaluated to determine the downwash along the line $y = 0$, $z = 0$ and along the line $y = 0$, $z = 0.1b$ for triangular wings of aspect ratios $2b/c_r = 1.6$ and 3.2. Eq. (24) was evaluated along the line $y = 0$, $z = 0$ for the same wings. Eq. (25) was evaluated at points along the line $y = 0$, $z = 0$ for rectangular wings of aspect ratios $b/c_r = 2$ and 4. The integrations were performed mechanically for Eqs. (23) and (25) and analytically for Eq. (24). The results are compared with the exact linearized solutions[2–4] in Figs. 11 to 13.

Discussion

The bent lifting-line solutions for the triangular wings are shown in Figs. 11a and 11b. The agreement with the exact solution is very good for all points except those within a one-half chord of the trailing edge. The agreement indicates that the bent lifting line is a good average representation of the triangular wing. The method should give even better agreement when used to

represent a swept wing, such as the one in Fig. 7a, because the bent lifting line would then more closely approximate the actual chordwise distribution of vorticity.

The discontinuity in the curves for $z = 0.1\ b$ designates large negative (upwash) values that become infinite on the Mach cone from the tip of the lifting line. Lifting-line solutions always yield this infinity when the loading at the tip has a one-half order singularity. The infinity may or may not exist in the exact linearized solution for the flow field about the original wing, depending on the plan-form configuration at the wing tip. Infinite upwash will exist on the downstream Mach cone from a wing tip formed by the intersection of a subsonic leading edge and a supersonic trailing edge, provided the subsonic edge is not in the free-stream direction at the intersection.[1]

The unbent lifting-line solutions for the triangular wings are presented in Fig. 12. The lifting line was placed at the three-quarter chord point to give the best average agreement with the exact linearized solution. The center of pressure for these wings is at the two-thirds chord point. The agreement is not so good as that obtained with the bent lifting line and indicates that the bent lifting line is more suitable for computing downwash behind triangular wings. The smaller aspect ratio wing ($2b/c_r = 1.6$) is in better agreement with the exact linearized solution because of the rapidity with which the downwash approaches the asymptotic value at infinity.

The unbent lifting-line solutions for the rectangular wings are presented in Fig. 13. The downwash obtained with the lifting line at the one-half chord point is in excellent agreement with the exact linearized solutions. The location of the center of pressure is at the 4/9 and the 10/21 chord points for aspect ratios 2 and 4, respectively. These calculations suggest that the best chordwise position for the unbent lifting line is at, or slightly downstream of, the wing center of pressure.

A more accurate estimate of the downwash in the $z = 0$ plane, close to the trailing edge, may be obtained by judiciously fairing the curve obtained by the lifting-line method to the known value of downwash at the trailing edge. At a subsonic trailing edge satisfying the Kutta condition, $-w/\alpha U$ is unity, whereas at a supersonic trailing edge, $-w/\alpha U$ can be computed using the method of Lagerstrom and Graham.[2]

Concluding Remarks

The downwash computations based on lifting-line theory are in close agreement with those based on exact-linearized theory. Thus, lifting-line methods can be used to obtain the linearized solution for the downwash behind supersonic wings. It should be noted, however, that linearized theory assumes the trailing vortex sheet to be in the $z = 0$ plane and thereby neglects the displacement and distortion of the vortex sheet. In addition, the load distributions indicated by linearized theory may be modified by viscous effects and by larger magnitudes of perturbation velocities than are permitted by linear theory. An experimental program, such as that conducted by Silverstein, Katzoff, and Bullivant[10] for wings in subsonic flight, is ultimately required to determine the necessary modifications to theory which will result in good agreement with practice.

References

[1] Mirels, Harold, and Haefeli, Rudolph C., *Line Vortex Theory for Calculation of Supersonic Downwash*, N.A.C.A. T.N. No. 1925, 1949.

[2] Lagerstrom, P. A., and Graham, Martha E., *Downwash and Sidewash Induced by Three-Dimensional Lifting Wings in Supersonic Flow*, Rep. No. SM-13007, Douglas Aircraft Company, Inc., April, 1947.

[3] Heaslet, Max A., and Lomax, Harvard, *The Calculation of Downwash behind Supersonic Wings with an Application to Triangular Plan Forms*, N.A.C.A. T.N. No. 1620, 1948.

[4] Lomax, Harvard, and Sluder, Loma, *Downwash in the Vertical and Horizontal Planes of Symmetry behind a Triangular Wing*, N.A.C.A. T.N. No. 1803, 1949.

[5] Robinson, A., and Hunter-Tod, J. H., *Bound and Trailing Vortices in the Linearized Theory of Supersonic Flow and the Downwash in the Wake of a Delta Wing*, Report No. 10, College Aero. (Cranfield), October, 1947.

[6] Robinson, A., *On Source and Vortex Distributions in the Linearized Theory of Steady Supersonic Flow*, Report No. 9, College Aero. (Cranfield), October, 1947.

[7] Schlichting, H., *Airfoil Theory at Supersonic Speed*, N.A.C.A. T.M. No. 897, June, 1939.

[8] Heaslet, Max A., and Lomax, Harvard, *The Use of Source-Sink and Doublet Distributions Extended to the Solution of Arbitrary Boundary Value Problems in Supersonic Flow*, N.A.C.A. T.M. No. 1515, 1948.

[9] Evvard, John C., *Theoretical Distribution of Wave Drag and Lift in the Vicinity of Wing Tips at Supersonic Speeds*, N.A.C.A. T.N. No. 1382, 1947.

[10] Silverstein, Abe, Katzoff, S., and Bullivant, W. Kenneth, *Downwash and Wake behind Plain and Flapped Airfoils*, N.A.C.A. Report No. 651, 1939.

The Pulse Method for the Determination of Aircraft Dynamic Performance

R. C. SEAMANS, JR.,* B. P. BLASINGAME,† AND G. C. CLEMENTSON‡

Massachusetts Institute of Technology and U.S.A.F. Institute of Technology

SUMMARY

In this paper a method is described for evaluating an aircraft dynamic test involving the response of the aircraft to an applied displacement of a control surface. It is shown that the response can be expressed mathematically by means of a concept called a *performance operator*[1] and that with selected types of control surface motion of common occurrence the response can be related to the applied displacement more simply by means of a *performance function*. These two concepts are used extensively by Dr. C. S. Draper and his associates in the Instrumentation Laboratory of the Massachusetts Institute of Technology.

A general description is given of the performance operator and the performance function, following which a technique is described which permits the performance function of an aircraft to be determined from knowledge of its response to a pulse of less than 1-sec. duration. The performance function of a U.S. Air Force B-25 medium bomber, obtained by this technique, is correlated with the performance function computed from stability derivatives.

It is seen that the conventional analysis gives satisfactory results at low Mach Numbers and in the absence of aeroelastic effects. However, it is anticipated that, at high Mach Numbers and when aeroelastic effects cannot be ignored, experimental techniques such as outlined in this paper will be required to obtain the aircraft performance functions.

INTRODUCTION

THE INCREASED AERODYNAMIC DRAG resulting from transonic and supersonic speeds can severely limit the range capabilities of an aircraft. For this reason the stabilizing surfaces of transonic and supersonic aircraft are reduced to the minimum size that considerations of stability will permit. Therefore, it is almost a matter of course that an appraisal of the dynamic characteristics of a high-speed airplane is needed when the airplane is still in the design stage. Later, it must be expected that the prototype will be given not only the conventional flight tests but also dynamic tests that will enable artificial stability derivatives to be harmonized with the air frame and from which automatic features for landing, navigation, and special military purposes can be successfully incorporated.

Received May 2, 1949. Revised and received July 29, 1949.

* Associate Professor of Aeronautical Engineering and Director, Tracking Control Project, Instrumentation Laboratory.

† Major, U.S.A.F. Institute of Technology, temporarily assigned to Massachusetts Institute of Technology for graduate training.

‡ Major, U.S.A.F. Institute of Technology, temporarily assigned to Massachusetts Institute of Technology for graduate training.

The performance of an aircraft is difficult to analyze by strictly mathematical procedures because its response depends upon compressible fluid mechanics and involves, even for a rigid air frame, several degrees of freedom. For these reasons a method has been sought which will enable the complete performance characteristics of an aircraft to be determined from relatively simple practical tests. With this in view, the Instrumentation Laboratory, working under a contract with the U.S. Air Force, made extensive longitudinal and lateral tests on a B-26 (designated A-26 prior to October, 1948) medium bomber. Assistance in the tests was given by the Cornell Aeronautical Laboratory, who installed the necessary instrumentation and control equipment, conducted the required flights, and reduced the resulting flight data.

In the tests, the response of the airplane was determined as the result of separately applied displacements of the elevator, rudder, and ailerons. In each case, both sinusoidal and step displacements were used in order to investigate both steady-state and transient effects. The response to a sinusoidal input, as determined for several air speeds and center-of-gravity locations, agrees reasonably well with the response predicted by theoretical methods in both the longitudinal mode and the lateral mode at the low Mach Numbers used.

The dynamic performance resulting from step displacements agreed well with theory in the longitudinal tests; the agreement was reasonably good in the lateral tests for which the rudder motion provided the excitation. However, considerable difficulty was experienced with the aileron step displacements because, with only one degree of aileron, the bank angle reaches 30° before the airplane reaches a constant rate of roll. It was suggested by Major Clementson[2] that the difficulty could be overcome by using a pulse displacement rather than a step displacement. With the pulse method, the control surface is quickly returned to its equilibrium position after initiation of the disturbance. The method is simple to use, adequate data for transient evaluation can be obtained from only a few flights, and the further advantage is offered that the airplane is operated at nearly equilibrium conditions.

In June, 1948, a B-25 medium bomber was made available to the Instrumentation Laboratory by the U.S. Air Force to make possible an investigation of the pulse method. For the purpose, the Laboratory has

installed a stop mechanism in the airplane so that the pilot can apply elevator pulses. There are two stops in the mechanism: One of them is located so that when the control column is held against it the pilot can trim the elevator for the desired air speed and altitude configuration; the second stop is adjusted before flight to give the desired elevator travel. The pilot introduces the pulse by moving the control column from the stop giving trimmed flight to the other stop and back again to the initial stop in a selected interval of time. The stop mechanism is provided with a quick disengage as a safety measure and to permit recovery from long-period phugoid oscillations that may be incurred at low air speeds.

Instruments have been installed for recording elevator position, rate of pitch, and normal acceleration. During a flight of 2-hour duration, there is time to apply several pulses at each of three air speeds and to make static calibrations of the recording equipment both before and after obtaining the pulse data. The accuracy of the indications of the elevator pulse displacement and response is greater than with indications involving a step input, because all of the required quantities can be considerably greater in magnitude and at the same time the total change in the pitch angle can be considerably reduced.

The procedure for reducing the pulse data into a form similar to that obtained directly from sinusoidal tests involves a Fourier Transformation. Computing machines, such as the Corodi Analyzer, are designed for this specific mathematical application, and other computing machines may be adapted to this purpose. An alternate, approximate method is outlined in this paper. Using this approximate method, a pulse response may easily be transformed by graphical vector summation. A computing machine based on this approximate Fourier Transform has been constructed. The machine permits the real and imaginary parts of this vector summation to be recorded continuously as functions of frequency, the new independent variable.

(I) Definition of the Performance Operator and the Performance Function

The airplane in flight can be considered a single *operating component*, which receives certain inputs and which produces outputs that are functions of the inputs. For present purposes, the principal inputs are the control surface displacements and the power-plant thrust; the principal outputs are the angle of attack, aerodynamic yaw, air speed, angular velocity, and linear acceleration. In general, the output quantities differ from the input quantities in dimension, magnitude, and integral or differential order. The relationships of the outputs to the inputs can be determined from the kinematic and dynamic equations of motion of the airplane. All of these equations can be summarized in the general form:

$$q_{(\text{out})} = \{P\}_{A(q_{\text{in}}q_{\text{out}})}\, q_{(\text{in})} \tag{1}$$

The term $\{P\}$ in this equation designates the performance operation required to convert the input to the output quantity. The subscript, A, indicates the component or system under investigation, in this case the airplane, A. The subscripts q_{in} and q_{out} within the parentheses show by their designations and order the desired input and output quantities.

As an example, consider the performance of an airplane required when investigating stabilization about its roll axis. The input to the airplane in this case is the aileron displacement δ_a, and the resulting output is the angle of roll, φ. The airplane performance operator that describes the relationship is written $\{P\}_{A[\delta_a\varphi]}$.

It is possible to describe the lateral response to aileron displacement in terms of three linear differential equations with constant coefficients, provided the airplane is restricted in motion to small deviations from equilibrium. But this restriction does not hold when the airplane is in a diving turn. In this case at least eight nonlinear equations are required to specify the motion of the airplane.

With the performance operator it becomes possible at least to express the angle of roll in terms of the aileron motion. In the form of Eq. (1), we can write:

$$\varphi = \{P\}_{A(\delta_a\varphi)}\, \delta_a \tag{2}$$

It must be emphasized that the performance operator notation primarily summarizes the operations required to establish the output quantity for a given input variation. It yields a solution of the performance equations only when the input quantity is specified, and then only by using conventional mathematical procedure.

The performance of a large number of useful components can be expressed by a single linear differential equation having constant coefficients. This equation may be written:

$$\ldots + a_2 \frac{d^2q_{(\text{out})}}{dt^2} + a_1 \frac{dq_{(\text{out})}}{dt} + a_0 q_{(\text{out})} = b_0 q_{(\text{in})} + b_1 \frac{dq_{(\text{in})}}{dt} + b_2 \frac{d^2q_{(\text{in})}}{dt^2} + \ldots \tag{3}$$

This is one of the possible kinds of relationships between the output and the input implied in the performance operator definition of Eq. (1)—i.e.,

$$\{P\}_{(\,)(q_{\text{in}}q_{\text{out}})} = \left\{ \frac{b_0}{a_0}(\,) + \frac{b_1}{a_0}\frac{d}{dt}(\,) + \frac{b_2}{a_0}\frac{d^2}{dt^2}(\,) + \ldots - \frac{a_1}{a_0}\frac{dq_{(\text{out})}}{dt} - \frac{a_2}{a_0}\frac{d^2q_{(\text{out})}}{dt^2} \ldots \right\} \tag{4}$$

The dynamic characteristics are described mathematically by Eq. (4) and specify a particular component when the coefficients (a's and b's) are known. The output response depends upon these dynamic characteristics and upon the time variation of the input.

Several types of inputs are considered in this paper. For the special class of sinusoidal input functions, certain simplifications in the relation between output and input quantities result. It is convenient to use the complex exponential notation, $e^{j\omega t}$ for these types of functions. This term has a unit magnitude and implies rotation in the complex plane at an angular frequency, ω, expressed in radians per unit time. The angular position of the exponential term, measured with respect to the real axis, is equal to the product of the angular frequency and the elapsed time, t. It can be seen that the complex exponential is periodic, having a repetition rate of $\omega/2\pi$ and a repetition time, called the period, of $2\pi/\omega$.

An input quantity that has a complex-plane rotation, similar to $e^{j\omega t}$ but with an initial phase angle $(PA)_{(\text{in})}$ and an amplitude $q_{(\text{in})a}$, can be expressed by

$$q_{(\text{in})} = q_{(\text{in})a}\, e^{j[\omega t + (PA)_{(\text{in})}]} \tag{5}$$

The complex form of Eq. (5) is particularly convenient when differential equations are to be solved, because the operation of either differentiation or integration involves only the multiplication or division by $j\omega$. In addition, any periodic quantity can be expressed as an infinite series of complex exponentials rotating both positively and negatively at frequencies that are integral multiples of a fundamental frequency, ω_1. This series, called a Fourier Series, pairs the exponentials in such a way that their summation is a real quantity. Sine and cosine functions can be expressed using only two terms of the Fourier Series. More complicated functions, such as the square wave and the sawtoothed wave, require an infinite number of terms for mathematical exactness, but usually a limited number is satisfactory for engineering purposes.

It is known from the elementary theory of linear differential equations that, when the input is described by a complex exponential, the *steady-state output* has the same angular frequency but has a different amplitude $q_{(\text{out})a}$ and phase angle, $(PA)_{(\text{out})}$—that is,

$$q_{(\text{out})} = q_{(\text{out})a}\, e^{j[\omega t + (PA)_{(\text{out})}]} \tag{6}$$

It can be seen from a comparison of Eqs. (5) and (6) that the ratio of the steady-state output to the input is independent of time because the term $e^{j\omega t}$ is factorable. This ratio is termed the performance function,* $(PF)_{(\ )(q_{\text{in}}q_{\text{out}})}$, so that by definition

$$(PF)_{(\ )(q_{\text{in}}q_{\text{out}})} = \frac{q_{(\text{out})a}}{q_{(\text{in})a}}\, e^{j[(PA)_{(\text{out})} - (PA)_{(\text{in})}]}$$

$$= (AR)_{(\ )(q_{\text{in}}q_{\text{out}})} e^{j(PA)_{(\ )(q_{\text{in}}q_{\text{out}})}} \tag{7}$$

In Eq. (7), the ratio of the output amplitude to the input amplitude is called the amplitude ratio, AR, and the difference in phase between the output and the input is called the phase angle, PA. The scheme of subscripts established with the performance operator is used for designating the performance function for a particular application. The term *vector performance operator*, which was used in the previous article[1] has confused the distinction between an operator and a function. The distinction can be explained by noting from Eqs. (5), (6), and (7) that, with a complex exponential input,

$$q_{(\text{out})} = (PF)_{(\ )(q_{\text{in}}q_{\text{out}})}\, q_{(\text{in})a}\, e^{j[\omega t + (PA)_{(\text{in})}]} \tag{8}$$

and from Eqs. (1) and (5),

$$q_{(\text{out})} = \{P\}_{(\ )(q_{\text{in}}q_{\text{out}})}\, q_{(\text{in})a}\, e^{j[\omega t + (PA)_{(\text{in})}]} \tag{9}$$

so that

$$e^{j\omega t}(PF)_{(\ )(q_{\text{in}}q_{\text{out}})} = \{P\}_{(\ )(q_{\text{in}}q_{\text{out}})}\, e^{j\omega t} \tag{10}$$

Eq. (10) shows that the product of the complex exponentia' $e^{j\omega t}$ and the performance function results from the operation, $\{P\}$, carried out on the complex exponential. The performance function affects the amplitude and phase of the complex exponential representing the output quantity but does not operate on the exponential in the truly mathematical sense.

The performance function depends upon the angular frequency. The relationship for a linear differential equation with constant coefficients, determined by combining Eqs. (3), (5), and (8), is

$$(PF)_{(\ )(q_{\text{in}}q_{\text{out}})} = \frac{b_0 + b_1(j\omega)^1 + b_2(j\omega)^2 + \ldots + b_m(j\omega)^m}{a_0 + a_1(j\omega)^1 + a_2(j\omega)^2 + \ldots a_n(j\omega)^n} \tag{11}$$

The nth integer appearing in the denominator of Eq. (11) is usually greater than the mth integer shown in the numerator, in which case the performance function approaches zero as the angular frequency approaches an infinite value.

(II) Relation of the Performance Function to a Generalized Response

The dynamic characteristics of an operating component can be completely specified either in terms of its performance function or in terms of its response to a unit impulse (UIR). When the response to a unit impulse is known either by direct measurement or by analysis, the response to any input may be evaluated by use of the real convolution integral, a procedure commonly used to determine airplane structure loads due to prescribed control deflections. This integral,[3] sometimes identified with Duhamel, states the relation between the input and output of a component or system as

$$q_{(\text{out})}(t) = \int_0^t q_{(\text{in})}(\tau)\, [(UIR)(t-\tau)]_{(\ )(q_{\text{in}}q_{\text{out}})}\, d\tau \tag{12}$$

or, substituting $\tau' = t - \tau$ into Eq. (12) and then drop-

* The performance function is equivalent to the frequency response or transfer function used by other authors.

ping the primes,

$$q_{(out)}(t) = \int_0^t q_{(in)}(t-\tau)[(UIR)(\tau)]_{(\ )(q_{in}q_{out})}\,d\tau \quad (13)$$

The response of a component can be obtained by convolving the input quantity and the unit impulse response according to either Eq. (12) or (13). It should be noted that the output quantity can be determined at any time, t, and, hence, these equations can be used to study either transient or steady-state effects. Steady-state conditions are approached as the time becomes infinitely large.

Since this mathematical operation combines the input quantity with component characteristics to give the output quantity, it can be seen that

$$[P]_{(\ )(q_{in}q_{out})} = \int_0^t (\ )[(UIR)(t-\tau)]_{(\ )(q_{in}q_{out})}d\tau \quad (14)$$

Computing machines for operating on the input in the manner of Eq. (14) are in existence as, for example, the Cinema Integraph. An approximate arithmetic procedure proposed by Tustin[4] requires a summation based on the response to triangles of finite duration.

Generally, in the study of closed-loop dynamic systems, benefits result from a transformation that permits the use of a complex variable, rather than time, as the independent variable. There are a number of transformations, such as the Fourier Transform and the LaPlace Transform, which can be utilized. The LaPlace Transform has the most general application, and a great many engineering treatments of its development are available. The LaPlace Transform is used in this section to show the relation between the performance function and the unit impulse response of a component or system, although it is a more powerful method than is needed for much of the analysis discussed in this paper. The special properties of the pulse allow the Fourier Transform to be used in place of the LaPlace Transform in a large number of cases.

The complex variable, s, of the LaPlace Transform has a real part, α, and an imaginary part ω—that is, $s = \alpha + j\omega$—and the transform is defined as

$$[LT][q(t)] = \int_0^\infty q(t)e^{-st}dt \quad (15)$$

For the Fourier Transform, the lower limit of the integral in Eq. (15) is changed to $-\infty$, and the complex variable is taken simply as $j\omega$.

A theorem[5] that has important application states that convolution can be reduced to multiplication after transforming the dependent variables in the manner of Eq. (15). Application of this theorem to either Eq. (12) or (13) gives

$$[LT][UIR]_{(\ )(q_{in}q_{out})} = \frac{[LT][q_{(out)}(t)]}{[LT][q_{(in)}(t)]} \quad (16)$$

Eq. (16) can be used whenever the input quantity and the impulse response are transformable—that is, whenever their insertion in Eq. (15) leads to a convergent integral. Since the complex variable, s, includes a finite, real part that may be made large, a divergent input quantity is transformable provided it is of exponential order. Similar restrictions are placed on the transformation of the unit impulse response. As a consequence, the response of any stable or unstable component having linear performance equations with constant coefficients can be determined from Eq. (16).

The relationship of the performance function to the unit impulse can be established by the convolution integral of Eq. (13). Because this integral is developed for general input functions, it is valid for the complex exponential input of Eq. (5). The transient response to a periodic input of this type is of little importance and is not taken into account in the original definition of the performance function. The steady-state response to the complex exponential input is:

$$q_{(out)}(t) = \int_0^\infty q_{(in)a}\,e^{j[\omega(t-\tau)+(PA)_{(in)}]} \times [UIR](\tau)]_{(\ )(q_{in}q_{out})}d\tau$$

$$= q_{(in)a}e^{j[\omega t+(PA)_{(in)}]}\int_0^\infty e^{-j\omega t} \times [(UIR)(t)]_{(\ )(q_{in}q_{out})}\,dt \quad (17)$$

A comparison of Eqs. (8), (15), and (16) shows that

$$(PF)_{(\ )(q_{in}q_{out})} = [LT][UIR]_{(\ )(q_{in}q_{out})}\,|_{\,s=j\omega} = \frac{[LT][q_{(out)}(t)]}{[LT][q_{(in)}(t)]}\bigg|_{s=j\omega} \quad (18)$$

When a mathematical expression for the unit impulse response exists, the performance function can be determined from its transform by substituting $j\omega$ for the complex variable, s, as indicated in Eq. (18).

However, it is usually possible to short-cut the LaPlace Transform when the performance function is evaluated experimentally. For the case of physically realizable components, the output quantity is zero prior to $t = 0$, when the pulse occurs at some positive time. Hence, the lower limit of integration implied by Eq. (18) may be replaced by $-\infty$ instead of zero without loss of generality. Then, since the condition $s = j\omega$ is required,

$$(PF)_{(\ )(q_{in}q_{out})} = \frac{\int_{-\infty}^{\infty} q_{(out)}(t)e^{-j\omega t}dt}{\int_{-\infty}^{\infty} q_{(in)}(t)e^{-j\omega t}dt} = \frac{[FT][q_{(out)}(t)]}{[FT][q_{(in)}(t)]} \quad (19)$$

This equation shows that the performance function equals the ratio of the Fourier Transform of the output quantity to the Fourier Transform of the input quantity. Eq. (19) may be used to obtain values for the performance function at any angular frequency, ω, provided the integrals contained in the equation are convergent.

The performance function carries the dimensions of the input and the output quantities. It is convenient

to define a parameter, independent of frequency, which carries these dimensions. This parameter, named the sensitivity $S_{(\ )(q_{in}q_{out})}$, equals the value of the performance function at zero frequency when such a value exists, so that from Eq. (19)

$$S_{(\ )(q_{in}q_{out})} = \int_{-\infty}^{\infty} q_{(out)}(t)\,dt \Big/ \int_{-\infty}^{\infty} q_{(in)}(t)\,dt \quad (20)$$

The sensitivity can be determined from an experimental response record by dividing the area under the output curve by the area under the input curve. The sensitivity equals the ratio of b_0 to a_0, the coefficients contained in Eq. (11).

The sensitivity of certain components may have a value that is inconvenient to use. The sensitivity of the longitudinal response of the airplane is not usually considered for autopilot design because it includes the effect of both the long-period and short-period modes. In such cases, a reference sensitivity $S_{(\ )(q_{in}q_{out})(\text{ref.})}$ is defined which carries the dimensions of the input and the output quantities. The value of the reference sensitivity is selected for maximum convenience.

If the input and output are known as analytical mathematical functions, the performance function may be evaluated by direct application of Eq. (19). However, frequently the input and output are available only as recorded plots on oscillograph paper. The problem, then, is one of approximating these curves so that an evaluation of the performance function can be obtained.

(III) Determination of the Performance Function from Pulse Response Data

In Section (II) the performance function is shown to be the ratio of the Fourier Transforms of the output and input quantities. Special computing machines for taking the exact Fourier Transformer may not be available, in which case methods presented in this and the following part of the paper can be employed. It is felt that, even when special computing machines are accessible, the methods outlined herein may prove more economical and nearly as accurate.

A convenient method of approximating any curve[6] is by the use of a series of pulses occurring at definite time intervals. A useful pulse for this purpose is the unit triangular pulse $[(UT)(t)]$, defined in Fig. 1, which leads directly to approximating any curve by a series of chords of the curve. As shown, the pulse occurs during the interval from $-\Delta\tau$ to $\Delta\tau$ and is zero at all other times. The pulse attains its maximum value at zero time and, consequently, is symmetrical about the origin. Its height is unity, and therefore the value of the pulse at any time is nondimensional.

Shown in Fig. 1 with the unit triangular pulse is a similar but more general type called simply a triangular pulse $[(T)(t)]$. Like the former, it has a time duration of $2\Delta\tau$ and is symmetrical about the origin. Unlike the unit triangular pulse, its height, T_a, is not fixed but can

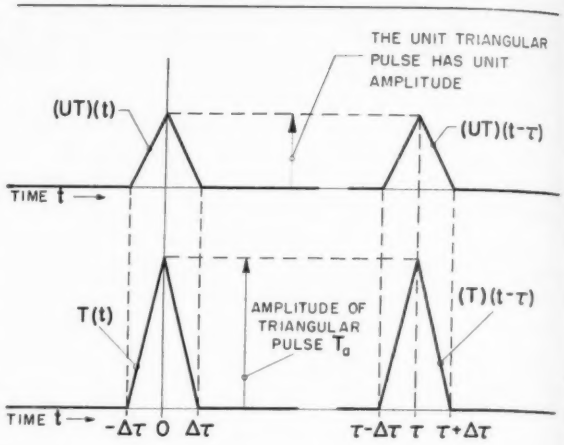

Fig. 1. Definition of unit triangular pulse and general triangular pulse.

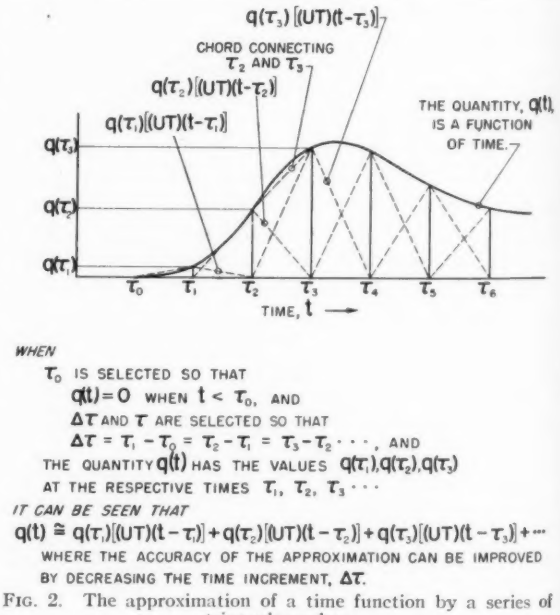
q(τ3)[(UT)(t-τ3)]
CHORD CONNECTING τ2 AND τ3
q(τ2)[(UT)(t-τ2)]
q(τ1)[(UT)(t-τ1)]
THE QUANTITY, q(t), IS A FUNCTION OF TIME.
q(τ3)
q(τ2)
q(τ1)
τ0 τ1 τ2 τ3 τ4 τ5 τ6
TIME, t
WHEN
τ0 IS SELECTED SO THAT
q(t) = 0 WHEN t < τ0, AND
Δτ AND τ ARE SELECTED SO THAT
Δτ = τ1 − τ0 = τ2 − τ1 = τ3 − τ2 · · · , AND
THE QUANTITY q(t) HAS THE VALUES q(τ1), q(τ2), q(τ3)
AT THE RESPECTIVE TIMES τ1, τ2, τ3 · · ·
IT CAN BE SEEN THAT
q(t) ≅ q(τ1)[(UT)(t − τ1)] + q(τ2)[(UT)(t − τ2)] + q(τ3)[(UT)(t − τ3)] + · · ·
WHERE THE ACCURACY OF THE APPROXIMATION CAN BE IMPROVED BY DECREASING THE TIME INCREMENT, Δτ.

Fig. 2. The approximation of a time function by a series of triangular pulses.

be selected to give the best possible approximation of a given quantity.

When a triangular pulse occurs not at time zero but at any time, τ, the unit triangular pulse is designated as $[(UT)(t-\tau)]$ and the general triangular pulse is $[(T)(t-\tau)]$. Since the two pulses differ only in height, they are related by the expression

$$[(T)(t-\tau)] = T_a[(UT)(t-\tau)] \quad (21)$$

Fig. 2 shows how the triangular pulse is used to approximate a general quantity $q(t)$ which varies with time. The initial time τ_0 is fixed at a time when the quantity $q(t)$ is zero, and the later instants of time τ_1, τ_2, τ_3 are arrived at by successive increments of the constant time interval $\Delta\tau$. The corresponding values of $q(t)$ are $q(\tau_1)$, $q(\tau_2)$, $q(\tau_3)$. In terms of the corresponding unit triangular pulses, the function $q(t)$ is given at time t by:

$$q(t) = q(\tau_1)[(UT)(t-\tau_1)] + q(\tau_2)[(UT)(t-\tau_2)] + \ldots \quad (22)$$

The sum of two linear functions of some independent variable is itself a linear function of the variable. Hence, for example, the series of triangles in the region between τ_2 and τ_3 is the straight line joining the ordinates $q(\tau_2)$ and $q(\tau_3)$, since one of the linear functions occurring in this interval is zero at τ_2 and the other is zero at τ_3. By applying a similar reasoning to the remaining time intervals, it can be seen that Eq. (22) expresses $q(t)$ as the sum of the successive chords. It is clear that the accuracy of the approximation can be made arbitrarily good by reducing the time duration of the pulse $\Delta\tau$.

Now the approximate Fourier Transform of the function of time can be written as the summation of the Fourier Transform of each of the triangular pulses in the time series. In order to simplify the resulting summation, reference is made to a Fourier Transform theorem. This theorem can be stated as follows: "If the Fourier Transform $F(\omega)$ of a function of time, $f(t)$, exists, then the Fourier Transform of $f(t-\tau)$ is $e^{-j\omega\tau}F(\omega)$." A delay, τ, in the time domain is equivalent to a phase-angle lag in the frequency domain equal to the product of the time delay and the angular frequency. In terms of a unit triangle,

$$[FT][(UT)(t-\tau)] = e^{-j\omega\tau}[FT][(UT)(t)] \quad (23)$$

The series of triangular pulses used to approximate the quantity, $q(t)$, are evenly spaced along the time scale, as shown in Fig. 2. Since the first matching triangle is delayed by $\tau_1 + \Delta\tau$ and the time interval between successive triangles is $\Delta\tau$, the nth triangle is delayed $\tau_0 + n\Delta\tau$ with respect to zero time. Consequently, transformation of Eq. (22), followed by substitution of Eq. (23), yields

$$[FT][q(t)] = \{q(\tau_1)e^{-j\omega\Delta\tau} + q(\tau_2)e^{-j2\omega\Delta\tau} + \ldots + q(\tau_n)e^{-jn\omega\Delta\tau} + \ldots\}e^{-j\omega\tau_0}[FT][(UT)(t)] \quad (24)$$

The exponential terms appearing in the series of Eq. (24) have magnitudes that depend upon the value of the quantity $q(t)$ at τ_1, τ_2, τ_3, etc. The vectors are rotated negatively from the real axis of the complex plane by an angle proportional to the integer, n, the time increment, $\Delta\tau$, and the angular frequency, ω. Although it might appear that any angular frequency can be inserted in Eq. (24), the approximation is not satisfactory when $\omega\Delta\tau$ is in excess of $\pi/2$ rads. If this restriction does not allow a high enough angular frequency, the interval $\Delta\tau$ must be made smaller.

The Fourier Transform of the unit triangle must also be included in Eq. (24) when the complete transform of the quantity is desired. This transformation is discussed in Appendix A, and is plotted as a function of $\omega\Delta\tau$ in Fig. 16. Since the unit triangular pulse, $(UT)(t)$, is symmetrical about the origin, it is an even function, and its transform has zero phase angle.

When Fourier Transforms are used to determine the performance function, it is only necessary to know the transform of the output relative to the input. Thus, when the same τ_0 and $\Delta\tau$ are chosen for each quantity, the combination of Eqs. (19) and (24) gives

$$(PF)_{(\ )(q_{in}q_{out})} = \left.\frac{\sum q_{out}(\tau_n)e^{-jn\omega\Delta\tau}}{\sum q_{in}(\tau_n)e^{-jn\omega\Delta\tau}}\right|_{n=1,2,3,\ldots} \quad (25)$$

The summations of Eq. (25) can be effected either (1) by direct graphical addition of the complex quantities or (2) by resolving the complex quantities into their real and imaginary parts before carrying out the addition.* A Fourier synthesizer based on method (2) has been built for this purpose. The synthesizer consists of electromagnetic resolvers, the rotors of which are geared in the ratio 1:2:3: ..... Potentiometers are used to introduce the correct amplitudes, and the outputs are summed electrically and recorded. The details of the synthesizer are given in Appendix B.

An example is included to illustrate the direct graphical addition of the complex quantities. A critically damped, second-order system is selected for this purpose. A critically damped system has a damping ratio, DR (ratio of actual damping to that required for critical damping), of 1. One other parameter is needed to define the dynamic characteristics of the second-order system. The undamped natural frequency, ω_n, is a convenient parameter to use. The undamped natural frequency is the frequency at which the system would oscillate in radians per unit time if, after removing its damping, the system were excited by an impulse. For this example, the undamped natural frequency is $\pi/10$ rad. per sec.

The response of this second-order system to a unit triangle is shown in Fig. 3. The time duration of the pulse is 2 sec., and the resulting response returns to equilibrium in about 25 sec. The maximum excursion of the response is only 11.4 per cent of the input, but, because the static sensitivity of this system is unity, the time integrals of the input and the output are equal.

The determination of the performance function by graphical summation is shown in Fig. 4. Values for the addition are obtained from Fig. 3 using a time interval, $\Delta\tau$, of 1 sec. Consequently, the input and output ordinates used in Eq. (25), are the values of these quantities at 1, 2, 3, . . . sec. However, since the input quantity is zero at 2 sec. and all subsequent times, Eq. (25) reduces in this example to:

* This latter method is well adapted to computing machine operations since the functions $\cos(n\omega\Delta\tau)$ and $\sin(n\omega\Delta\tau)$ may be tabulated on card files.

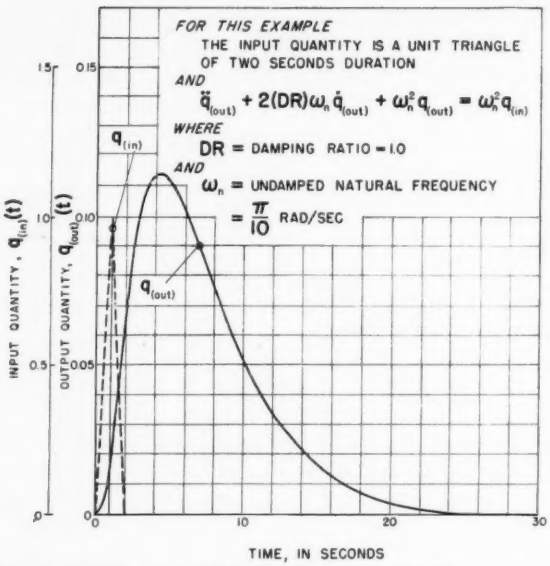

FIG. 3. Response of a critically damped second-order system to a triangular pulse.

$$(PF)_{(\ )(q_{in}q_{out})} = e^{j\omega\Delta\tau} \sum_{n=1}^{n=25} q_{(out)(\tau_n)}\, e^{-jn\omega\Delta\tau}$$

The upper limit of the summation is the 25th ordinate in as much as the pulse response returns to zero in 25 sec.

The evaluation of the performance function is shown for a frequency of seven-tenths of the undamped natural frequency. Consequently, each consecutive term in the summation is rotated 0.07π rad. or 12.6° with respect to its preceding term. The angular orientation of the terms up to and including the 25th are laid off on the rose of Fig. 4. The values of the output quantity at the times τ_n are read directly from the curve of Fig. 3. It can be seen that the summation has a magnitude of 0.67 and a phase lag of 82.6°, so that

$$(PF)_{(\ )(q_{in}q_{out})} = e^{j12.6}\,[0.67\, e^{-j82.6°}] = 0.67\, e^{-j70°}$$

Hence, at a frequency of seven-tenths of the undamped natural frequency, the amplitude ratio of a critically damped second order system is 0.67 and the phase angle is −70° (the minus sign indicating a lag).

Nondimensional plots of the amplitude ratio and the phase angle of a second-order system are presented in Fig. 14. The frequency is expressed nondimensionally as the ratio of the forced frequency, ω, and the natural frequency of the system, ω_n, making

$$FR = \text{frequency ratio} = \omega/\omega_n \qquad (26)$$

It can be seen that the result of the graphical summation of Fig. 4 agrees with the generalized performance function data of Fig. 14.

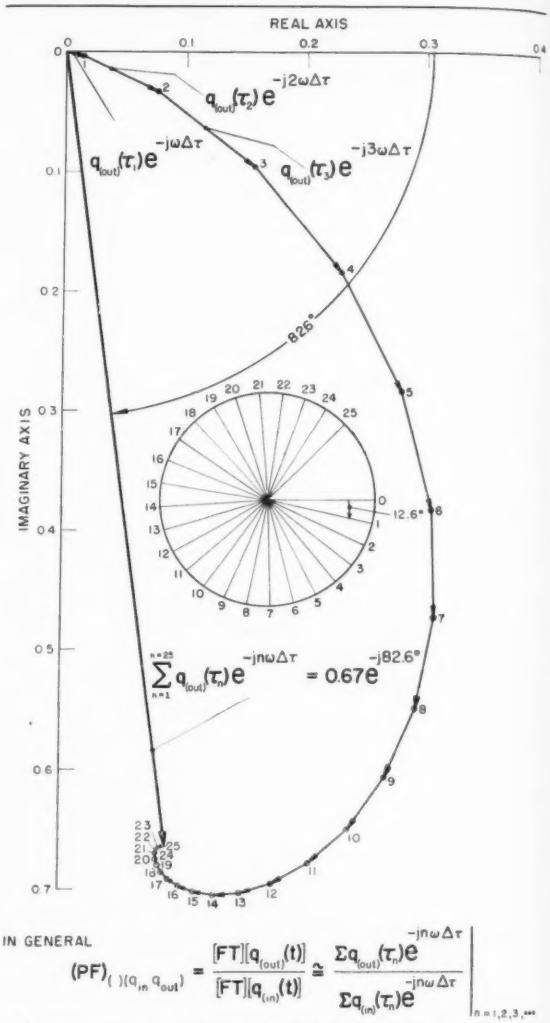

IN GENERAL

$$(PF)_{(\ )(q_{in}q_{out})} = \frac{[FT][q_{(out)}(t)]}{[FT][q_{(in)}(t)]} \cong \left.\frac{\Sigma q_{(out)}(\tau_n)e^{-jn\omega\Delta\tau}}{\Sigma q_{(in)}(\tau_n)e^{-jn\omega\Delta\tau}}\right|_{n=1,2,3,\cdots}$$

VALUES FOR SUMMATION OBTAINED FROM FIG. -3

WITH $\Delta\tau = 1$ SECOND

SO THAT $\tau_1, \tau_2, \tau_3, \cdots$ ARE THE VALUES OF TIME AT 1,2,3, ··· SECONDS RESPECTIVELY

FOR THIS EXAMPLE

$\omega = 0.7\omega_n$

AND $\omega\Delta\tau = 0.07\pi = 12.6$ DEGREES

ALSO

$q_{(in)}(\tau_1) = 1\ ;\ q_{(in)}(\tau_2) = q_{(in)}(\tau_3) = \cdots = 0$

HENCE

$$(PF)_{(\ )(q_{in}q_{out})} = e^{j\omega\Delta\tau} \sum_{n=1}^{n=25} q_{(out)}(\tau_n)\, e^{-jn\omega\Delta\tau}$$

$$= e^{j12.6°}\left[0.67\, e^{-j82.6°}\right] = 0.67\, e^{-j70°}$$

FIG. 4. Determination of the performance function by graphical summation.

(IV) Extension of the Pulse Method to Lightly Damped System

The approximate method for determining the performance function outlined in Section (III) is suited to components having a well damped or slightly oscillatory response. Direct application of this method to a component having a markedly oscillatory response becomes prohibitively tedious, inasmuch as many terms are required before the series of Eq. (25) converges. An ex-

ample of this type is the lateral response of an airplane that has an oscillatory mode often referred to as "Dutch Roll." When a highly oscillatory mode occurs, its period of oscillation and rate of decay can usually be measured directly. Hence, an equation for the oscillatory mode $q_{(\text{out})(\text{osc.})}(t)$ can be written from which the Fourier Transform can be obtained directly. The remaining portion of the response $q_{(\text{out})(\text{rem.})}(t)$ can be transformed by the approximate method previously demonstrated. The validity of this procedure is implicit in the assumption that the performance of the component can be represented by a linear differential equation, so that

$$q_{(\text{out})}(t) = q_{(\text{out})(\text{osc.})}(t) + q_{(\text{out})(\text{rem.})}(t) \tag{27}$$

and, from Eq. (19),

$$(PF)_{(\ )(q_{\text{in}}q_{\text{out}})} = \frac{[FT][q_{(\text{out})(\text{osc.})}(t)]}{[FT][q_{(\text{in})}(t)]} + \frac{[FT][q_{(\text{out})(\text{rem.})}(t)]}{[FT][q_{(\text{in})}(t)]} \tag{28}$$

During the time interval in which the input pulse is applied, the system has a forced response and a transient response. However, the instant the input returns to zero, the output is a transient that is completely dependent upon the characteristics of the system. The transient is the sum of exponentials of the form e^{rt}, where r is a root of the system characteristic equation. When any of the roots have positive real parts, the system is divergent and unstable; when all roots have negative real parts, the transient is stable; when roots with imaginary parts exist, they appear in conjugate pairs. Such a pair of exponentials gives an oscillatory mode, which can be written for $t > 0$

$$q_{(\text{out})(\text{osc.})}(t) = \left\{q_{(\text{out})(\text{osc.})a}\, e^{-(DR)\omega_n t}\right\} \times \sin\left\{\omega_n\sqrt{1-(DR)^2}\,t + (PA)_{(\text{osc.})}\right\} \tag{29}$$

It can be seen that the real part of the roots leading to the oscillatory mode of Eq. (29) is equal to $-(DR)\omega_n$ and the imaginary parts are $\pm\omega_n\sqrt{1-(DR)^2}$. The damping ratio DR and the angular undamped natural frequency ω_n are convenient parameters even though the system is third-order or higher. By using these parameters, nondimensional plots originally intended for second-order systems can be utilized directly.

One such plot permits the damping ratio to be found for a particular transient. The heights of successive peaks are measured, and the transient peak ratios can be determined. When the mth peak is compared with a reference peak, m_r, the transient peak ratio, $[(TP)R]$, according to Eq. (29), is

$$[(TP)R] = e^{-(m-m_r)[\pi(DR)/\sqrt{1-(DR)^2}]} \tag{30}$$

Consequently, the ratio is independent of the natural frequency, depending only upon the damping ratio and the difference in the order of the peaks, $m - m_r$ ($m - m_r = 1$ for adjacent peaks). The curves of Fig. 5, which are based on Eq. (30), are useful when evaluating the damping ratio.

The discussion of the previous paragraph presupposes a datum from which the peak heights can be ascertained. With a second-order system, the datum is the final steady-state response, but with a higher-order system, it must be estimated. For example, the datum shown in Fig. 6 is the average of the upper and lower envelopes of the oscillatory mode. Since the ratio of the heights of adjacent peaks is 0.85, the damping ratio in this case is 0.05.

The undamped natural frequency is calculated from the damping ratio and the measured period of oscillation, $T_{(\text{osc.})}$. A sinusoid repeats every 2π rad.; hence, from Eq. (29),

$$\omega_n = 2\pi/T_{(\text{osc.})}\sqrt{1-(DR)^2} \tag{31}$$

In the example of Fig. 6, the period is 8 sec., so that the undamped natural frequency becomes 0.78 rad. per sec.

The oscillatory mode is seldom zero initially (when $t = 0$), especially since the actuating pulse is of finite duration. For this reason, the phase angle of the oscillation, $(PA)_{\text{osc.}}$, must be determined so that the time delay is properly taken into account. For example, in the case shown in Fig. 6, the phase angle is 44°, which is equivalent to a time delay of approximately one-eighth of the period of oscillation. Once the damping ratio, natural frequency, and phase angle have been found, the only unknown in Eq. (29) is the amplitude of the oscillation, $q_{(\text{out})(\text{osc.})a}$. The amplitude can be calculated so that Eq. (29) matches the response at any time t and, hence, at every time t.

It is convenient to express the Fourier Transform of the oscillatory mode as a function of the frequency ratio defined in Eq. (26). Then, substitution of Eq. (29) into Eq. (15) with s replaced by $j\omega$ gives

$$[FT][q_{(\text{out})(\text{osc.})}(t) = \left\{\frac{q_{(\text{out})(\text{osc.})a}\sin(PA)_{\text{osc.}}}{\omega_n^2(CT)_{\text{osc.}}}\right\} \times \left\{\frac{1 + j(FR)\omega_n(CT)_{\text{osc.}}}{1-(FR)^2 + j2(FR)(DR)}\right\} \tag{32}$$

where

$(CT)_{\text{osc.}}$ = a characteristic time of the oscillatory mode

$$= \frac{\sin(PA)_{\text{osc.}}}{\omega_n[\sqrt{1-(DR)^2}\cos(PA)_{\text{osc.}} + (DR)\sin(PA)_{\text{osc.}}]} \tag{33}$$

The actual evaluation of the frequency function of Eq. (32) is facilitated by the use of nondimensional plots of the amplitude ratio and phase angle, as given in Figs. 14 and 15.

The performance function equals the sum of the Fourier Transforms of the oscillatory mode and the remainder function, divided by the Fourier Transform of the input quantity, in conformity with Eq. (28). The

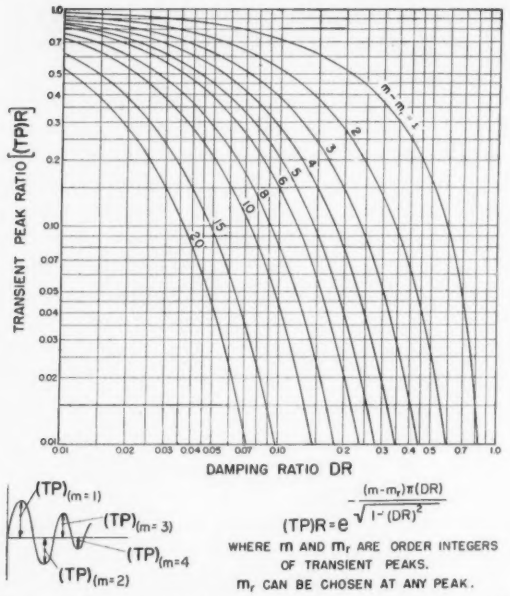

FIG. 5. Diagram showing the relationship of the transient peak ratio to the damping ratio, for the transient solution of a second-order differential equation with constant coefficients.

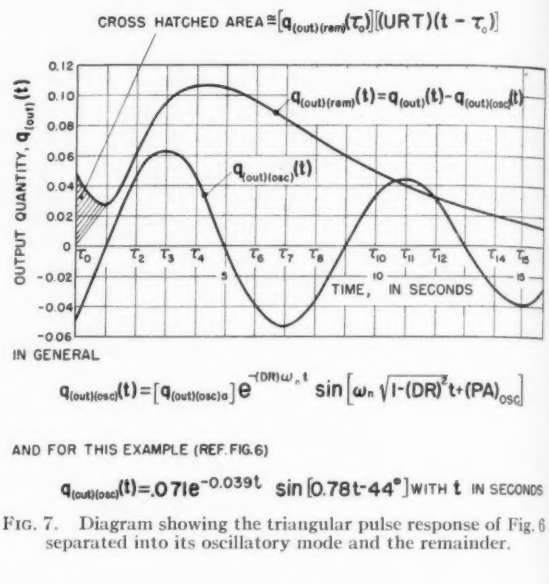
CROSS HATCHED AREA ≅ [q_(out)(rem)(τ_0)][(URT)(t - τ_0)]
OUTPUT QUANTITY, q_(out)(t)
q_(out)(rem)(t) = q_(out)(t) - q_(out)(osc)(t)
q_(out)(osc)(t)
TIME, IN SECONDS
IN GENERAL
q_(out)(osc)(t) = [q_(out)(osc)a] e^(-(DR)ω_n t) sin [ω_n √(1-(DR)^2) t + (PA)_osc]
AND FOR THIS EXAMPLE (REF. FIG. 6)
q_(out)(osc)(t) = .071 e^(-0.039t) sin [0.78t - 44°] WITH t IN SECONDS

FIG. 7. Diagram showing the triangular pulse response of Fig. 6 separated into its oscillatory mode and the remainder.

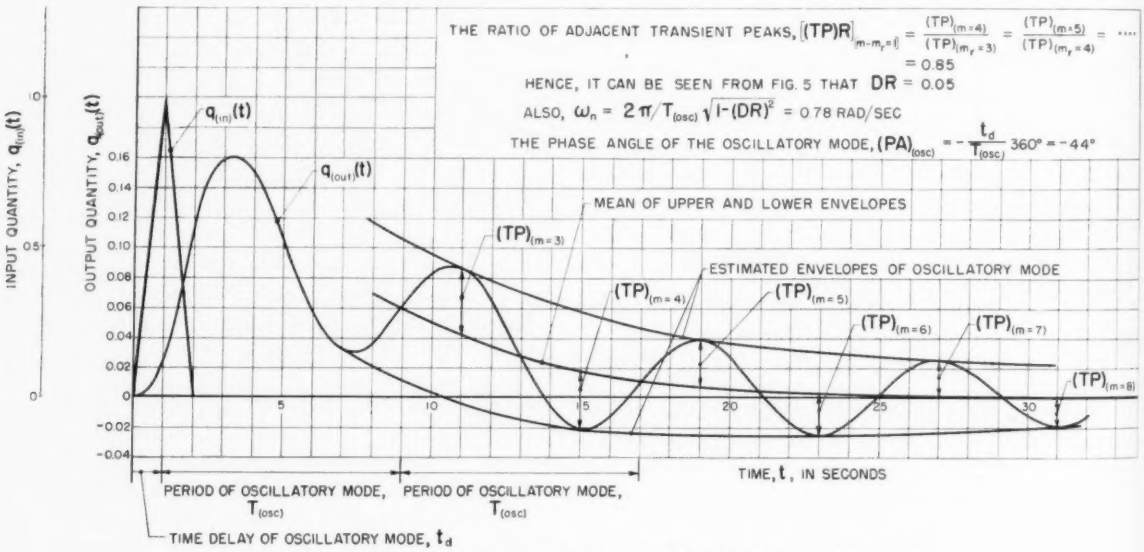
THE RATIO OF ADJACENT TRANSIENT PEAKS, [(TP)R]_(m-m_r=1) = (TP)_(m=4)/(TP)_(m_r=3) = (TP)_(m=5)/(TP)_(m_r=4) = ... = 0.85
HENCE, IT CAN BE SEEN FROM FIG. 5 THAT DR = 0.05
ALSO, ω_n = 2π/T_(osc) √(1-(DR)^2) = 0.78 RAD/SEC
THE PHASE ANGLE OF THE OSCILLATORY MODE, (PA)_(osc) = -(t_d/T_(osc)) 360° = -44°
INPUT QUANTITY, q_(in)(t)
OUTPUT QUANTITY, q_(out)(t)
q_(in)(t)
q_(out)(t)
MEAN OF UPPER AND LOWER ENVELOPES
ESTIMATED ENVELOPES OF OSCILLATORY MODE
(TP)_(m=3)
(TP)_(m=4)
(TP)_(m=5)
(TP)_(m=6)
(TP)_(m=7)
(TP)_(m=8)
TIME, t, IN SECONDS
PERIOD OF OSCILLATORY MODE, T_(osc)
PERIOD OF OSCILLATORY MODE, T_(osc)
TIME DELAY OF OSCILLATORY MODE, t_d

FIG. 6. The triangular pulse response of a system with a highly oscillatory mode.

remainder function, called the output remainder quantity, $q_{(out)(rem.)}(t)$, equals the difference between the total output quantity and the oscillatory mode. Fig. 7 shows the triangular pulse response of Fig. 6 separated into the oscillatory mode and the remainder.

The Fourier Transform of the remainder is obtained by the approximate method of Section (III), excepting in one particular. The remainder is zero prior to time τ_0, but at time τ_0 it has a finite value equal in magnitude but opposite in sign to the oscillatory mode. The resulting instantaneous change in magnitude cannot be matched by a triangular pulse that is isosceles in shape; consequently, a right triangular pulse is required.*

* Experience gained recently on the lateral response indicates that it may be simpler and more accurate to commence the oscillatory mode at a time, t_p, when its value is zero $[q_{(out)(osc.)}(t) = 0]$. Then the right triangle is unnecessary, the phase angle $(PA)_{osc.}$ is eliminated, and the remainder $q_{(out)(rem.)}(t)$ remains equal to the output quantity, $q_{out}(t)$, minus the oscillatory mode for $t > t_p$; but for $t < t_p$, the remainder and the output are equal. A study of techniques for testing lightly damped systems was conducted by Comdrs. Bain, Michaelis, and Wootton and is discussed in their Master's Thesis entitled, "Investigation of Aircraft Lateral Motion Performance Function by Pulse Technique," M.I.T., September, 1949.

The right triangular pulse attains its maximum value instantaneously and then decreases linearly with time, reaching zero after time $\Delta\tau$ has elapsed. Consequently, the right triangular pulse has a duration half that of the regular isosceles triangular pulse described in Section (III). The unit right triangular pulse is shown in Fig. 17 of Appendix A, and the Fourier Transform of the unit right triangular pulse is presented in Fig. 18 of the same Appendix. Since the unit right triangular pulse, $[(URT)(t)]$, is unsymmetrical, its transform includes both an amplitude and a phase angle. The phase angle approaches 90° as the frequency becomes infinitely great.

The shaded part of Fig. 7 is nearly equal to the product of the ordinate, $[q_{(\text{out})(\text{rem.})}(\tau_0)]$, and a unit right triangular pulse. As a result, the total remainder can be expressed

$$q_{(\text{out})(\text{rem.})}(t) = [q_{(\text{out})(\text{rem.})}(\tau_0)][(URT)(t)] + \sum_{n=1,2,\ldots} [q_{(\text{out})(\text{rem.})}(\tau_n)][(UT)(t-\tau_n)] \quad (34)$$

Then, with the input quantity represented as a series of isosceles triangular pulses, substitution of Eqs. (32) and (34) into Eq. (28) gives

$$(PF)_{(\ )(q_{\text{in}}q_{\text{out}})} = \frac{[FT][q_{(\text{out})(\text{osc.})}(t)] + [q_{(\text{out})(\text{rem.})}(\tau_0)][FT][(URT)(t)]}{[FT][(UT)(t)]} \sum_{n=1,2\ldots} q_{(\text{in})}(\tau_n)e^{-jn\omega\Delta\tau} + \left.\frac{\sum[q_{(\text{out})(\text{rem.})}(\tau_n)]e^{-jn\omega\Delta\tau}}{\sum[q_{(\text{in})}(\tau_n)]e^{-jn\omega\Delta\tau}}\right|_{n=1,2,\ldots} \quad (35)$$

Although the complete equation for the performance function appears formidable, the work is reduced to the determination of the constants for the oscillatory mode; the summation of two exponential series; the selection of proper values from Figs. 14, 15, 16, and 18; and the addition of the complex quantities of Eq. (35). This procedure for the example of Figs. 6 and 7 gives the performance function of Fig. 8, represented in terms of amplitude and phase angle. The amplitude and phase angle are shown as functions of the frequency ratio, which is the ratio of the angular frequency to the undamped natural frequency of the oscillatory mode. An amplitude peak occurs when these two frequencies are nearly equal. If a component with the characteristics of this example were included in a closed-loop system, this peak, unless compensated, would tend to make the system unstable.

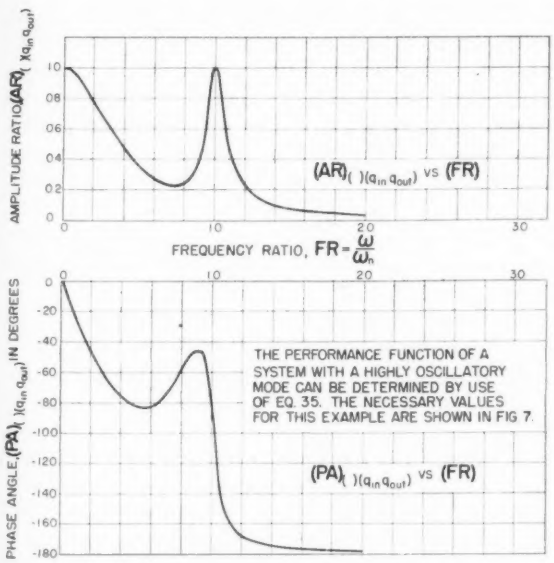
AMPLITUDE RATIO $(AR)_{(\ )(q_{in}q_{out})}$
$(AR)_{(\ )(q_{in}q_{out})}$ VS (FR)
FREQUENCY RATIO, $FR=\frac{\omega}{\omega_n}$
PHASE ANGLE $(PA)_{(\ )(q_{in}q_{out})}$ IN DEGREES
THE PERFORMANCE FUNCTION OF A SYSTEM WITH A HIGHLY OSCILLATORY MODE CAN BE DETERMINED BY USE OF EQ. 35. THE NECESSARY VALUES FOR THIS EXAMPLE ARE SHOWN IN FIG 7.
$(PA)_{(\ )(q_{in}q_{out})}$ VS (FR)

FIG. 8. Performance function obtained from the triangular pulse response of Fig. 6.

Some dynamic systems include a component that is inherently unstable in one of its modes. For example, the characteristic equation of certain aircraft contains a divergence-producing root, and the resulting motion of the aircraft is usually referred to as the "spiral divergence." It might seem that such aircraft could not be included in an automatically controlled system without producing instability. This is not the case; in fact, in certain systems, unstable components and subloops may be intentionally created to produce improved overall system performance.

Since slightly unstable components are not only to be expected, but on occasions to be preferred, adequate methods for determining their performance functions experimentally are required. The performance function is a multiplying factor that relates the output response to a complex exponential input *after steady-state conditions are reached.* However, an unstable operating component never attains steady-state unless the component is imbedded in a stabilizing closed loop. When this is done, the entire loop can be excited, and the resulting input and output of the unstable component can be measured. Flight tests have demonstrated the effectiveness of this technique for steady-state sinusoidal inputs. It is suggested that the pulse inputs might be applied in place of sinusoidal inputs. The artificial stabilization would bring the aircraft back to equilibrium, and, hence, the Fourier Transform of the input and output would exist and the performance function could be evaluated either from Eq. (19) or from the approximate relationship of Eq. (25).

(V) Flight Test

The most attractive features of the pulse method for obtaining airplane performance functions are its economy in equipment, installation time, and required flight time. In all probability the greatest saving is realized by having the human pilot initiate the forcing function. This eliminates an automatic pilot installation, which would be required if the frequency response characteristics were to be obtained directly. Moreover, experience has shown that the flying time can be cut to one-third of that required with direct oscillation of the

control surfaces. As a direct result of the economy in flying time, sufficient flight-test data can readily be obtained to cross-check and resolve any discrepancies that may appear in the test results.

The pulse method is in many ways similar to both the short-period longitudinal test and the lateral rudder-kick test, which are standard flight tests to obtain qualitative information as to the transient response of an aircraft. The principal difference, however, is that the latter tests are normally made for the control-free airplane, whereas the pulse method is used to obtain the control-fixed oscillation about the original equilibrium flight configuration.

In order to ensure oscillation about the original equilibrium condition, an equilibrium control position stop must be provided. Theoretically, this stop alone is sufficient; however, unless a stop is also provided to control the magnitude of the pulse, it is extremely difficult to set the oscillograph sensitivities to give reasonable response traces. The time and funds available for flight test dictate the form of the control surface jig. It may be a simple, double chain arrangement, or a more elaborate mechanism like that shown in Fig. 9. The stop mechanism shown in this figure was designed by C. E. Muzzey, of the Flight Test Section of the M.I.T. Instrumentation Laboratory. The mechanism consists of a removable rack that rides on a sliding rack. The sliding rack is pivoted at the control column and is free to slide (except when constrained as noted below) in a slide pivoted to the air frame. This slide contains a hinged gate When the gate is closed against the slide block, it provides a double stop that limits the control column motion. When the gate is open, the control column is completely free. The purpose of the hinged gate arrangement is to allow the pilot to completely free the airplane so that he can control the long-period oscillation that becomes predominant after the short-period oscillation has subsided.

In making a pulse test, the pilot executes the following simple steps:

(1) He trims the airplane in equilibrium flight at the test speed and pressure altitude.

(2) When equilibrium flight has been obtained, he moves the trim stop into position, taking care not to disturb the equilibrium flight condition as the trim stop is moved into place.

(3) He moves the control rapidly against the opposite stop and returns it to the trim stop in accordance with the pulse duration time desired. Experience has shown that a control pulse of 1° sec. will initiate a reasonable transient response in an airplane of medium size.

(4) He holds the control securely against the trim stop until the oscillation has subsided.

The following variables were recorded during each transient on an oscillograph, shown in Fig. 10: (1) normal acceleration, (2) rate of pitch angle, and (3) elevator position. The measuring system used in this flight test program was largely composed of components

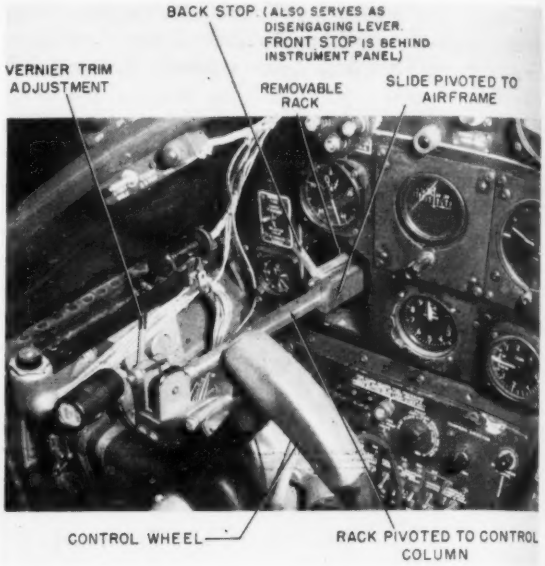
BACK STOP (ALSO SERVES AS DISENGAGING LEVER. FRONT STOP IS BEHIND INSTRUMENT PANEL)
VERNIER TRIM ADJUSTMENT
REMOVABLE RACK
SLIDE PIVOTED TO AIRFRAME
CONTROL WHEEL
RACK PIVOTED TO CONTROL COLUMN

FIG. 9. Photograph of stop mechanism for control column.

previously designed for other applications by the Instrumentation Laboratory of M.I.T.

The normal accelerometer used for measuring the normal acceleration includes a temperature-controlled viscous damper. The damper temperature is regulated by a thermoswitch and is held to close temperature tolerance. For these tests, the damping ratio was 1.0 and the undamped natural frequency 10 cycles per sec. The uncertainty of this accelerometer is ± 0.005 gravity.

The rate-of-pitch indicator is a single degree of freedom gyro computer, which was modified for these tests to obtain a damping ratio of 0.7. The undamped natural frequency of this instrument is 5 cycles per sec.; its uncertainty is ± 1 millirad. per sec.

The elevator displacement is indicated by the electromagnetic type of signal generator called a microsyn. This instrument is a variable-transformer type designed by Dr. R. K. Mueller, of the Instrumentation Laboratory M.I.T., for fire control applications where the angular displacement of a shaft must be measured within $^1/_2$ millirad.

The normal accelerometer and the rate-of-pitch gyro are also furnished with a microsyn signal generator. The output from each of the signal generators was amplified before being recorded. Filters were used on the first flight tests but were found to be unnecessary. The oscillograph record shown in Fig. 11 is unfiltered data.

Both static calibrations and dynamic corrections must be applied to all test results to correct for instrumentation errors. The dynamic corrections can be obtained from direct sinusoidal oscillation of the instrument in the laboratory. The frequency response characteristics are more conveniently determined after installation by applying either a step function or pulse to the instrument, by recording the transient response, and by com-

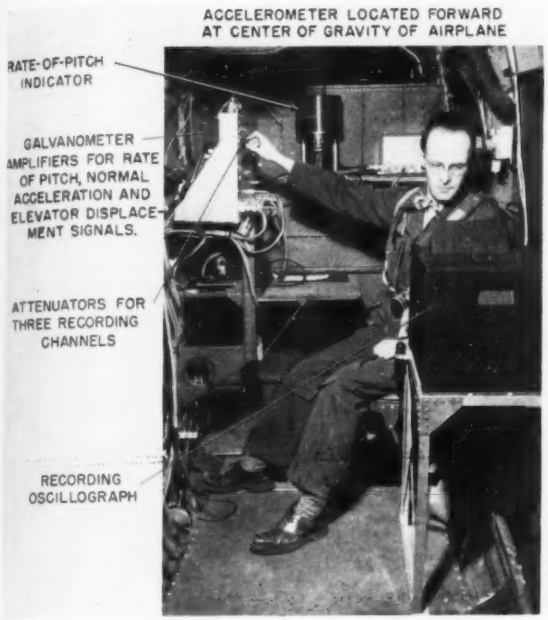
ACCELEROMETER LOCATED FORWARD AT CENTER OF GRAVITY OF AIRPLANE
RATE-OF-PITCH INDICATOR
GALVANOMETER AMPLIFIERS FOR RATE OF PITCH, NORMAL ACCELERATION AND ELEVATOR DISPLACEMENT SIGNALS.
ATTENUATORS FOR THREE RECORDING CHANNELS
RECORDING OSCILLOGRAPH

FIG. 10. Photograph of flight-test instrumentation located in aft compartment.

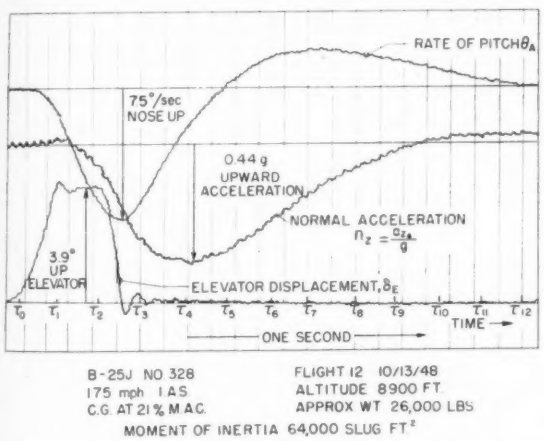
RATE OF PITCH θ_A
75°/sec NOSE UP
0.44 g UPWARD ACCELERATION
NORMAL ACCELERATION $n_z = \frac{a_{z_A}}{g}$
3.9° UP ELEVATOR
ELEVATOR DISPLACEMENT, δ_E
t_0 t_1 t_2 t_3 t_4 t_5 t_6 t_7 t_8 t_9 t_{10} t_{11} t_{12}
TIME
ONE SECOND
B-25J NO 328
175 mph IAS
C.G. AT 21% M.A.C.
FLIGHT 12 10/13/48
ALTITUDE 8900 FT.
APPROX WT 26,000 LBS
MOMENT OF INERTIA 64,000 SLUG FT²

FIG. 11. Oscillograph record showing rate of pitch and normal acceleration response of an aircraft to an applied elevator pulse displacement.

puting the frequency response. The means for providing a sinusoidal input are not readily available, whereas a pulse or step function can be easily applied.

Static calibrations of the measuring system caused more difficulty than the dynamic calibrations. Experience gained in this flight-test program has shown that the only way to be certain of static calibrations is to use frequent in-flight calibrations. In this manner any drift or change in the sensitivity of a channel is determined, and the proper corrections can be applied to the measured data.

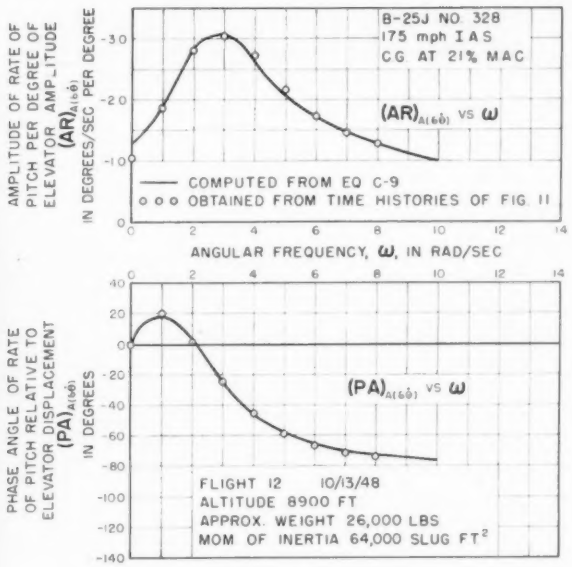
AMPLITUDE OF RATE OF PITCH PER DEGREE OF ELEVATOR AMPLITUDE $(AR)_{A(\delta\dot{\theta})}$ IN DEGREES/SEC PER DEGREE
B-25J NO 328
175 mph IAS
CG AT 21% MAC
$(AR)_{A(\delta\dot{\theta})}$ vs ω
COMPUTED FROM EQ C-9
o o o OBTAINED FROM TIME HISTORIES OF FIG. 11
ANGULAR FREQUENCY, ω, IN RAD/SEC
PHASE ANGLE OF RATE OF PITCH RELATIVE TO ELEVATOR DISPLACEMENT $(PA)_{A(\delta\dot{\theta})}$ IN DEGREES
$(PA)_{A(\delta\dot{\theta})}$ vs ω
FLIGHT 12 10/13/48
ALTITUDE 8900 FT
APPROX. WEIGHT 26,000 LBS
MOM OF INERTIA 64,000 SLUG FT²

FIG. 12. Comparison of rate of pitch performance function of airplane obtained from elevator pulse displacement with performance function obtained from theoretical considerations.

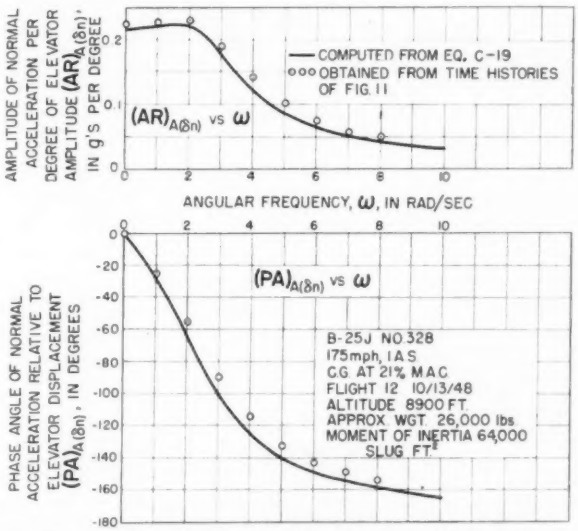
AMPLITUDE OF NORMAL ACCELERATION PER DEGREE OF ELEVATOR AMPLITUDE $(AR)_{A(\delta n)}$, IN g'S PER DEGREE
COMPUTED FROM EQ. C-19
o o o OBTAINED FROM TIME HISTORIES OF FIG. 11
$(AR)_{A(\delta n)}$ vs ω
ANGULAR FREQUENCY, ω, IN RAD/SEC
PHASE ANGLE OF NORMAL ACCELERATION RELATIVE TO ELEVATOR DISPLACEMENT $(PA)_{A(\delta n)}$, IN DEGREES
$(PA)_{A(\delta n)}$ vs ω
B-25J NO 328
175mph, IAS
C.G. AT 21% M.A.C.
FLIGHT 12 10/13/48
ALTITUDE 8900 FT.
APPROX WGT 26,000 lbs
MOMENT OF INERTIA 64,000 SLUG FT²

FIG. 13. Comparison of normal acceleration performance functions of airplane obtained from elevation pulse displacement with performance function obtained from theoretical considerations.

(VI) Correlation of Aircraft Performance Functions Obtained Experimentally and Theoretically

Correlation of the results obtained by pulse data with possible results obtained by direct sinusoidal oscillations of the elevator was not attempted because the automatic pilot installation and subsequent flying would have extended the program beyond reasonable limits. In place of direct sinusoidal oscillation data, it was decided to use the theoretical performance equation of the airplane and, as far as possible, use only static flight-test data in determining the stability derivatives.

The theoretical performance functions[8] required for this discussion are derived in Appendix C. Eq. (C-9) for rate-of-pitch response and Eq. (C-19) for normal acceleration response are reproduced here:

$$(PF)_{A(\delta\ddot{\theta})} = S_{A(\delta\ddot{\theta})(\text{ref.})} \frac{1 + j(FR)\omega_n(CT)_{A(\delta\ddot{\theta})}}{1-(FR)^2 + j2(DR)(FR)} \quad \text{(C-9)}$$

$$(PF)_{A(\delta n)} = S_{E(\delta n)} + S_{A(\delta n)(\text{rem.})} \times \frac{1 + j(FR)\omega_n(CT)_{A(\delta n)}}{1 - (FR)^2 + j2(DR)(FR)} \quad \text{(C-19)}$$

When written in this manner, the frequency-variant portions of the performance functions have a characteristic numerator and denominator. Consequently, separate nondimensional curves can be plotted of each function and the curves used to compute the aircraft performance functions. These nondimensional curves are presented in Figs. 14 and 15. To use the curves, the characteristic parameters ω_n, $(CT)_{A(\ )}$, and (DR) must be calculated from the stability derivatives according to their equations given in Appendix C. The numerator is then evaluated as a function of the parameter $\omega_n(CT)_{A(\ )}$; the denominator, as a function of the damping ratio (DR). The aircraft performance function is then found by a straight algebraic process involving complex numbers. These nondimensional curves are extremely useful to determine quickly the effects of changes in the center of gravity, air speed, and altitude upon the dynamic performance of the airplane. The smooth curves of Figs. 12 and 13 were calculated from these equations for the values of the stability derviatives given in Appendix C.

The normal acceleration performance function [Eq. (C-19)] is especially interesting because it contains a separate sensitivity, $S_{E(\delta n)}$. The inverse transform of this sensitivity gives an impulse in the time domain. However, the inverse transform of the product of this sensitivity and the direct transform of a finite pulse are equal to the pulse in the time domain scaled by this sensitivity. Therefore, the system response to a finite pulse will include a similar finite pulse occurring at the same time as the input pulse. Hence, one would expect to find a "pip" in the normal acceleration response. This has been observed experimentally. Although Fig. 11 shows only a small initial negative bulge in the normal acceleration response, similar records for shorter pulse time durations have exhibited sharp "pips." Physically, this "pip" has a simple explanation: In order to rotate the wing so as to achieve an increased angle of attack, it is necessary for the tail to be depressed by the elevator. The first effect of this action is to decrease the total lift of the airplane because of the loss of lift on the tail. From Eqs. (C-19) and (C-20) it can be seen that the area of this "pip" is directly proportional to Z_δ and, hence, represents the loss of total lift on the airplane caused by the elevator deflection.

The experimental data points plotted on Figs. 12 and 13 were computed from Fig. 11 and corrected for instru-

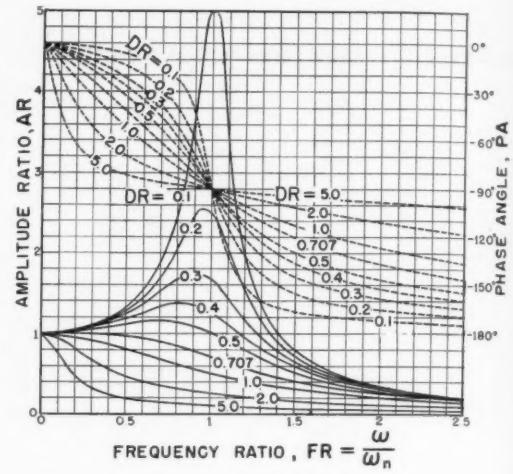

FIG. 14. Relationship between the performance function, $1/[1 - (FR)^2 + j\,2(DR)(FR)]$, and the frequency ratio.

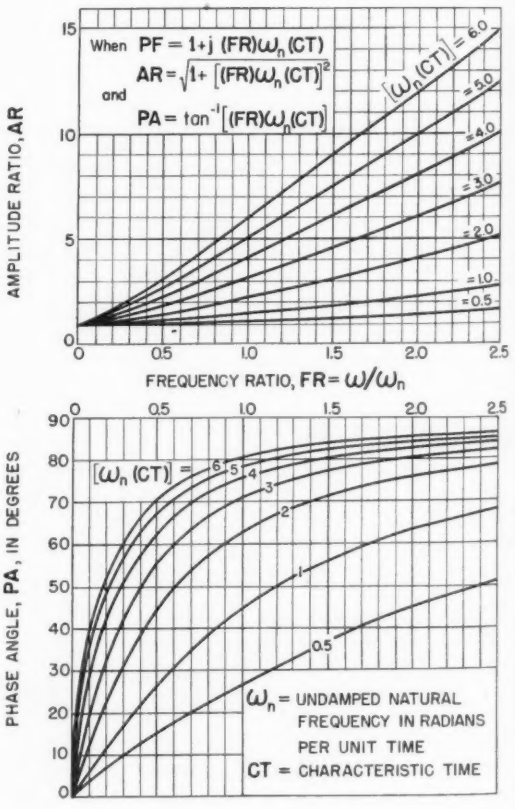

FIG. 15. Relationship between the performance function, $[1 + j(FR)\omega_n(CT)]$, and the frequency ratio.

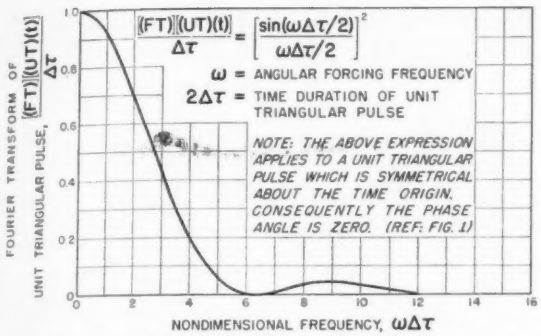
$\frac{(FT)(UT)(t)}{\Delta\tau} = \left[\frac{\sin(\omega\Delta\tau/2)}{\omega\Delta\tau/2}\right]^2$
ω = ANGULAR FORCING FREQUENCY
2Δτ = TIME DURATION OF UNIT TRIANGULAR PULSE
NOTE: THE ABOVE EXPRESSION APPLIES TO A UNIT TRIANGULAR PULSE WHICH IS SYMMETRICAL ABOUT THE TIME ORIGIN. CONSEQUENTLY THE PHASE ANGLE IS ZERO. (REF: FIG. 1)
FOURIER TRANSFORM OF UNIT TRIANGULAR PULSE, $\frac{(FT)(UT)(t)}{\Delta\tau}$
NONDIMENSIONAL FREQUENCY, ωΔτ

FIG. 16. Fourier transform of unit triangular pulse which is symmetrical about the time origin.

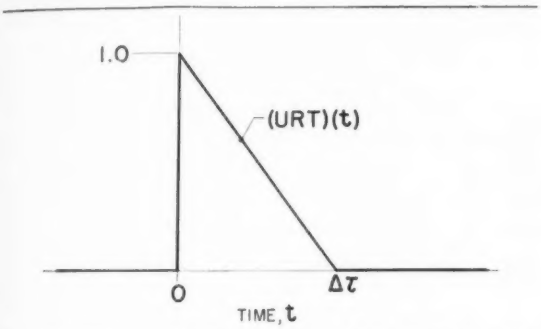

FIG. 17. Diagram defining the unit right triangular pulse.

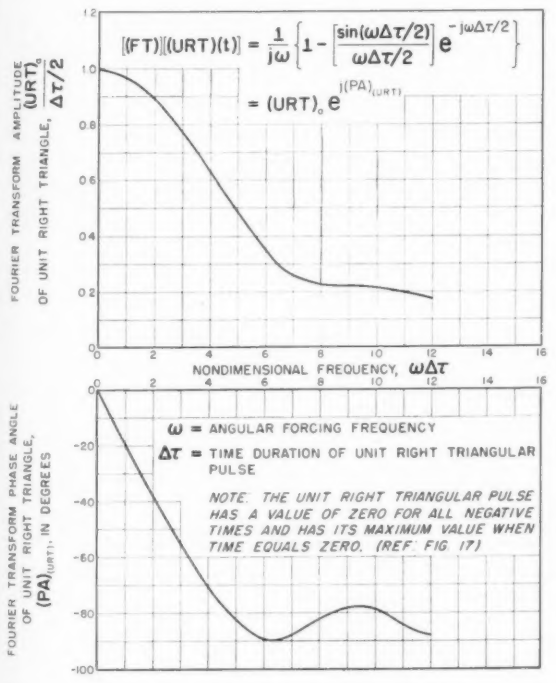
$[(FT)][(URT)(t)] = \frac{1}{j\omega}\left\{1 - \left[\frac{\sin(\omega\Delta\tau/2)}{\omega\Delta\tau/2}\right] e^{-j\omega\Delta\tau/2}\right\}$
$= (URT)_o e^{j(PA)_{(URT)}}$
FOURIER TRANSFORM AMPLITUDE OF UNIT RIGHT TRIANGLE, $\frac{(URT)_o}{\Delta\tau/2}$
NONDIMENSIONAL FREQUENCY, ωΔτ
ω = ANGULAR FORCING FREQUENCY
Δτ = TIME DURATION OF UNIT RIGHT TRIANGULAR PULSE
NOTE: THE UNIT RIGHT TRIANGULAR PULSE HAS A VALUE OF ZERO FOR ALL NEGATIVE TIMES AND HAS ITS MAXIMUM VALUE WHEN TIME EQUALS ZERO. (REF: FIG. 17)
FOURIER TRANSFORM PHASE ANGLE OF UNIT RIGHT TRIANGLE, $(PA)_{(URT)}$, IN DEGREES

FIG. 18. Fourier transform of unit right triangular pulse in terms of amplitude and phase angle.

ment errors. The performance functions were reduced by the Fourier Analyzer described in Appendix B and were checked by the graphical method described in Section (III).

The degree of correlation between the experimental points and the smooth curves should not be interpreted as a measure of the accuracy of predicting the airplane performance functions from theoretical equations. The major drawback to calculating the performance function is that, in general, the aerodynamic parameters will not be known accurately enough to give good results and the equations themselves will have to be extended to account for aeroelastic and Mach Number effects. However, where the performance functions have already been determined experimentally for a number of flight configurations, fitted stability derivatives can be used to interpolate the flight-test configurations.

CONCLUSIONS

(1) The pulse technique of determining airplane performance functions is a feasible flight-test method.

(2) The use of the pulse method for determining the airplane performance functions will save in equipment, installation time, and required flying time.

(3) The instrumentation as used in the flight-test program has low enough uncertainty levels and sufficient sensitivity to determine the performance variables to the degree of accuracy required for dynamic analysis.

(4) The airplane theoretical performance equations are especially useful when interpolating dynamic flight-test data.

(5) The Fourier Synthesizer and Analyzer has a definite advantage over any of the conventional harmonic analyzers for two reasons: (a) Transforms can be made directly from oscillograph records, and, hence, data need not be plotted to any special scale; (b) the transforms are obtained as continuous functions of frequency instead of selected frequency points.

(6) The approximation of a time function by a series of short chords will give accurate transforms at low frequencies and can be extended to any frequency desired by decreasing the time increment $\Delta\tau$.

APPENDIX A—FOURIER TRANSFORM OF UNIT TRIANGULAR PULSES

In Section (IV), a method is described for approximating the Fourier Transform of a response that has a lightly damped oscillatory mode. This method requires the Fourier Transform of the unit triangular pulse and the unit right triangular pulse. It is convenient to have the Fourier Transforms[9] of the unit triangular pulse and the unit right triangular pulse available in curve form so that their values need not be computed for the frequencies of interest. These curves and a brief explanation of their derivation are presented in this appendix.

The unit triangular pulse is symmetrical about the time origin and has a time duration $2\Delta\tau$, so that, prior to time $-\Delta\tau$ and after time $\Delta\tau$, its magnitude is zero. According to the definition of the unit triangular pulse as described in this appendix and as shown in Fig. 1,

$$\begin{aligned}(UT)(t) &= 0, \quad \text{for } t < -\Delta\tau \\ (UT)(t) &= 1 + (t/\Delta\tau), \quad \text{for } -\Delta\tau < t < 0 \\ (UT)(t) &= 1 - (t/\Delta\tau), \quad \text{for } 0 < t < \Delta\tau \\ (UT)(t) &= 0, \quad \text{for } \Delta\tau < t\end{aligned}$$

The use of these conditions for the unit triangular pulse permits its Fourier Transform to be expressed as

$$[FT][(UT)(t)] = \int_{-\infty}^{\infty} [(UT)(t)]e^{-j\omega t}\,dt = \Delta\tau\left[\frac{\sin\,\omega\,\Delta\tau/2}{\omega\,\Delta\tau/2}\right]^2 \quad \text{(A-1)}$$

Since the unit triangular pulse is an even function, its transform has an amplitude but no phase angle. The amplitude is plotted in Fig. 16 as a function of the nondimensional frequency $\omega\Delta\tau$. The amplitude of the transform has a value of $\Delta\tau$ at zero frequency and is reduced to zero when the nondimensional frequency equals 2π rad. In order to extend the useful range of frequencies, the time increment $\Delta\tau$ can be decreased.

A quantity with an abrupt change in value at the origin cannot be matched by a symmetrical triangular pulse. Consequently, the unit right triangular pulse shown in Fig. 17 is defined. The unit right triangular pulse is zero for all negative times, has a height of unity at the origin, and decreases to zero at $\Delta\tau$. This definition may be stated mathematically:

$$\begin{aligned}(URT)(t) &= 0, \quad \text{for } t < 0 \\ (URT)(t) &= 1 - (t/\Delta\tau), \text{ for } 0 < t < \Delta\tau \\ (URT)(t) &= 0, \quad \text{for } \Delta\tau < t\end{aligned}$$

With the unit right triangular pulse defined in this fashion, its Fourier Transform becomes

$$[FT][(URT)(t)] = \int_{-\infty}^{\infty} [(UT)(t)]e^{-j\omega t}dt = \frac{1}{j\omega}\left\{1 - \left[\frac{\sin\,\omega\Delta\tau/2}{\omega\Delta\tau/2}\right]e^{-j\omega\Delta\tau/2}\right\} \quad \text{(A-2)}$$

The Fourier Transform of Eq. (A-2) contains both a real and an imaginary part. Hence, the transform of the unit right triangular pulse has an amplitude and a phase angle, both of which vary with frequency. Values for the amplitude and phase angle can be obtained from Fig. 18.

Appendix B—The Fourier Synthesizer

The resolution of a series of complex exponentials into the sum of their real and imaginary parts is an operation frequently encountered in the process of transforming either from the time domain to the frequency domain or from the frequency domain to the time domain. When large amounts of data are to be reduced, the need for a specially constructed synthesizer becomes apparent. The Instrumentation Laboratory at M.I.T. has built the electromechanical synthesizer shown in Fig. 19. This unit consists of an assembly of twelve synchros. The rotors of these synchros are geared together either in the ratio 1:2:3 . . . or in the ratio 1:3:5 . . . . The second of these ratios is used exclusively for inverse transformations involving the response of a component to an applied step function. The stator of a synchro can be set in any angular position to account for the phase angle of the complex exponential term it is representing. The output from each synchro is the voltage induced across a stator winding. This voltage is attenuated by means of a Helipot potentiometer to give the desired magnitude of the complex exponential term. The attenuated voltages from the synchros are added electrically. The resulting voltage is amplified, rectified, and impressed on the galvanometer of a Sanborn Recorder. The recorder produces a trace on 2-in. paper.

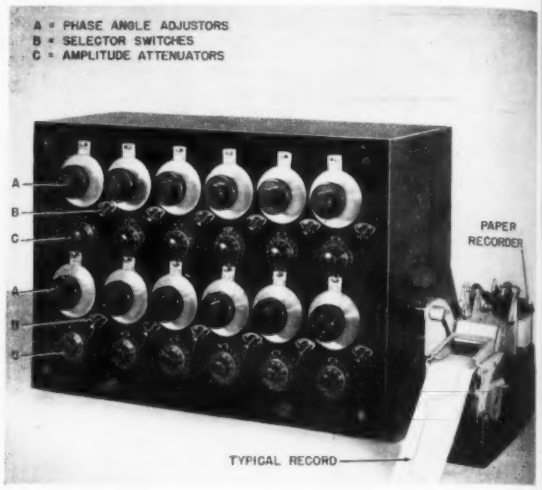

Fig. 19. Photograph of Fourier synthesizer.

The use of the synthesizer for evaluating the series of complex exponentials of Eq. (24) may be described in the following manner: The series of Eq. (24) can be written

$$\begin{aligned}q\text{-series} &= \sum_{n=1,2,3,\ldots} q(\tau_n)e^{-jn\omega\Delta\tau} \\ &= \sum_{n=1,2,3,\ldots} q(\tau_n)\cos n\omega\Delta\tau - j\sum_{n=1,2,3\ldots} q(\tau_n)\sin n\omega\Delta\tau \\ &= R_e\,[q\text{-series}] + jI_m\,[q\text{-series}] \quad \text{(B-1)}\end{aligned}$$

The amplitude and phase angle of the series can be readily determined, since

$$[q\text{-series}] = [q\text{-series}]_a e^{j(PA)_{[q\text{-series}]}} \quad \text{(B-2)}$$

Then

$$[q\text{-series}]_a = \sqrt{\{R_e\,[q\text{-series}]\}^2 + \{I_m[q\text{-series}]\}^2} \quad \text{(B-3)}$$

and

$$(PA)_{[q\text{-series}]} = \tan^{-1}\{I_m[q\text{-series}]/R_e[q\text{-series}]\} \quad \text{(B-4)}$$

The stators of the synchros are oriented so that, with the phase angle setting at zero, the voltage induced across each synchro secondary is proportional to cos Ⓗ, where Ⓗ is the angular position of the rotor. With a gear ratio of 1:2:3 . . . n . . . , the rotor position can be related to the rotor position of the fundamental rotor, Ⓗ, simply as nⒽ$_1$. However, the real part of the nth term of Eq. (B-1) depends upon cos $n\,\omega\Delta\tau$; consequently, the nondimensional frequency, $\omega\Delta\tau$, is equivalent to the angular position of the rotor representing the fundamental complex exponential. Since both the synthesizer and the recorder are driven at constant speed, the timing line of the recording paper can be calibrated in terms of angular frequency, ω. The galvanometer current is proportional to the sum of the cosine voltages, each properly attenuated, and, consequently, the ordinate can be calibrated in terms of $R_e[q\text{-series}]$.

Recalling that sin Ⓗ = −cos (90 + Ⓗ), it is seen that, by simply rotating each stator by 90°, the $I_m[q\text{-series}]$ is obtained. It is anticipated that the synchros will be replaced by magnetic resolvers having secondary windings in space quadrature, so that eventually both the real and imaginary parts can be obtained simultaneously.

Appendix C—Aircraft Longitudinal Response

In this appendix the equations of motion are developed that are used to calculate the theoretical response curves for comparison with the experimentally determined response curves. Since experimental pulse data have been obtained to date primarily for the longitudinal response, only the longitudinal equations are considered. The derivation of the classical linearized equations of motion are not pertinent to this paper and, consequently, are abstracted from Volume V of Durands' *Aerodynamic Theory*. From page 129 of Volume V, the longitudinal equations may be written as:

$$\dot{u} + g\text{Ⓗ} = uX_u + wX_w + \dot{\text{Ⓗ}}X_{\dot{\text{Ⓗ}}} \quad \text{(C-1)}$$

$$\dot{w} - u_0\dot{\text{Ⓗ}} = uZ_u + wZ_w + \delta Z_\delta \quad \text{(C-2)}$$

$$\ddot{\text{Ⓗ}} = uM_u + \dot{w}M_{\dot{w}} + \dot{\text{Ⓗ}}M_{\dot{\text{Ⓗ}}} + wM_w + \delta M_\delta \quad \text{(C-3)}$$

It has been shown by Rea[10] that, for frequencies greater than 0.5 rad. per sec., the variation in air speed is negligible. Hence, the above set of differential equations can be reduced from three to two—i.e., for $u = \dot{u} = 0$,

$$-u_0\,\dot{\text{Ⓗ}} + \dot{w} - wZ_w = \delta Z_\delta \quad \text{(C-4)}$$

$$\ddot{\text{Ⓗ}} - \dot{\text{Ⓗ}}M_{\dot{\text{Ⓗ}}} - \dot{w}M_{\dot{w}} - wM_w = \delta M_\delta \quad \text{(C-5)}$$

When the elevator input displacement is expressed in the complex exponential form, $\delta_e e^{j\omega t}$, the solution of Eqs. (C-4) and (C-5) gives

$$w = (PF)_{A(\delta w)}\delta_e e^{j\omega t} \quad \text{(C-6)}$$

$$\dot{\text{Ⓗ}} = (PF)_{A(\delta\dot{\text{Ⓗ}})}\delta_e e^{j\omega t} \quad \text{(C-7)}$$

where

$$(PF)_{A(\delta w)} = S_{A(\delta w)(\text{ref.})}\frac{1 + j(FR)\omega_n(CT)_{A(\delta w)}}{1 - (FR)^2 + j2(DR)(FR)} = (AR)_{A(\delta w)}e^{j(PA)A(\delta w)} \quad \text{(C-8)}$$

$$(PF)_{A(\delta\dot{\text{Ⓗ}})} = S_{A(\delta\dot{\text{Ⓗ}})(\text{ref.})}\frac{1 + j(FR)\omega_n(CT)_{A(\delta\dot{\text{Ⓗ}})}}{1 - (FR)^2 + j\,2(DR)(FR)} = (AR)_{A(\delta\dot{\text{Ⓗ}})}e^{j(PA)A(\delta\dot{\text{Ⓗ}})} \quad \text{(C-9)}$$

In Eqs. (C-8) and (C-9) it has been found convenient to define the following characteristic parameters:

$$\omega_n = \sqrt{Z_w M_{\dot{\text{Ⓗ}}} - u_0 M_w} \quad \text{(C-10)}$$

$$(DR) = -[M_{\dot{\theta}} + Z_w + u_0 M_{\dot{w}}] \div 2\sqrt{Z_w M_{\dot{\theta}} - u_0 M_w} \quad \text{(C-11)}$$

$$(FR) = \omega/\omega_n \quad \text{(C-12)}$$

$$S_{A(\delta\dot{\text{Ⓗ}})(\text{ref.})} = (Z_\delta M_w - Z_w M_\delta)/(Z_w M_{\dot{\text{Ⓗ}}} - u_0 M_w) \quad \text{(C-13)}$$

$$(CT)_{A(\delta\dot{w})} = (M_\delta + Z_\delta M_{\dot{w}})/(M_w Z_\delta - M_\delta Z_w) \quad \text{(C-14)}$$

$$S_{A(\delta w)(\text{ref.})} = (u_0 M_\delta - M_{\dot{\text{Ⓗ}}} Z_\delta)/(Z_w M_{\dot{\text{Ⓗ}}} - u_0 M_w) \quad \text{(C-15)}$$

$$(CT)_{A(\delta w)} = Z_\delta/(u_0 M_\delta - M_{\dot{\text{Ⓗ}}} Z_\delta) \quad \text{(C-16)}$$

Eq. (C-8), however, involves linear velocity along the Z axis, which is an inconvenient output quantity for experimental measurements. A more convenient quantity to measure in flight is normal acceleration, n_z. Eqs. (C-8) and (C-9) can be combined to give a performance function in terms of normal acceleration, since

$$n_z = (\dot{w} - u_0\dot{\text{Ⓗ}})/g \quad \text{(C-17)}$$

making

$$(PF)_{A(\delta n)} = \frac{(j\omega)}{g}(PF)_{A(\delta w)} - \frac{u_0}{g}(PF)_{A(\delta\dot{\text{Ⓗ}})} \quad \text{(C-18)}$$

After carrying out the indicated operations and simplifying, the performance function can be written

$$(PF)_{A(\delta n)} = S_{E(\delta n)} + S_{A(\delta n)(\text{rem.})}\frac{1 + j(FR)\omega_n(CT)_{A(\delta n)}}{1 - (FR)^2 + j\,2(FR)(DR)} \quad \text{(C-19)}$$

where

$$S_{E(\delta n)} = Z_\delta/g \quad \text{(C-20)}$$

$$S_{A(\delta n)(\text{rem.})} = \frac{Z_w}{g}\left[\frac{u_0 M_\delta - Z_\delta M_{\dot{\theta}}}{Z_w M_{\dot{\theta}} - u_0 M_u}\right] \quad \text{(C-21)}$$

$$CT_{A(\delta n)} = CT_{A(\delta w)} \quad \text{(C-22)}$$

In addition,

$$S_{A(\delta n)(\text{ref.})} = S_{E(\delta n)} + S_{A(\delta n)(\text{rem.})} = (u_0/g)S_{A(\delta\dot{\text{Ⓗ}})(\text{ref.})} \quad \text{(C-23)}$$

Eqs. (C-9) and (C-19) can be used to calculate the aircraft theoretical performance functions. The theoretical response curves in Section (VII) are calculated from these equations using the following numeral data:

Physical Data

$I_y = 64{,}000$ slug ft.^{2} (measured)
$W = 26{,}000$ lbs.
$S_{(\text{wing})} = 610$ ft.^{2} $\qquad S_{(\text{tail})} = 132.5$ ft.^{2}
$C_{(\text{wing})} = 9.67$ ft. $\qquad l_{(\text{tail})} = 25.9$ ft.

Aerodynamic Data (175 m.p.h., 21 per cent M.A.C.)

$\left(\frac{dC_L}{d\alpha}\right)_A = 5.25$ per rad., from flight test
SM = static margin $= -0.15$, from flight test
$\frac{dC_m}{d\alpha} = -0.79$ per radian, from flight test
$\left(\frac{dC_L}{d\alpha}\right)_t \eta_t = 3.9$ per rad., computed
$\frac{d\epsilon}{d\alpha} = 0.4$, computed $\qquad \frac{dC_m}{d\delta_e} = -1.3$ per rad., computed

Computed Stability Derivatives

175 m.p.h., 21 per cent M.A.C., 10,000 ft., Pressure Altitude

$$M_\delta = \left(\frac{dc_m}{d\delta_e}\right)\frac{S_w C_w}{I_y} q = -9.8\ (1/\text{sec.}^2)$$

$$Z_\delta = \left(\frac{dc_m}{d\delta_e}\right)\frac{S_w C_w}{m l_t} q = -30.4\ (\text{ft./sec.}^2)$$

$$M_w = \left(\frac{dc_m}{d\alpha}\right)\frac{S_w C_w}{I_y u_0} q = -0.0192\ (1/\text{ft. sec.})$$

$$Z_w = -\left(\frac{dC_L}{d\alpha}\right)_A \frac{q S_w}{m u_0} = -1.065\ (1/\text{sec.})$$

$$M_{\dot{w}} = -\left(\frac{dC_L}{d\alpha}\right)_t \eta_t \frac{d\epsilon}{d\alpha}\frac{l_t^2 S_t q}{I_y u_0^2} = -0.00176\ (1/\text{ft.})$$

$$M_{\dot{\mathfrak{W}}} = -(1.2)\left(\frac{dC_L}{d\alpha}\right)_t \eta_t \frac{q S_t l_t^2}{I_y u_0} = -1.72\ (1/\text{sec.})$$

Characteristic Parameters for Use in Eqs. (C-9) and (C-19)

$\omega_n = 2.78$ rad./sec. from Eq. (C-10)
$(DR) = 0.6$ from Eq. (C-11)
$S_{A(\delta\dot{\mathfrak{W}})(\text{ref.})} = -1.28 \frac{\text{deg./sec.}}{\text{deg.}}$ from Eq. (C-13)
$(CT)_{A(\delta\dot{\mathfrak{W}})} = 0.995$ sec. from Eq. (C-14)
$S_{E(\delta n)} = -0.0165$ g/deg. from Eq. (C-20)
$S_{A(\delta n)(\text{rem.})} = 0.229$ g/deg. from Eq. (C-21)
$(CT)_{A(\delta n)} = 0.010$ sec. from Eq. (C-22)

REFERENCES

[1] Seamans, R. C., Jr., Bromberg, B. G., and Payne, L. E., *Application of the Performance Operator to Aircraft Automatic Control*, Journal of the Aeronautical Sciences, Vol. 15, No. 9, September, 1948.

[2] Clementson, G. C., *Investigation of the Response of an Aircraft to a Finite Pulse Input*, Thesis for M.S., M.I.T., 1948.

[3] von Kármán, Theodore, and Biot, Maurice A., *Mathematical Methods in Engineering*, p. 403; McGraw-Hill Book Company, Inc., New York, 1940.

[4] Tustin, A., *A Method of Analyzing the Behavior of Linear Systems in Terms of a Time Series*, The Journal of the Institution of Electrical Engineers, Vol. 94, Part IIA, No. 1, 1946.

[5] Gardner, Murray F., and Barnes, John L., *Transients in Linear Systems*, Vol. I; John Wiley & Sons, Inc., New York, 1945.

[6] Brown, G. S., and Campbell, P. P., *Principles of Servomechanism*, Chapt. 11; John Wiley & Sons, Inc., New York, 1948.

[7] Draper, C. S., and Bentley, G. P., *Design Factors Controlling the Dynamic Performance of Instruments*, A.S.M.E. Transactions, July, 1940.

[8] Van Meter, J. T., *The Effect of Various Flight Configurations of an Airplane*, Thesis for M.S., M.I.T., 1948.

[9] Electronic Training Staff of the Cruft Laboratory, Harvard University, *Electronic Circuits and Tubes;* McGraw-Hill Book Company, Inc., New York, 1947.

[10] Rea, James B., *Automatic Tracking Control of Aircraft*, Sc.D. Thesis, M.I.T., 1947.

Changes of Address

Since the Post Office Department does not as a rule forward magazines to forwarding addresses it is important that the Institute be notified of changes in address 30 days in advance of publishing date to ensure receipt of every issue of the JOURNAL and REVIEW.

Notices should be sent directly to:

Institute of the Aeronautical Sciences, Inc.
2 East 64th Street, New York 21, New York

The Theoretical Lateral-Stability Derivatives for Wings at Supersonic Speeds

ARTHUR L. JONES*

Ames Aeronautical Laboratory, N.A.C.A.

SUMMARY

Results available on lateral-stability derivatives for wing plan forms at supersonic speeds are summarized. The effects of aspect ratio and Mach Number are studied primarily, and subsonic values for the derivatives are included in the investigation of the Mach Number effects. Nonlinearities in the sideslip variation of the yawing and rolling moments are considered briefly, and the effects of combining a wing and body are indicated for two of the derivatives.

INTRODUCTION

THE PRIMARY FIELD of application for stability derivatives is the calculation of the motion of an airplane. A stability derivative, expressed in simple terms, is the ratio of the force or moment produced by motion along or around one of the airplane axes to the magnitude of the motion. These derivatives appear as coefficients in the classical set of six linear differential equations derived for the motion of the airplane on the basis of small disturbances. The application of these equations, three of which apply to longitudinal motion and three to lateral motion, to the study of the stability of the airplane motions is generally referred to as dynamic-stability analysis in contrast to the more widely applied static-stability analysis.

In the past 10 or 15 years, dynamic-stability analysis has become more and more popular as a tool for the aircraft designer and the research analyst. The interest in this type of analysis seems to be reaching a new zenith in the design and study of guided missiles. The stepup in speed of aircraft which has occurred in this 10- to 15-year period does not materially affect the classical form of the equations of motion. The increase in speed, however, does have a significant effect on the values for the stability derivatives that appear as the coefficients of these equations. In fact, in the transition from subsonic to supersonic speeds, changes in the sign, as well as the magnitude, of the derivatives occur in some cases.

It is the purpose of this paper to summarize the lateral-stability derivatives that have been calculated for wing plan forms traveling at supersonic speeds. The wings considered have no dihedral or twist. Longitudinal-stability derivatives will not be included in the summary, although a considerable amount of investigation to obtain these derivatives has been carried out. No experimental comparisons will be made, inasmuch as the experimental data that exist on supersonic stability derivatives are classified at the present time. The main objective of the summary will be to study the effects of aspect ratio and of Mach Number on the derivatives. Other results of interest will also be included, and, in view of the fact that this paper is a summary and the results are of paramount interest, only a brief discussion of the methods of calculation will be given.

There are nine lateral-stability derivatives. Rolling, yawing, and sideslip each contribute a side force, a rolling moment, and a yawing moment. For the wing alone, the magnitudes of the three side-force derivatives C_{Y_p}, C_{Y_r}, and C_{Y_β} are extremely small and their contribution to the motion of the airplane is, in general, insignificant. Thus, the only stability derivatives with which we shall be concerned are, in coefficient form:

C_{l_p} = the damping in roll
C_{n_p} = the yawing moment due to rolling
C_{l_r} = the rolling moment due to yawing
C_{n_r} = the damping in yaw
C_{l_β} = the rolling moment due to sideslip, or "the effective dihedral angle"
C_{n_β} = the yawing moment due to sideslip or "the directional stability."

SYMBOLS AND COEFFICIENTS

A = aspect ratio (b^2/S)
b = span of wing measured normal to plane of symmetry
B = $\sqrt{M^2 - 1}$
c_r = chord of wing root
C_l = rolling-moment coefficient (rolling moment/qSb)
C_n = yawing-moment coefficient (yawing moment/qSb)
C_Y = side-force coefficient (side force/qS)
C_{l_p} = $\partial C_l/\partial(pb/2V)$
C_{l_r} = $\partial C_l/\partial(rb/2V)$
C_{l_β} = $\partial C_l/\partial\beta$
C_{n_p} = $\partial C_n/\partial(pb/2V)$
C_{n_r} = $\partial C_n/\partial(rb/2V)$
C_{n_β} = $\partial C_n/\partial\beta$
C_{Y_p} = $\partial C_Y/\partial(pb/2V)$
C_{Y_r} = $\partial C_Y/\partial(rb/2V)$
C_{Y_β} = $\partial C_Y/\partial\beta$
l = overall longitudinal length of sweptback wing
m = slope of right wing tip relative to plane of symmetry (see Fig. 1)
M = free-stream Mach Number
p = rate of roll, rad. per sec.
q = free-stream dynamic pressure

Presented at the Aerodynamics Session, Annual Summer Meeting, I.A.S., Los Angeles, July 21–22, 1949.

* Aeronautical Research Scientist.

r = rate of yaw, rad. per sec.
S = area of wing
V = free-stream velocity
α = angle of attack, rad.
β = sideslip angle (positive when sideslipping to right), deg.

Subscript

w = wing alone

Method of Analysis

Of the theoretical approaches that are available for the analysis of problems in supersonic fluid dynamics, the one that has seen the greatest application in the calculation of supersonic stability derivatives for wing plan forms is the linearized theory of compressible flow as applied to thin airfoils. This is a potential theory, and its application reduces the study of supersonic lifting-surface problems to a process of fitting potential solutions of the well-known wave equation of mathematical physics to the somewhat simplified boundary conditions of thin-airfoil theory. Once the potential solutions corresponding to the boundary conditions are known for a given wing plan form, the pressures acting normal to the plate and the pressures on the subsonic leading edges,* usually referred to as the edge suction pressures, can be determined. From these pressures the lift and drag forces and the various moments can be obtained by straightforward integrations.

With regard to the accuracy of the calculated results, it should be noted that, although the theory is based on the assumptions of small angles of attack and correspondingly small perturbation velocities, the similarly restricted theory in subsonic flow has yielded surprisingly accurate results. Furthermore, comparisons that have been made, such as in reference 1, between the available supersonic experimental data on lift-curve slope and the theoretical values based on the linearized compressible-flow theory are encouraging. The lift-curve slope is, of course, a longitudinal derivative. Furthermore, it is dependent on the total or integrated pressure and not the distribution of the pressure. This favorable comparison, therefore, is somewhat indirect, but, when it is coupled with the fact that the lateral derivatives considered herein are not very sensitive to small shifts in the spanwise centers of pressure (being dependent on fairly large lateral moment arms), the indication is that the linearized theory should provide fairly good estimates of the potential-flow contribution to the lateral derivative, at least insofar as general trends and orders of magnitude are concerned. Certain of the viscous effects, such as the contribution of skin friction to C_{n_r}, can be evaluated independently and added to the potential flow contributions. Thus, it is possible that the present results will be sufficiently accurate to preclude widespread application of a more elaborate theoretical method or complete recourse to experimental results. In an instance where a rather precise value for a derivative is desired, however, an experimental result or a more comprehensive theoretical investigation may be required.

As previously mentioned, one of the first steps in the solution of the general problem of lifting-surface analysis is the establishment of the boundary conditions. Sideslip and roll provide no great difficulties in this respect. A sideslipped flat plate at an angle of attack can be represented by a uniform distribution of the downwash perturbation velocity over the plan form. The rolling wing is readily represented by a linear spanwise variation of the downwash perturbation velocity. The yawing wing, however, is not so easily prescribed in terms of the boundary conditions; in fact, the yawing wing is not truly adaptable to a steady-state solution through a substituted warping or some such artifice and should be considered as an unsteady-flow problem. At the present time, derivatives based on an unsteady flow analysis for the yawing wing are not available. Results for these derivatives calculated through the use of strip theory and other approximations, however, are included in the results presented.

In view of the boundary-condition situation and taking into consideration the nonlinearities that are involved in the sideslip analysis and the complication of the yawing-moment derivatives due to the edge-suction force, it is not surprising that the preponderance of the reported calculations of lateral-stability derivatives are for the damping-in-roll derivative, C_{l_p}. Beyond this one derivative, however, the bulk of the material generally available on lateral-stability derivatives has come from a group, headed by Dr. H. S. Ribner, in the Stability-Analysis Section at the Langley Aeronautical Laboratory of the N.A.C.A. and a group in the Theoretical Aerodynamics Section of the Ames Aeronautical Laboratory. Most of the results on supersonic stability derivatives that will be presented and discussed in this paper have come from one of these two sources.

The values given for the derivatives are referred to the stability axes system.[2] This is a right-handed system of three orthogonal axes—namely, the longitudinal axis, the vertical axis, and the lateral axis of the aircraft. The axes are fixed in the airplane and travel with it. They are oriented in a manner such that the longitudinal axis is in the plane of symmetry, positive forward, and aligned with the free-stream vector at zero sideslip. The vertical axis is positive downward and the lateral axis is positive in the direction toward the right wing tip. The signs for the moments follow the right-hand screw rule.

The angle of attack α is measured in radians, and the sideslip angle β in degrees, wherever they occur herein.

* In the terminology that has become associated with supersonic flow analysis, the term "subsonic edge" refers to an edge swept behind the Mach cone, from which it follows that the velocity normal to the edge is subsonic; the term "supersonic edge" refers to an edge swept ahead of the Mach cone.

Results and Discussion

The presentation and discussion of the results will be divided into four categories: (1) the variation of the derivatives with aspect ratio; (2) the variation of the derivatives with Mach Number for both subsonic and supersonic speeds; (3) the variation of C_l and C_n with sideslip; and (4) the effects of wing-and-body combinations.

Four types of plan forms will be considered in this study. These plan forms, shown in Fig. 1 for an aspect ratio of 4, are characteristic of the supersonic wing configurations that are frequently proposed. They fit the following descriptions: (1) rectangular; (2) trapezoidal with tips raked out at a slope of 0.5; (3) triangular with apex forward; and (4) swept back and tapered to points at the wing tips, having subsonic leading edges, supersonic trailing edges, and a ratio of root chord to overall length of 0.5.

The sweptback plan form just described was selected because more data were available for it than for any other of the sweptback type. It is unfortunate that this plan form has not been analyzed as yet for conditions that make the leading edge supersonic or the trailing edge subsonic. With regard to this situation it can be said, however, that the sweptback plan forms as a class present a rather complex integration problem and, consequently, require rather long and tedious calculation procedures. All this accounts for the rather limited extent of the curves presented for the sweptback plan form.

In the following discussion, the stability derivative coefficients—that is, the nondimensional form of the derivatives that are plotted on the graphs—usually will be referred to as the "derivatives" for simplicity and brevity.

The Variation of the Derivatives with Aspect Ratio

The variations with aspect ratio of the six derivatives under consideration are shown in Figs. 2 through 7. These results are presented for $B = 1$ (B is the Mach Number parameter $\sqrt{M^2 - 1}$) and were obtained from the data and expressions contained in references 3 through 9.

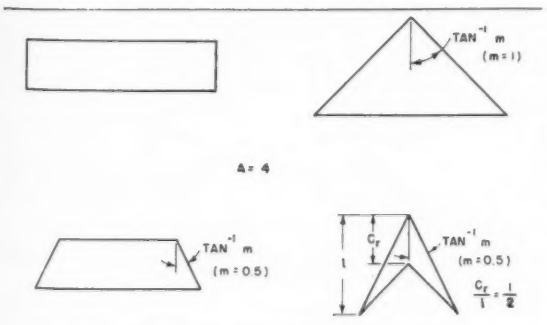

FIG. 1. Plan-form types investigated. $A = 4$.

The Damping in Roll, C_{l_p}.—The negative values for C_{l_p} evident in Fig. 2 indicate damping of the rolling motion which is to be expected for unstalled wings. As might also have been anticipated, the derivatives, in general, increase in magnitude with increasing aspect ratio. The one exception is the supersonic-edged triangular plan form for which C_{l_p} remains constant at $-1/3$. The trapezoidal and rectangular plan forms approach asymptotically the two-dimensional value of $-2/3$.

For the ratio of c_r/l of 0.5, the aspect ratio of the sweptback wings is given by $8m$, where m is the slope of the leading edge, as compared with $4m$ for the triangular wing. Thus it can be determined from Fig. 2 that, for equal leading-edge slopes, the sweptback wing, which has twice the aspect ratio of the triangular wing, provides the greater damping in roll.

The Yawing Moment Due to Rolling, C_{n_p}/α.—The leading-edge suction forces, as well as the normal forces, contribute to the value of C_{l_p}/α. The normal-force contribution is, for practical purposes, $-\alpha C_{l_p}$ and is independent of the longitudinal location of the moment center. The contribution of the edge-suction force, however, is quite dependent on the moment-center location. Thus, the magnitude and, in some cases, the sign of this derivative can be altered by a chordwise shift of the moment center. These statements apply also to the other derivatives that contribute yawing moments, C_{n_r} and C_{n_β}. For the particular plan forms under consideration, the values presented for the yawing-moment derivatives correspond to the following moment-center locations: $c_r/2$ for the rectangular and trapezoidal plan forms; $2c_r/3$ aft of the leading-edge apex for the triangular plan form; and $2l/3$ aft of the leading-edge apex for the sweptback plan forms. Subsequent calculations have shown, however, that, for any location of the moment center between those indicated and the leading edge, the results presented may be considered as fairly typical.

It is evident from Fig. 3 that the variation of C_{n_p}/α with aspect ratio is similar to the C_{l_p} variation. The values of the derivative generally increase with increasing aspect ratio, only in this case it is in algebraic rather than absolute magnitude because of the shift in the horizontal axis and the inversion of the vertical axis.

The Rolling Moment Due to Yawing, C_{l_r}/α.—The results for this derivative are presented in Fig. 4. The analysis presented in reference 6 is based on a strip theory and, for $B = 1$, predicts zero as the value for C_{l_r}/α for the rectangular wing. This analysis extended to any closely related trapezoidal plan form yields the same result.

The triangular and sweptback plan forms with subsonic leading edges show, in general, an increase in C_{l_r}/α with an increase in aspect ratio. Furthermore

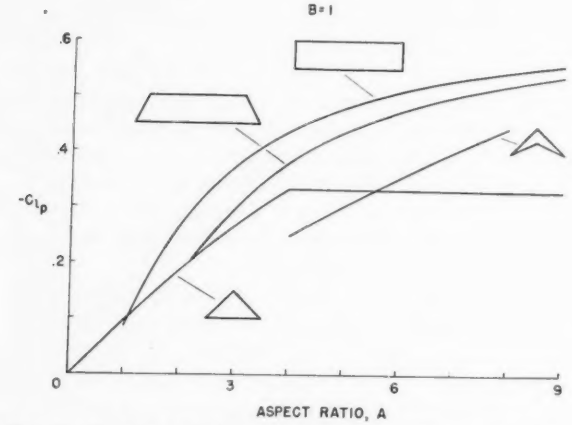

FIG. 2. Variation of damping-in-roll derivative with aspect ratio. $B = 1$.

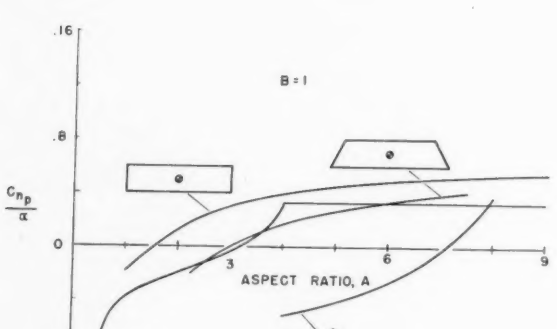

FIG. 3 Variation of yawing-moment-due-to-roll derivative with aspect ratio. $B = 1$.

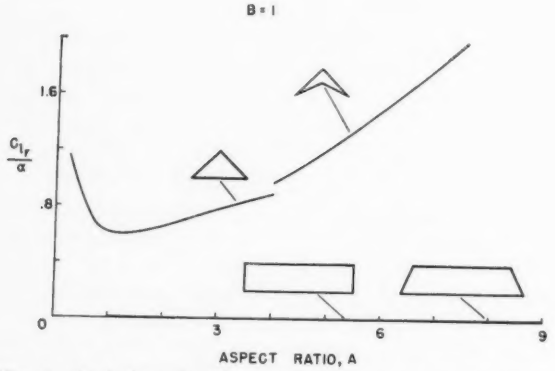

FIG. 4. Variation of rolling-moment-due-to-yawing derivative with aspect ratio. $B = 1$.

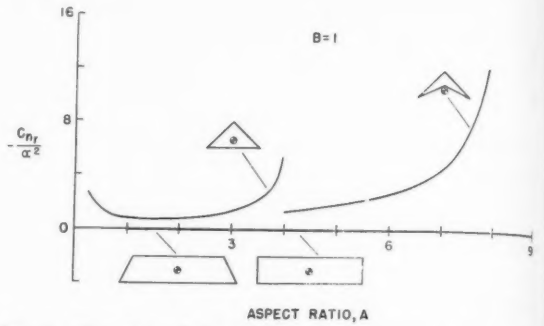

FIG 5. Variation of damping-in-yaw derivative with aspect ratio. $B = 1$.

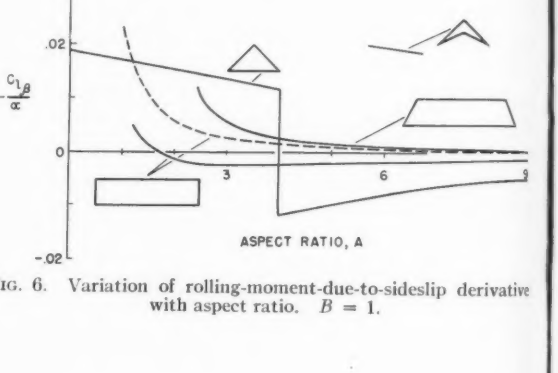

FIG. 6. Variation of rolling-moment-due-to-sideslip derivative with aspect ratio. $B = 1$.

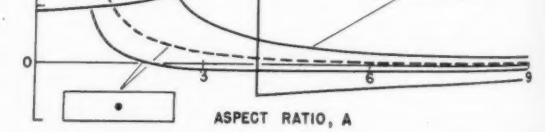

FIG. 7. Variation of yawing-moment-due-to-sideslip derivative with aspect ratio. $B = 1$.

in this case, as in the C_{l_p} case, equal leading-edge slopes generally yield greater magnitudes of C_{l_r}/α for the sweptback plan forms than for the triangular plan forms. In references 4 and 7, the sources of the results for triangular and sweptback plan forms, the belief is expressed that, if the analysis were to be carried out for supersonic leading edges, a reversal in the sign C_{l_r} would occur. It is also stated, with regard to the approximations involved in the analysis, that, although the spanwise increase in speed is taken into account, the spanwise variation in Mach Number is not included.

The Damping in Yaw, C_{n_r}/α^2.—The values of C_{n_r}/α^2 shown in Fig. 5 are for a potential flow. No effects of profile drag are included. Thus, the major contributions to this derivative are again the normal-force moment, represented by $-\alpha C_{l_r}$, and the moment due to the edge-suction force.

As might have been anticipated, the variations of C_{n_r}/α^2 fit the descriptions given for C_l/α for each of the plan forms.

In general, the value of C_{n_r} contributed by the wing will be dependent on the effects of viscosity. Furthermore, for an aircraft having fuselage and tail components, the contribution of the wing alone to the value of C_{n_r} for the complete configuration is likely to be small.

The Dihedral Effect, $C_{l\beta}/\alpha$.—There are two curves shown in Fig. 6 for the rectangular plan forms. The dotted curve from reference 6 represents a result based on the hypothesis that the Kutta condition does not hold at the trailing tip for small angles of sideslip. The solid curve from reference 5, on the other hand, represents a value of the derivative based on the assumption that the Kutta condition holds throughout the sideslip range. Experimental results will be needed to determine eventually just what condition or changes in condition are prevalent at the trailing tip during sideslip. At the Mach Number considered, $M = 1.41$ or $B = 1$, the two curves differ in sign throughout most of the aspect-ratio range. Both curves, however, show a general decrease in magnitude as the aspect ratio increases.

The trapezoidal plan form selected for this investigation provides positive dihedral effect throughout the aspect-ratio range at this Mach Number. As shown in reference 5, however, this result cannot be generalized to apply to all trapezoidal plan forms of this type. For a different tip slope, the sign of the derivative can change within the aspect-ratio range shown.

The results for the triangular plan form indicate a reversal from positive to negative dihedral effect as the leading edge becomes supersonic. This is essentially a Mach Number, rather than an aspect ratio, effect, and the primary result of increasing the aspect ratio is a reduction in the magnitude of the derivative.

Although only a limited aspect-ratio range is shown for the sweptback wing, the results indicate that this plan form is behaving similarly to the subsonic-edged triangular plan form and, thus, probably will continue to do so when the leading edges becomes supersonic. Curves for both subsonic-leading-edge and supersonic-leading-edge sweptback plan forms of different types, presented in reference 5, indicate the probability of this behavior.

The Directional Stability, $C_{n\beta}/\alpha^2$.—The differences between the magnitudes of the plotted values of $C_{r\beta}/\alpha^2$ and $C_{l\beta}/\alpha$ are due to the yawing moments contributed by the leading-edge-suction forces. The suction forces generally tend to increase the directional stability over that contributed by the normal-force component $-\alpha C_{l\beta}$ alone. The variations with aspect ratio for $C_{n\beta}/\alpha^2$ are much the same as those for $C_{l\beta}/\alpha$, with the exception that the suction effects cause the derivatives for the subsonic-edged triangular and sweptback plan forms to increase rather than to decrease in magnitude as the aspect ratio is increased.

The effects of assuming that the Kutta condition does not hold on the trailing tip are shown again by the dotted curve for the rectangular plan form.[6] Further details on the sideslip variations of C_n/α^2 and C_l/α and the effect of the Kutta condition are given in a later section of this paper.

Variation with Mach Number

The four plan forms selected for the investigation of Mach Number effects are shown in Fig. 1. By choosing the aspect ratio of these plan forms to be 4, the leading-edge slopes of the triangular and sweptback wings were fixed at 1.0 and 0.5, respectively.

The variations of the stability derivatives with Mach Number have been extended to cover the subsonic, as well as the supersonic, velocity régime in order to provide a more interesting and significant comparison The values of the derivative for $M = 0$ were obtained from references 9 through 14 for all but the trapezoidal plan form. The results for the rectangular plan form, however, will be approximately correct for the trapezoidal plan form at subsonic speeds. The references just cited contain some experimental, as well as calculated, results, and some of the experimental values are included in the subsonic portions of the curves of Figs. 8 through 13. With the exception of C_{n_r}, the values for the derivatives at $m = 0$ were approximately corrected for the effects of compressibility, and thereby extended to $M \approx 0.95$, by the methods of reference 15.

The Damping in Roll, C_{l_p}.—The curves for the C_{l_p} variation with Mach Number, shown in Fig. 8, follow a similar pattern for each plan form. The general trend is a slight increase in the magnitude of C_{l_p} as the Mach Number increases and approaches unity, followed by some transition through the sonic speed to a comparable value of C_{l_p} and a fairly rapid decrease in magnitude at the low supersonic Mach Numbers. The curves then tend to level off, however, and begin a rather asymptotic approach to the axis as the Mach Number is further increased.

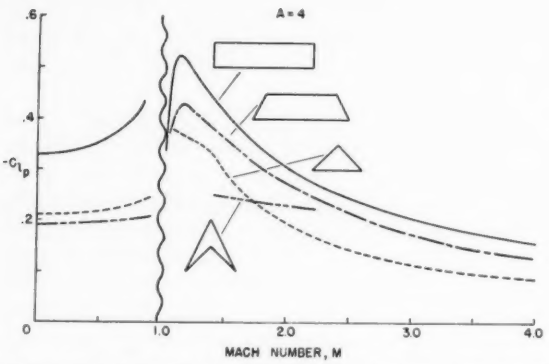

FIG. 8. Variation of damping-in-roll derivative with Mach Number. $A = 4$.

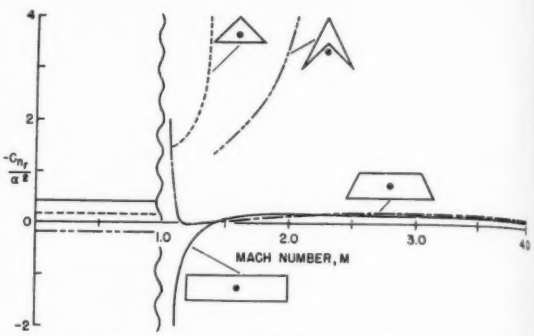

FIG. 11. Variation of damping-in-yaw derivative with Mach Number. $A = 4$.

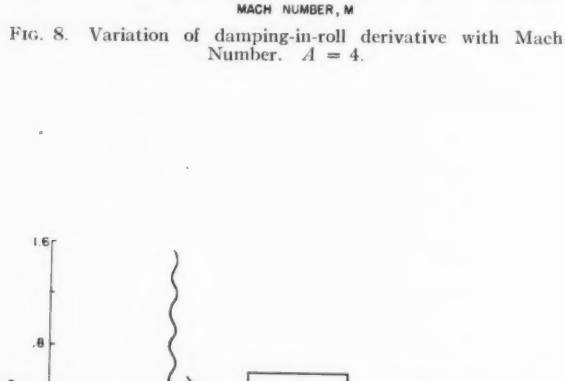

FIG. 9. Variation of yawing-moment-due-to-roll derivative with Mach Number. $A = 4$.

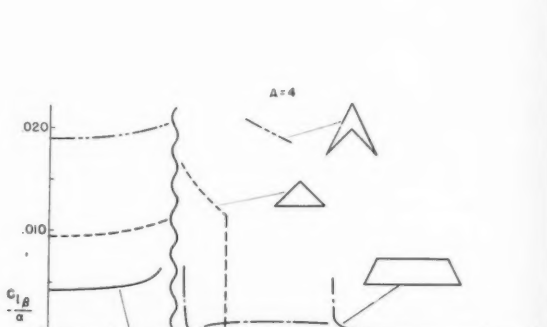

FIG. 12. Variation of rolling-moment-due-to-sideslip derivative with Mach Number. $A = 4$.

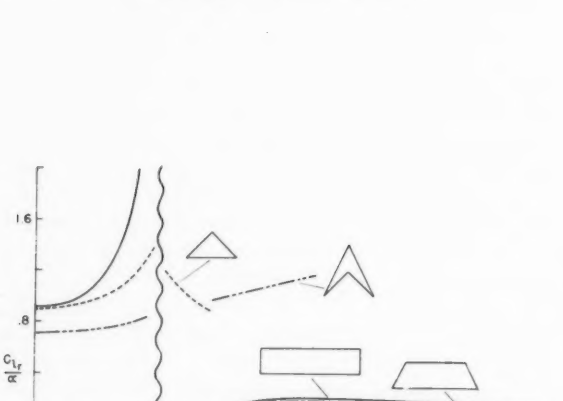

FIG. 10. Variation of rolling-moment-due-to-yawing derivative with Mach Number $A = 4$.

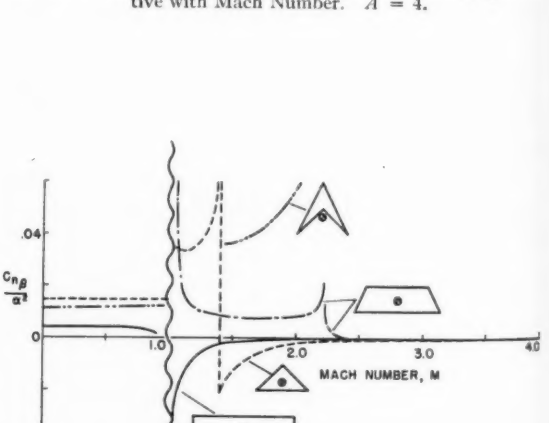

FIG. 13. Variation of yawing-moment-due-to-sideslip derivative with Mach Number. $A = 4$.

The Yawing Moment Due to Rolling, C_{np}/α.—The negative sign of this derivative, which is associated with these plan forms at subsonic speeds, changes to a positive one at various supersonic Mach Numbers for all the plan forms. For the rectangular plan forms this reversal occurs at the sonic speed, $M = 1$. For the trapezoidal, triangular, and sweptback plan forms it occurs at supersonic speeds.

With regard to the magnitudes of the derivatives, it is evident that, in general, a decrease in the magnitude of C_{np}/α takes place as the supersonic Mach Number increases. It is likely that, once the leading edges of the sweptback plan form become supersonic, this plan form would follow the trend of the others.

The Rolling Moment Due to Yawing, C_{lr}/α.—The curves for the rectangular and trapezoidal plan forms, shown in Fig. 10, indicate that reversals in the sign of this derivative occur at the sonic speed and exist up to $M = 1.41$. There are no changes in the sign of C_{lr}/α for the triangular and sweptback wings, however. As the Mach Number is increased, the magnitudes of the derivatives for all the plan forms increase as the sonic speed is approached and, in general, decrease at the supersonic speeds.

The Damping in Yaw, C_{nr}/α^2.—The reversals of the sign of C_{nr}/α^2 for the rectangular and trapezoidal plan forms which occur when the sonic speed is exceeded hold only until the Mach Number 1.41 is reached. The value for the triangular wing shows a sizable jump in magnitude at the sonic speed but no reversal in sign; whereas the value for the sweptback wing shows both. The lack of damping in yaw for the sweptback wing at subsonic speeds occurs only at large angles of sweep. This same condition in the cases of the rectangular and trapezoidal wings at the low supersonic speeds, however, is due to the Mach Number effects on the spanwise distribution of the loading.[4, 7]

As mentioned previously, the values of C_n shown in Fig. 11 represent only the potential flow contribution of the wing alone. The other aircraft components, such as the fuselage and the vertical tail, and the viscous effects will generally contribute a large part of the magnitude of this derivative.

The Dihedral Effect, $C_{l\beta}/\alpha$.—The curve for the triangular plan form, shown in Fig. 12, indicates that this plan form loses its positive dihedral effect when its leading edges become supersonic. The resulting negative dihedral effect diminshes rapidly, however, as the Mach Number is further increased. The data available in reference 5 on sweptback plan forms indicate that the sweptback wing considered would probably behave in a similar fashion.

For the rectangular plan form, the switch from positive to negative dihedral effect occurs at $M = 1$. No curve has been shown for the case where the Kutta condition on the trailing tip is neglected, but it should suffice to say that this curve would indicate positive dihedral effect throughout most of the supersonic Mach Number range. At the particular aspect ratio of 4, the trapezoidal plan form with slightly raked-out tips maintains a positive dihedral effect throughout the Mach Number range. As indicated previously in the aspect-ratio study, that result cannot be generally extended to all trapezoids of this type. The aspect ratio and the amount of tip rake are rather critical factors with regard to the value of this derivative at supersonic speeds.

On the supersonic side of the Mach Number range, the magnitudes of $C_{l\beta}/\alpha$ generally tend to decrease with increasing Mach Number for all plan forms.

The Directional Stability, $C_{n\beta}/\alpha^2$.—The curves for $C_{n\beta}/\alpha^2$ shown in Fig. 13 follow the same general trends as the curves for $C_{l\beta}/\alpha$. As explained previously in the discussion of the variation of these derivatives with aspect ratio, any differences in the curves for $C_{n\beta}/\alpha^2$ and $C_{l\beta}/\alpha$ at supersonic speeds are due to the effect of leading-edge suction on $C_{n\beta}/\alpha^2$.

Variation of C_l *and* C_n *with Sideslip*

The nonlinearities in the sideslip variations, which are illustrated by the C_n/α^2 and C_l/α curves for triangular and rectangular plan forms in Figs. 14 and 15, are of special interest. The solid curves, taken from references 5 and 8, illustrate the three types of nonlinearities commonly occurring: (1) the warped but still continu-

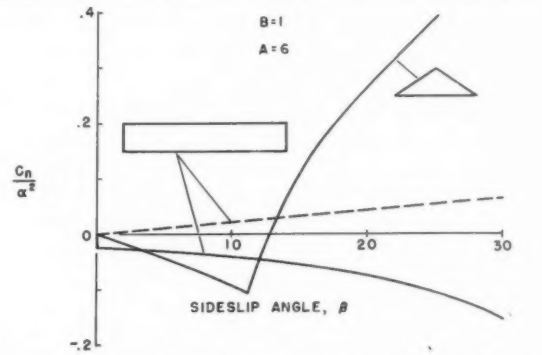

FIG. 14. Variation of yawing moment with sideslip. $B = 1$, $A = 6$.

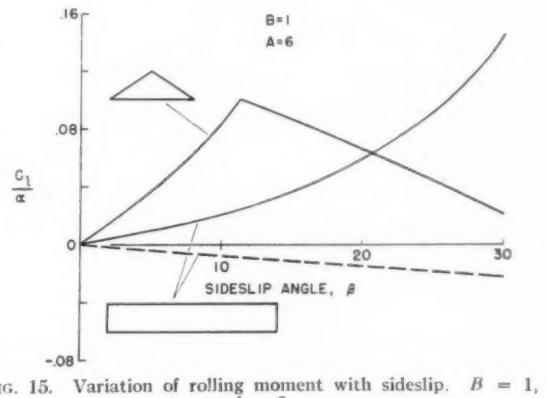

FIG. 15. Variation of rolling moment with sideslip. $B = 1$, $A = 6$.

ous curve present in both the rectangular and triangular cases; (2) the break in the curve for the triangular wing; and (3) the sudden jump in the curve at zero sideslip for the rectangular wing. The first type is due mainly to the generally nonlinear edge-suction effects. The second type occurs usually as an edge passes through a Mach cone and changes from a subsonic edge with suction to a supersonic edge without suction, or vice versa. The third type is usually caused by an edge passing through the free-stream direction and changing from a leading edge with suction to a trailing edge without, or vice versa. This third type of nonlinearity occurs if the Kutta condition is assumed to exist at the trailing tip. The dotted curve for the rectangular plan form in Fig. 14, obtained from reference 6, represents the assumption that the Kutta condition does not hold. It can be seen that, in addition to eliminating the jump in the curve, the latter assumed condition changes the sign of the slope of the curve. This change in the sign of the derivative is also evident in the C_l variations plotted in Fig. 15.

Effects of Wing-and-Body Combinations

It is certain that the values of the stability derivatives for the wing alone will be modified somewhat by the addition of a body such as a fuselage. Unfortunately, not much material is available as yet on the lateral-stability derivatives for wing-and-body combinations. Some idea, however, of the effects on C_{l_β} and C_{l_p} of adding a fuselage can be obtained for low-aspect-ratio plan forms from references 16 and 17, respectively. These results are based on a theory derived particularly for low-aspect-ratio wings and slender bodies. This theory is applicable throughout the whole Mach Number range, including the sonic speed.

Fig. 16 contains the ratios of these derivatives for the wing and body combined to those for the wing alone, $(\ )/(\ )_w$, as a function of the ratio of the diameter of the body to the wing span, D/b. A triangular wing and a circular cylindrical body are represented. The entire wing area, submerged as well as exposed, is the reference area on which the coefficients are based. As might be expected, the ratio $C_{l_\beta}/(C_{l_\beta})_w$ diminishes steadily as the ratio D/b increases. The rate of decrease of $C_{l_\beta}/(C_{l_\beta})_w$ also increases steadily. A rather remarkable result was obtained for the C_{l_p} ratio, however. For values of D/b less than 0.4, the ratio of $C_{l_p}/(C_{l_p})_w$ is greater than 1. This indicates that the interference due to the body either increases or favorably redistributes the wing loading for this range of D/b. At higher values of D/b, however, the C_{l_p} ratio tends toward zero as might be reasonably anticipated.

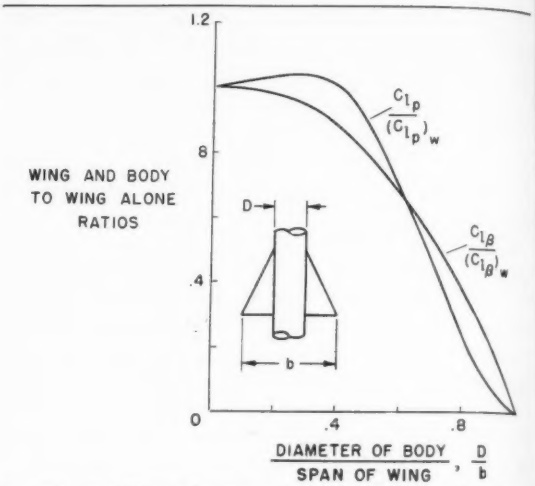

FIG. 16. Stability-derivative ratios for the damping in roll and the dihedral effect of a wing-and-body combination.

CONCLUDING REMARKS

From the foregoing collection of material on the lateral stability derivatives at supersonic speeds it is possible to pick out a few definite trends. The magnitudes of the supersonic derivatives in coefficient form, for instance, are fairly comparable to those encountered at subsonic speeds. The effect of increasing the aspect ratio is, in general, an increase in the magnitudes of the stability derivatives due to rolling and yawing and a decrease in the magnitudes of the derivatives due to sideslip.

With regard to the effects of Mach Number, the magnitudes of the derivative coefficients generally tend to increase as the sonic speed is approached from the subsonic side and to decrease as the Mach Number is increased on the supersonic side.

One of the most interesting aspects of the behavior of the results was the reversal in sign for some of the derivatives. These reversals usually occurred either at the sonic speed or at supersonic speeds as the subsonic leading edge changed to a supersonic leading edge. Of the derivatives contributed by the wing alone, those contributing rolling moments, C_{l_p}, C_{l_r}, and C_{l_β} are the most significant in their effect on the stability of the aircraft. Two of these, C_{l_r} and C_{l_β}, show reversals in sign from their usual subsonic values. The change in having the right wing drop instead of pick up when the right wing speeds up in yaw or when sideslipping to the right will probably pose serious stability problems at supersonic flight speeds. Further analysis is needed, however, in order to bring out the complete physical significance of all the trends and magnitudes of the derivatives presented.

REFERENCES

[1] Vincenti, Walter G., *Comparison Between Theory and Experiment for Wings at Supersonic Speeds*, Proceedings of the Joint Conference of the I.A.S. and R.Ae.S., New York, May 24–26, 1949 (to be published).

[2] Glauert, H., *A Non-Dimensional Form of the Stability Equations of an Aeroplane*, R. & M. 1093, British A.R.C., 1927.

(*Continued on page 59*)

Influence of Acceleration on Aerodynamic Characteristics of Thin Airfoils in Supersonic and Transonic Flight*

C. S. GARDNER† AND H. F. LUDLOFF‡
New York University

ABSTRACT

An attempt has been made to derive the aerodynamic characteristics, in the supersonic and transonic range, of a two-dimensional airfoil moving at uniformly accelerated speed; it is assumed that the airfoil is thin and the shocks resulting from its motion are extremely weak. Under these conditions, the airfoil motion may be treated as a time-dependent perturbation problem, which can be solved by means of "Possio solutions." The solutions for lift, drag, and pressure on the airfoil surface turn out to be elliptic integral expressions, whose arguments depend on the Mach Number and on an acceleration parameter.

The evaluation of these solutions is carried out in a different manner, depending on whether the transonic or the supersonic range is considered. In Section (A), the solution at supersonic speeds is expanded in *positive* powers of the acceleration parameter β. The influence of acceleration turns out to be extremely small. In Section (B), *the transonic* range is treated, by expanding the expressions for lift and drag, at $M = 1$, into a series starting with the *negative* one-fourth power of β. This elucidates why, at $M = 1$, the theoretical expressions for the aerodynamic parameters remain *finite* in the case of *accelerated* motion but become infinite in the limit of stationary flight speed ($\beta = 0$). In Section (C), a physical discussion of the results for wedges and diamond profiles is given: The curves representing the aerodynamic parameters as a function of the Mach Number have a more or less pronounced maximum at $M = 1$, depending on the value of the flight acceleration β. The application of a validity criterion shows that for sufficiently "large" β the results can be taken quantitatively, while at "small" β the results have only qualitative meaning.

NOTATION

x, y, t	= coordinates of point P in reference system, fixed in still air
ξ	= coordinate in reference system, fixed in moving airfoil
σ	= strength of "temporary source" in Possio solution
ξ, τ	= coordinates of "temporary source" in Possio solution
a	= sound speed in still air
p, ρ	= static pressure, density in still air
$M = U/a$	= instantaneous Mach Number
l	= chord length of airfoil
α	= angle of attack of chord
δ	= vertex angle of wedge profile, semivertex angle of diamond profile
b	= acceleration
$\beta = -2bl/a^2$	= dimensionless acceleration parameter

Based on a paper presented by H. F. Ludloff at the Aerodynamics Session, Seventeenth Annual Meeting, I.A.S., New York, January 24–27, 1949.

* This investigation was carried out under contract with O.N.R., Fluid Mechanics Branch.

† Research Associate.

‡ Associate Professor, Daniel Guggenheim School of Aeronautics, College of Engineering.

INTRODUCTION

THE PATH OF A uniformly accelerated, two-dimensional thin airfoil can be represented in the x-t plane as a strip between two parabolic arcs (see Fig. 1), the width of the strip being l, where l is the chord length. If the airfoil is assumed to produce small disturbances, any point inside the strip may be considered to be a source of disturbance waves propagating with sound speed. The velocity field can be derived from a perturbation potential that has to fulfill the differential equation of "sound" waves, and the solution of this equation may be represented as an integral over "Temporary Sources" (Possio's Solutions[1]), which are distributed over the parabolic strip mentioned before:

$$\varphi(x, y, t) = \int\int \frac{\sigma(\xi, \tau)}{\sqrt{(t - \tau)^2 - (1/a^2)[(x - \xi)^2 + y^2]}}$$

At a given station P on the airfoil surface, only those disturbances will be felt which are within the shaded area of Fig. 1, that is limited by the "sound speed lines," passing through P. Thus the domain of integration has to be extended over this shaded area.

The characteristic difference between the supersonic and subsonic case is indicated in Fig. 1. While in supersonic motion the pressure at P is influenced only by a small finite source area, whose vertex is at P and whose base is the parabolic path CD of the leading edge, in the subsonic case the sound speed-lines through P cut off the whole lower part of the parabolic, source-covered strip. This means that during the subsonic flight, the whole previous history of the airfoil motion will influence the pressure distribution, lift, and drag, while during the supersonic flight the airfoil flies through undisturbed air.

Thus it may be noted that the aerodynamic characteristics at $M = 1$ will be different, depending on whether the airfoil has been accelerating from subsonic speeds or decelerating from supersonic speeds.

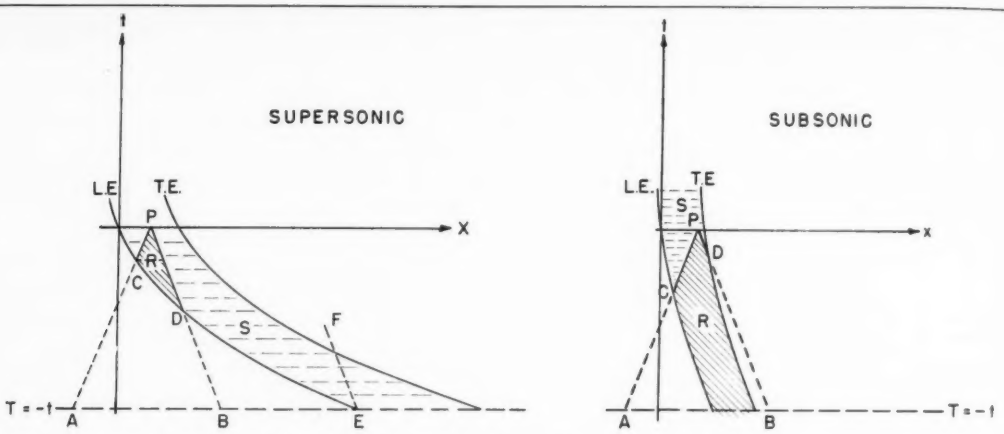

FIG. 1. Path of motion of decelerating airfoil in x-t plane.

The present investigation deals with the change of aerodynamic characteristics during a decelerating flight, starting at supersonic speeds (see author's note,[2] December, 1948). It turns out that the influence of deceleration is hardly appreciable at supersonic speeds (slightly more appreciable, if the airfoil flies at a finite angle of attack). But in the transonic range (see Fig. 3), the shape of the pressure-, drag-, and lift-curves (i.e., c_D vs. M, etc.), as derived from this theory, depends strongly on the value of the acceleration parameter β. While the theory becomes invalid in the limit of stationary flight speed (i.e., for $\beta = 0$), its degree of validity increases rapidly with increasing β-value [see Section (C, 3)]. Already at $\beta \sim 0.02$, the theory is as good an approximation as the linearized theory in the supersonic range. For $\beta \neq 0$ all curves have a marked maximum at $M = 1$, but *all parameters remain finite and vary continuously through the transonic range.*

The finiteness of c_D, etc., at $M = 1$ for accelerated motion, as in contrast to the infinite c_D-value attained for stationary speed, is made plausible in Fig. 2. It is seen that the parabolic strip of Fig. 1 becomes a straight strip for stationary speed; consequently the shaded integration area becomes of infinite extent for $\beta = 0$—i.e., the integral expressions for c_D, c_L, and c_p diverge for constant speed.

In more precise terms: At supersonic speeds, the aerodynamic quantities may be expanded in positive powers of β, so long as $M - 1 > \sqrt{\beta}$. However, in the vicinity of $M = 1$ (i.e., for $M - 1 < \sqrt{\beta}$) the elliptic integral, representing the pressure, drag, or lift value, has to be expanded in a different manner—i.e., by a series starting with a negative one-fourth power of β. This elucidates the fact that in the limiting case of constant flight speed ($\beta = 0$), the well-known divergent values for lift and drag are obtained, while for uniformly accelerated speed, all aerodynamic parameters, as lift, drag, and pressure on the airfoil surface, remain finite at $M = 1$.

A singular behavior is evidenced by the theoretical pressure value right at the leading edge, which can be shown to be finite at supersonic speeds, but becomes infinite as $x^{-1/4}$ at sound speed, and logarithmically infinite at subsonic speeds. The latter can be anticipated, in analogy to the stationary thin airfoil theory. Of course, this singularity of the pressure at the leading edge leaves the lift and drag values finite.

At the conclusion of these considerations, it has been checked, to what extent the results of the linearized theory around $M = 1$ may be expected to be in fair agreement with actual conditions. Therefore a validity criterion is discussed in Section (C, 3). Its application shows that under certain conditions—i.e., for small thickness ratio [and small A.R.; see Section (C, 3)]—the results derived here should be valid approximations, while in other cases the conclusions drawn for the transonic range are merely of qualitative nature. In this connection, one may also consult a recent paper by Lin, Reissner, and Tsien,[3] in which it is explained why linearized treatment of slender bodies in the transonic range becomes legitimate for sufficiently large accelerations.

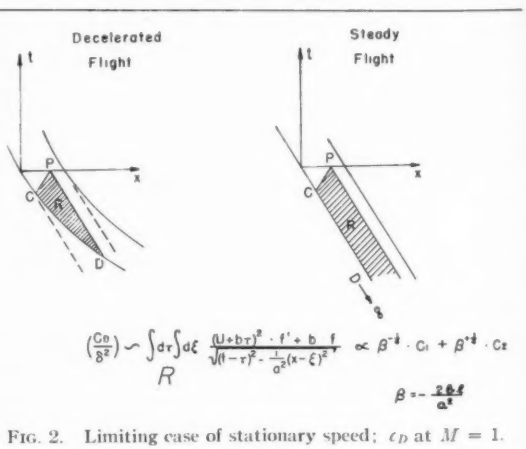

FIG. 2. Limiting case of stationary speed; c_D at $M = 1$.

(A) Computation of Drag and Lift of a Decelerating Thin Airfoil in Supersonic Flight

(1) *Formulation of the Analytic Problem*

Suppose a thin airfoil moves with uniformly accelerated, supersonic speed $U + bt$ into still air, in the direction of the negative x-axis. In coordinates, fixed in the airfoil, the upper profile surface may be given by: $y = f(\bar{x})$; here $f(0) = f(l) = 0$, l being the chord length (see Fig. 4). In coordinates fixed in still air, $y = f[x + Ut + (1/2)bt^2]$ where x, y, and t are so chosen that, at $t = 0$, the leading edge is at the origin $x = y = 0$. As it is assumed that the airfoil is thin and flat—i.e., $f << l$ and $f' << 1$—the disturbance, caused by the motion, is a small perturbation of the state of rest, and can be described by a perturbation potential φ which obeys the differential equation of disturbance waves:

$$\Delta\varphi - (1/a^2)\varphi_{tt} = 0 \tag{1}$$

a being the sound velocity in still air.

The pressure increment due to the disturbance is given by

$$\Delta p = -\rho(\varphi_t) \tag{2}$$

where ρ is the density of still air.

To determine the solution of Eq. (1), initial and boundary conditions must be specified. Assuming that the motion started at some past time $t = -T$, the initial conditions are

$$\varphi = 0, \quad \varphi_t = 0 \quad \text{at } t = -T \tag{3}$$

The boundary condition on the upper surface of the airfoil is in linearized approximation:

$$\varphi_y = (U + bt)f'[x + Ut + (1/2)bt^2]$$

at $y = 0$

$$0 < x + Ut + (1/2)bt^2 < l$$

for all $t > -T$.

Because of the symmetry of the flow pattern about $y = 0$, it follows that for $y = 0$ at a point of the x-t plane exterior to the airfoil, φ_y must be zero. Thus if the definition of f is extended so that $f(\bar{x}) = 0$ for $\bar{x} < 0$ or $\bar{x} > l$, it may be assumed that

$$\varphi_y = (U + bt)f'[x + Ut + (1/2)bt^2] \tag{4}$$

holds at $y = 0$ for *all* values of x and *all* values of $t > -T$. This extension of the definition of $f(x)$ will be useful in the course of the derivation [see Section (A, 2)].

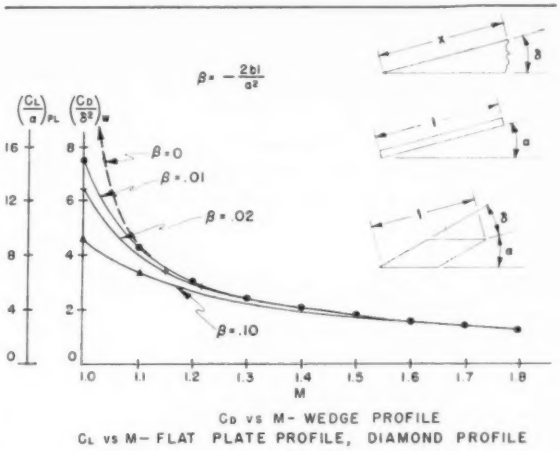

FIG. 3. c_D vs. M and c_L vs. M for wedge profile, at several β-values.

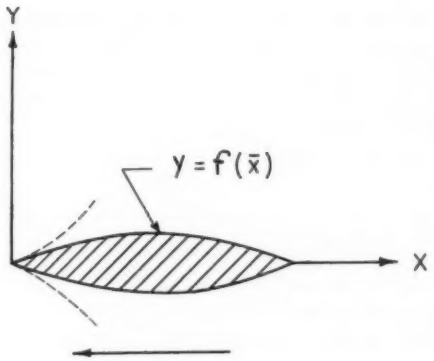

FIG. 4. Cross section of airfoil in x-y plane.

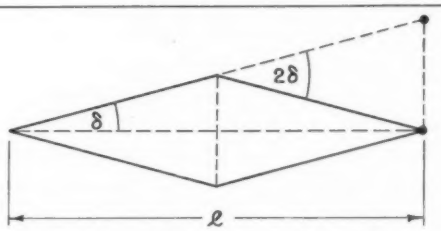

FIG. 5. Composition of diamond by wedges.

The solution of the initial-boundary problem defined by Eqs. (1), (3), and (4) can be given as the potential of a layer of temporary "sources" distributed over the x-t plane, the potential of a "source" of strength σ, located at $(\xi, 0, \tau)$ being

$$\sigma(\xi, \tau)/\sqrt{(t - \tau)^2 - (1/a^2)[(x - \xi)^2 + y^2]}$$

Thus

$$\varphi(x, y, t) = \int\int \frac{\sigma(\xi, \tau)}{\sqrt{(t-\tau)^2 - (1/a^2)[(x-\xi)^2 + y^2]}}\, d\xi\, d\tau \tag{5}$$

where the domain of integration is the region where $-T < \tau < t$ and the denominator is real. [Any point inside the so-defined ξ-τ domain may contribute to a disturbance felt at the point (x, y, t).] It has been shown by many authors[1,5] that, if φ is represented in this way, then

$$\lim_{y \to 0+} \varphi_y(x, y, t) = -\pi\sigma(x, t) \tag{6}$$

Thus substituting from Eqs. (4) and (6) into Eq. (5) and, since the airfoil surface is of primary interest, setting $y = 0$:

$$\varphi(x, 0, t) = -\frac{1}{\pi}\int_{-T}^{t} d\tau \int_{x-a(t-\tau)}^{x+a(t-\tau)} d\xi\, \frac{(U + b\tau)f'[\xi + U\tau + (1/2)b\tau^2]}{\sqrt{(t-\tau)^2 - (1/a^2)(x-\xi)^2}} \tag{7}$$

It is convenient to regard t as a third coordinate, so that the projection of the airfoil motion on to $y = 0$ traces out a parabolic strip in the x-t plane (see Fig. 1). If P is the point $(x, 0, t)$, it can be seen that the potential at P is given by an integral over the domain PAB cut out by the line $t = -T$ and the lines PA, PB along which $\xi = x \mp a(t - \tau)$—i.e., the lines representing the motion of a disturbance starting at $P(x, 0)$ and propagating with sound speed ("sound speed lines"). It may be seen that after a sufficient time has elapsed, the lines PA, PB both intersect the path of the leading edge before they intersect $t = -T$. It will be supposed that this is the case for all points P which are being considered. (Otherwise—i.e., if the line $t = -T$ is part of the boundary of the integration area—a transient effect connected with the start of the motion enters the problem.) The integrand then vanishes except over the shaded region PCD, since f' vanishes ahead of the leading edge. In particular, the integrand vanishes, as can be seen from Fig. 1, in a certain τ-interval say between $\tau = -T$ and $\tau = -T + t$. Thus, upon introducing a new integration variable $\bar{\tau} = t - \tau$, Eq. (7) can be written as

$$\varphi(x, 0, t) = \frac{1}{\pi}\int_{T}^{0} d\bar{\tau} \int_{x-a\bar{\tau}}^{x+a\bar{\tau}} d\xi\, \frac{[U + b(t-\bar{\tau})]f'[\xi + U(t-\bar{\tau}) + (1/2)b(t-\bar{\tau})^2]}{\sqrt{\bar{\tau}^2 - [(x-\xi)/a]^2}} \tag{8}$$

According to Eq. (2), the pressure at the surface of the airfoil is proportional to φ_t. To find φ_t, differentiate Eq. (8) and set afterward $t = 0$, which is a convenient transformation of the time coordinate, but no restriction of the generality, as the time zero point may be chosen at convenience:

$$\varphi_t(x, 0, 0) = \frac{1}{\pi}\int_{T}^{0} d\bar{\tau} \int_{x-a\bar{\tau}}^{x+a\bar{\tau}} d\xi\, \frac{(U - b\bar{\tau})^2 f''[\xi - U\bar{\tau} + (1/2)b\bar{\tau}^2] + bf'[\xi - U\bar{\tau} + (1/2)b\bar{\tau}^2]}{\sqrt{\bar{\tau}^2 - [(x-\xi)/a]^2}} \tag{9}$$

---

(2) *Expansion in Powers of a Deceleration Parameter* β

Since, in general, the acceleration of an airfoil is small compared to a standard acceleration a^2/l, a series expansion in terms of an acceleration parameter should be attempted. To obtain an expansion of $\varphi_t(x, 0, 0)$ in powers of b, the integrand in Eq. (9) may be expanded in a Taylor series and the series integrated term by term. Of course, this is possible only if f is an analytic function of its argument. However, this is in reality no restriction, as any f can be approximated uniformly throughout the domain of integration as exactly as desired, by an analytic function. The extended definition of $f(x)$ as introduced in Eq. (4) makes it possible to keep the integration limits in Eq. (9) free of b, so that only the integrand has to be expanded; this simplifies the procedure greatly.

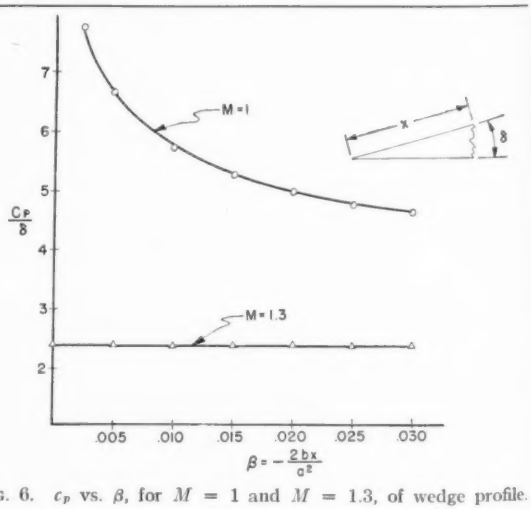

FIG. 6. c_p vs. β, for $M = 1$ and $M = 1.3$, of wedge profile.

Thus, expanding the numerator in Eq. (9):

$$\begin{aligned}(U-b\bar\tau)^2 f''[\xi - U\bar\tau + (1/2)b\bar\tau^2] + bf'[\xi - U\bar\tau + (1/2)b\bar\tau^2] \\ = (U - b\bar\tau)^2 \sum_{n=0}^{\infty} \frac{1}{n!}\left(\frac{b\bar\tau^2}{2}\right)^n f^{(n+2)}(\xi - U\bar\tau) + b\sum_{n=0}^{\infty}\frac{1}{n!}\left(\frac{b\bar\tau^2}{2}\right)^n f^{(n+1)}(\xi - U\bar\tau) \\ = U^2 f''(\xi - U\bar\tau) + \sum_{n=1}^{\infty}\frac{b^n}{2^n n!}[U^2\bar\tau^{2n} f^{(n+2)}(\xi - U\bar\tau) - 4nU\bar\tau^{2n-1} f^{(n+1)}(\xi - U\bar\tau) + \\ 2n(2n-1)\bar\tau^{2n-2} f^{(n)}(\xi - U\bar\tau)]\end{aligned} \tag{10}$$

where $f^{(k)}$ denotes the kth derivative of f. This expansion (10) must now be considered substituted into the numerator of Eq. (9).

In order to carry out the termwise integration, required by Eq. (9), the following procedure is used. If $g(x)$ is an arbitrary function, let $L(g)$ be defined by

$$L(g) = \frac{1}{\pi}\int_T^0 d\bar\tau \int_{x-a\bar\tau}^{x+a\bar\tau} d\xi \frac{Ug'(\xi - U\bar\tau)}{\sqrt{\bar\tau^2 - [(x-\xi)/a]^2}} \tag{11}$$

It can be seen that by setting b and t equal to zero in Eq. (8), $L(g)$ is the potential on the surface of an airfoil, whose profile is given by $y = g(x)$ and which moves at constant speed U in the direction of the negative x-axis. Thus, by the Ackert theory,

$$L(g) = -Ug(x)/\sqrt{M^2-1}, \quad \text{where } M = U/a$$

Now, it is to be noted that the kth integrated term of series (10) can be obtained by differentiating Eq. (11) k times with respect to U. Thus

$$I_k = \frac{1}{\pi}\int_T^0 d\bar\tau \int_{x-a\bar\tau}^{x+a\bar\tau} d\xi \frac{(-\bar\tau)^k g^{(k+1)}(\xi - U\bar\tau)}{\sqrt{\bar\tau^2 - [(x-\xi)/a]^2}} = \frac{\partial^k}{\partial U^k}\left[\frac{L(g)}{U}\right] = \frac{1}{a^k}\frac{\partial^k}{\partial M^k}\left[\frac{L(g)}{U}\right] = -\frac{g(x)}{a^k}\frac{\partial^k}{\partial M^k}\left(\frac{1}{\sqrt{M^2-1}}\right) \tag{12}$$

As shown in Appendix (1)

$$I_k = -\left[\frac{k!}{a^k(M^2-1)^{(k+1)/2}}\right] P_k\left(-\frac{M}{\sqrt{M^2-1}}\right) g(x) \tag{12a}$$

where $P_k(x)$ is the Legendre Polynomial of degree k. In particular, if $k = 2n$ and $g(x) = f^{(-n+1)}(x)$, meaning the n-fold repeated indefinite integral of $f'(x)$, Eq. (12) yields:

$$I_{2n} = \frac{1}{\pi}\int_T^0 d\bar\tau \int_{x-a\bar\tau}^{x+a\bar\tau} d\xi \frac{(\bar\tau)^{2n} f^{(n+2)}(\xi - U\bar\tau)}{\sqrt{\bar\tau^2 - [(x-\xi)/a]^2}} = -\frac{(2n)!}{a^{2n}(M^2-1)^{(2n+1)/2}} P_{2n} f^{(-n+1)}(x)$$

or, since $f^{(-n+1)}(x) = \int_0^x [(x-t)^{n-1}/(n-1)!]\, f'(t)dt$,

$$I_{2n} = -\left[\frac{(2n)!}{a^{2n}(M^2-1)^{(2n+1)/2}(n-1)!}\right] P_{2n}\left(-\frac{M}{\sqrt{M^2-1}}\right)\int_0^x (x-t)^{n-1} f'(t)dt \tag{13}$$

Similarly,

$$I_{2n-1} = -\frac{(2n-1)!}{a^{2n-1}(M^2-1)^n (n-1)!} P_{2n-1}\left(-\frac{M}{\sqrt{M^2-1}}\right)\int_0^x (x-t)^{n-1} f'(t)dt \tag{14}$$

and

$$I_{2n-2} = -\frac{(2n-2)!}{a^{2n-2}(M^2-1)^{(2n-1)/2}(n-1)!} P_{2n-2}\left(-\frac{M}{\sqrt{M^2-1}}\right)\int_0^x (x-t)^{n-1} f'(t)dt \tag{15}$$

In the termwise integration of the series expansion to be substituted in Eq. (9), Eqs. (13), (14), and (15) may be used and in addition the relation

$$(n+1)P_{n+1}(z) - (2n+1)zP_n(z) + nP_{n-1}(z) = 0$$

may be taken into consideration. Thus

$$\varphi_l(x, 0, 0) = -\frac{U^2 f'(x)}{\sqrt{M^2-1}} - \int_0^x \left\{ \sum_{n=1}^{\infty} \frac{b^n (2n-1)!(x-t)^{n-1}}{2^n a^{2n-2}(M^2-1)^{(2n+1)/2} n!(n-1)!} \times \right.$$

$$\left. \left[\frac{(M^2-4n)M}{\sqrt{M^2-1}} P_{2n-1} + (M^2-2n) P_{2n-2} \right] \right\} f'(t)dt \quad (16)$$

From Eq. (16), the pressure coefficient of a wedge profile of vertex angle δ (i.e., $f(x) = \delta x$) whose lower side is parallel to the flight direction, can be obtained as:

$$c_p = -\frac{2}{U^2}\varphi_l = \delta \left[\frac{2}{\sqrt{M^2-1}} - \frac{1}{2}\frac{(M^2+2)}{M^2(M^2-1)^{5/2}}\beta + \frac{3}{8}\frac{M^4+(27/4)M^2+1}{M^2(M^2-1)^{9/2}}\beta^2 \ldots \right] \quad (17)$$

where the acceleration parameter $\beta = -2bx/a^2$. Then the drag coefficient

$$c_D = \frac{1}{x}\int_0^x c_p \delta \, dx = \delta^2 \left[\frac{2}{\sqrt{M^2-1}} - \frac{1}{4}\frac{M^2+2}{M^2(M^2-1)^{5/2}}\beta + \frac{1}{8}\frac{M^4+(27/4)M^2+1}{M^2(M^2-1)^{9/2}}\beta^2 \ldots \right] \quad (18)$$

For *symmetrical* airfoils of chord length l, the drag coefficient is given by means of Eq. (2) as:

$$c_D = \frac{2}{\rho U^2 l}\int_0^l 2\Delta p(x) f'(x)dx = -\frac{4}{U^2 l}\int_0^l \varphi_l f'(x)dx \quad (19)$$

Thus

$$c_D = \frac{4}{\sqrt{M^2-1}}\frac{1}{l}\int_0^l [f'(x)]^2 dx + \frac{4}{l^2}\int_0^l dx \int_0^x dt \sum_{n=1}^{\infty}\left(-\frac{\beta}{4}\right)^n \frac{(2n-1)![(x-t)/l]^{n-1}}{M^2(M^2-1)^{(2n+1)/2} n!\,(n-1)!} \times$$

$$\left[\frac{(M^2-4n)M}{\sqrt{M^2-1}} P_{2n-1}\left(-\frac{M}{\sqrt{M^2-1}}\right) + (M^2-2n) P_{2n-2}\left(-\frac{M}{\sqrt{M^2-1}}\right) \right] f'(t) f'(x) \quad (20)$$

where now $\beta = -2bl/a^2$. Here it is assumed that the profile function $f(x)$ is subtended above the flight direction; therefore $f(l) \equiv\!\!\!\!/\; 0$, depending on whether the angle of attack is zero or not.

Indicating the first terms more explicitly, Eq. (20) yields for zero angle of attack:

$$c_D = \frac{4}{\sqrt{M^2-1}}\left(\frac{1}{l}\right)\int_0^l [f'(x)]^2 dx - \frac{3}{2}\beta^2 \frac{M^4+(27/4)M^2+1}{M^2(M^2-1)^{9/2}}\left(\frac{1}{l^3}\right)\int_0^l [f(x)]^2 dx - \frac{5}{64}\frac{\beta^3}{M^2(M^2-1)^{13/2}} \times$$

$$(24M^6 + 348M^4 + 303M^2 + 18)\left(\frac{1}{l^4}\right)\left[\int_0^l \bar{f}(x)dx\right]^2 - \ldots \quad (21)$$

Here, according to definition, $f(l) = 0$, so that the term proportional to the first power of β vanishes in this case.

In case of an angle of attack, $f(x)$ is resolved geometrically into a profile function of $f(x)$, subtended above the chord, and the angle of attack α of the chord; thus for symmetric airfoils:

$$c_D = \frac{4}{\sqrt{M^2-1}}\left[\alpha^2 + \frac{1}{l}\int_0^l \bar{f}'(x)^2 dx\right] - \frac{1}{2}\frac{M^2+2}{M^2(M^2-1)^{5/2}}\beta\alpha^2 +$$

$$\frac{1}{4}\frac{M^4+(27/4)M^2+1}{M^2(M^2-1)^{9/2}}\beta^2\left[\alpha^2 - 6\left(\frac{1}{l^3}\right)\int_0^l \bar{f}(x)^2 dx\right] + \ldots \quad (22)$$

here $\bar{f}(l) = 0$.

The lift coefficient of a symmetrical airfoil can be obtained by use of the relation

$$c_L = (2/l)\int_0^l c_p \, dx = -(4/lU^2)\int_0^l \varphi_l \, dx \quad (23)$$

Thus at an angle of attack α:

$$c_L = \frac{4}{\sqrt{M^2-1}}\alpha - \frac{\beta}{2}\frac{M^2+2}{M^2(M^2-1)^{5/2}}\alpha + \frac{\beta^2}{4}\frac{M^4+(27/4)M^2+1}{M^2(M^2-1)^{9/2}}\alpha + \ldots \quad (24)$$

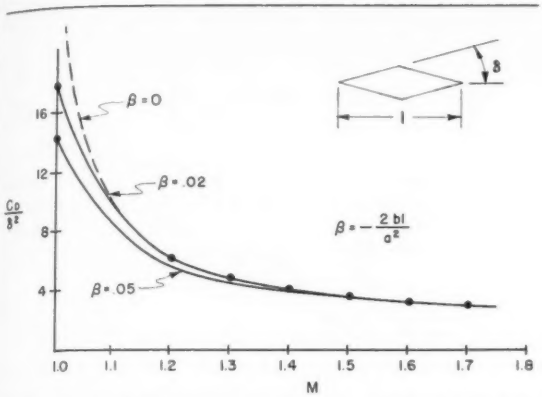

FIG. 7. c_D vs. M for diamond profile, at $\beta = 0.02$ and $\beta = 0.05$.

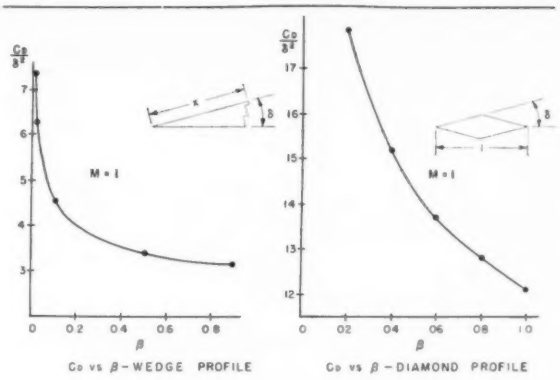

FIG. 8. c_D vs. β, at $M = 1$, for wedge and diamond.

Eqs. (18), (21), and (24) have been used to plot Figs. 3 and 7, in which c_D and c_L vs. M are represented at given values of β, for wedge and diamond profiles. The form of the above series indicates that the influence of the second and higher terms becomes appreciable only if $\beta \sim 0(M-1)$. Under actual conditions $\beta \lesssim 0.05$ [see end of Section (C, 2)].

(B) Computation of Aerodynamic Characteristics in the Transonic Range

(1) *Formulation of the Analytic Problem*

From Eqs. (18) to (24) it can be seen that, near $M = 1$, the series for c_p, c_D, and c_L diverge, as each term becomes infinite. It is shown in Appendix (2) that the series will converge, so long as $\beta < (M-1)^2$. If a representative value [see end of Section (C, 2)] of β—e.g., $\beta \sim 0.02$—is taken, the series expansions fail for $M \lesssim 1.14$, which means that the whole transonic regime must be represented in another manner. To investigate the transonic range, it is necessary to evaluate integrals (8) and (9), without making use of the benefits which an expansion in β may involve. In order to simplify the evaluation, the investigation will be restricted to diamond-shaped airfoil profiles, which can be considered composed of two wedges (see Fig. 5).

The present objective is, therefore, to compute the pressure distribution and the drag on a wedge profile of vertex angle δ and length x. Under these conditions, it is no longer profitable to make use of the extended definition of $f(x)$; but the actual integration limits have to be substituted in Eq. (8), explicitly. Thus, the integration in ξ and τ must be extended over the shaded area limited by the two "sound speed lines" going through P and the parabolic segment CD lying between them (see Fig. 1). The parabolic path of the leading edge is given by $\xi = -U\tau - (b/2)\tau^2$, and its intersections with the two sound speed lines $\xi = x \pm a(t-\tau)$ may be denoted by ξ_1, τ_1, and ξ_2, τ_2, respectively. It is appropriate to divide the area of integration into an upper triangular area and the rest of the domain, as indicated in Fig. 1. Thus, setting $x - \xi = \bar{\xi}$ and $f' = \delta$, Eq. (8) can now be written:

$$\varphi = -\frac{\delta}{\pi}\int_{t-\tau_1}^{t-\tau_2} d\bar{\tau} \int_{-a\bar{\tau}}^{x+U(t-\bar{\tau})+(1/2)\,b(t-\bar{\tau})^2} d\bar{\xi} \times \frac{U+b\,(t-\bar{\tau})}{\sqrt{\bar{\tau}^2 - \bar{\xi}^2/a^2}} - \frac{\delta}{\pi}\int_0^{t-\tau_2} d\bar{\tau} \int_{-a\bar{\tau}}^{a\bar{\tau}} d\bar{\xi}\, \frac{U+b(t-\bar{\tau})}{\sqrt{\bar{\tau}^2 - \bar{\xi}^2/a^2}} \tag{25}$$

In order to get the pressure distribution, relation (2) may again be used; φ_t is evaluated by differentiating Eq. (25) with regard to the upper and lower limits as well as under the integral sign; as a result of this, four line integrals and two surface integrals are obtained. Two of the line integrals cancel and a third one vanishes, so that finally:

$$\varphi_t = -\frac{\delta}{\pi}\int_{t-\tau_2}^{t-\tau_1} d\bar{\tau}\, \frac{[U+b(t-\bar{\tau})]^2}{\sqrt{\bar{\tau}^2 - (1/a^2)\,[x+U(t-\bar{\tau})+(b/2)(t-\bar{\tau})^2]^2}} - \frac{\delta b}{\pi}\int_{t-\tau_2}^{t-\tau_1} d\bar{\tau} \times \int_{-a\bar{\tau}}^{x+U(t-\bar{\tau})+(1/2)\,b(t-\bar{\tau})^2} \frac{d\bar{\xi}}{\sqrt{\bar{\tau}^2 - \bar{\xi}^2/a^2}} - \frac{\delta b}{\pi}\int_0^{t-\tau_2} d\bar{\tau} \int_{-a\bar{\tau}}^{a\bar{\tau}} \frac{d\bar{\xi}}{\sqrt{\bar{\tau}^2 - \bar{\xi}^2/a^2}} \tag{26}$$

While the third integral in Eq. (26) yields an elementary function, the first two can be reduced to combinations of complete and incomplete elliptic integrals of the first and second kinds. The pressure distribution following therefrom will be discussed later. Proceeding now to obtain the drag of the wedge profile, φ_t has to be integrated with regard to x, as indicated in Eq. (18). It can be shown that, putting $t = 0$, as before:

$$\int_0^x \varphi_t(x,0)dx = -\frac{\delta}{\pi}\int_{-\tau_2}^{-\tau_1} d\bar{\tau}\int_{-a\bar{\tau}}^{x\,-\,U\bar{\tau}\,+\,(1/2)\,b\bar{\tau}^2} d\bar{\xi}\,\frac{(U-b\bar{\tau})^2+b\,[x-\bar{\xi}-U\bar{\tau}+(b/2)\bar{\tau}^2]}{\sqrt{\bar{\tau}^2-\bar{\xi}^2/a^2}} -$$

$$\frac{\delta}{\pi}\int_0^{-\tau_2} d\bar{\tau}\int_{-a\bar{\tau}}^{+a\bar{\tau}} d\bar{\xi}\,\frac{(U-b\bar{\tau})^2+b[x-\xi-U\bar{\tau}+(b/2)\bar{\tau}^2]}{\sqrt{\bar{\tau}^2-\bar{\xi}^2/a^2}} \tag{27}$$

Differentiating Eq. (27) with regard to x again yields four line integrals and two surface integrals that after some calculation can be reduced to Eq. (26). This verifies Eq. (27), except for an integration constant which is determined by the condition that the drag has to vanish for $x = 0$.

(2) *Evaluation of Solution* (27)

To evaluate Eq. (27), the numerator of the integrand is split into two parts, one part depending on $\bar{\tau}$, the other on $\bar{\xi}$ only. In this way $\int_0^x \varphi_t\,dx$ is obtained as the sum of four double integrals, each of them containing $\bar{\xi}$ as well as $\bar{\tau}$ as integration variables. The integrations after $\bar{\xi}$ can be immediately evaluated and yield elementary functions. Upon substitution, the sum of the four outer integrals (over $\bar{\tau}$) yields, after introduction of the dimensionless quantities:

$$z = (b/a)\tau;\quad z_i = (b/a)\tau_i,\ i = 1, 2, 3, 4;\quad \beta = -2bx/a^2;\quad M = U/a \tag{28}$$

the following result:

$$-\,(\pi/\delta)\int_0^x \varphi_t\,dx \;=\; (J\;-\;L)(2a^2x/\beta) \tag{29}$$

here:

$$\left.\begin{aligned} J &= \int_{z_2}^{z_1} dz\,\frac{[M^2\beta-(1/2)\beta^2]+[(3/2)M\beta]z+(M^2)z^2+(3/2)Mz^3+(1/2)z^4}{\sqrt{(z_1-z)(z-z_2)(z-z_3)(z-z_4)}} \\ L &= \int_{z_2}^{z_1} dz\,\frac{[-(1/2)\beta^2]+(2M\beta)z+2[1+(\beta/2)-M^2]z^2-(2M)z^3-(1/2)z^4}{\sqrt{(z_1-z)(z-z_2)(z-z_3)(z-z_4)}} \end{aligned}\right\} \tag{30}$$

while $z_1 = -(M-1)+\sqrt{(M-1)^2+\beta}$, $z_2 = -(M+1)+\sqrt{(M+1)^2+\beta}$, $z_3 = -(M-1)-\sqrt{(M-1)^2+\beta}$, and $z_4 = -(M+1)-\sqrt{(M+1)^2+\beta}$; $z_1 > z_2 > z_3 > z_4$.

Both J and L are elliptic integrals of the same type, the numerator, say $R(z)$, and the denominator, say $P(z)$, being polynomials of fourth degree in z. The procedure by which either of the integrals is reduced consists of two steps. In the first step, the degree of the numerators of either J or L is reduced from four to two, by observing that

$$\int \frac{R(z)}{\sqrt{P(z)}}\,dz = \int \frac{d}{dz}[S(z)\sqrt{P(z)}]dz + \int \frac{T(z)}{\sqrt{P(z)}}\,dz$$

so that:

$$R \;=\; (1/2)SP' \;+\; S'P \;+\; T \tag{31}$$

where T is an unknown polynomial of degree two and S is an unknown polynomial of degree one. Since R and P are given polynomials of fourth degree, Eq. (31) yields five equations for the three unknown coefficients of T and the unknown two coefficients of S.

Thus, in Eq. (29), $J - L$ can be replaced by $\mathfrak{M}_1 - \mathfrak{M}_2$, where

$$\mathfrak{M}_i = \int_{z_2}^{z_1} dz\,\frac{A_i + H_iz + C_iz^2}{\sqrt{(z_1-z)(z-z_2)(z-z_3)(z-z_4)}};\quad i = 1, 2 \tag{32a}$$

In the second step, $\mathfrak{M}_i$ can be reduced by standard methods[6] to an expression of the form:

$$\mathfrak{M}_i \;=\; R_iK(k) \;+\; S_iE(k) \;+\; T_i\{(\pi/2) \;+\; [K(k) \;-\; E(k)]F(k',\,\theta) \;-\; K(k)E(k',\,\theta)\} \tag{32b}$$

Here the K or F, respectively, and the E are elliptic integrals of the first and second kinds. The R_i, S_i, and T_i may be expressed in terms of A_i, H_i, and C_i, and the latter ones again in terms of the coefficients in Eq. (30). With these substitutions $\mathfrak{M}_1$ and $\mathfrak{M}_2$ may be computed by means of Eq. (32b). Then the drag becomes, by use of Eqs. (29) and (32):

$$D' = \int_0^x \Delta p(x)\, f'(x)dx = \delta \int_0^x -\rho\varphi_t\, dx = \frac{2\delta^2 a^2 x\rho}{\pi\beta}\,(\mathfrak{M}_1 - \mathfrak{M}_2)$$

and

$$c_D = \frac{D'}{{}^1/_2\rho U^2 x} = \frac{4\delta^2}{\pi\beta M^2}\,(\mathfrak{M}_1 - \mathfrak{M}_2) \tag{33}$$

For arbitrary M and β, the quantities appearing in Eq. (32b) are given in Appendix (C).

As for all practical purposes $\beta \ll 1$, the evaluation of Eq. (33) is considerably expedited, if R_i, S_i, T_i, and the elliptic integrals, which according to Eq. (32b) compose $\mathfrak{M}_i$, are expanded in powers of $\beta^{1/4}$.

At $M = 1$, the expansion yields:

$$\left.\begin{aligned} R_1 &= \beta^{1/4}\frac{1}{\sqrt{2}}\left[-3 + \frac{1}{12}\beta^{1/2} + \ldots\right]; \qquad R_2 = \beta^{1/4}\frac{1}{\sqrt{2}}\left[-2 - \frac{5}{6}\beta^{1/2}\ldots\right] \\ S_1' &= \beta^{1/4}\frac{1}{\sqrt{2}}\left[6 + 3\,\frac{1}{24}\,\beta + \ldots\right]; \qquad S_2 = \beta^{1/4}\frac{1}{\sqrt{2}}\left[4 + \frac{19}{12}\beta + \ldots\right] \\ T_1 &= -6 + 4\beta \qquad\qquad ; \qquad T_2 = -4 \end{aligned}\right\} \tag{34a}$$

Expanding the elliptic integrals at $k = 1/\sqrt{2}$ and $\theta = \cot^{-1}(1/\sqrt{2})$, one gets:

$$\left.\begin{aligned} K &= \bar{K} + \frac{1}{4}(\bar{K} - 2\bar{E})\beta^{1/2} + \ldots 0(\beta) \\ E &= \bar{E} + \frac{1}{4}(\bar{K} - \bar{E})\beta^{1/2} + \ldots 0(\beta) \end{aligned}\right\} \tag{34b}$$

$$[\pi/2 + (K - E)F(k', \theta) - KE(k', \theta)] = (1/2\sqrt{2})\beta^{1/4}[(2\bar{E} - \bar{K}) - (1/6)\bar{K}\beta^{1/2} + \ldots]$$

here

$$\bar{K} = K(1/\sqrt{2}) \text{ and } \bar{E} = E(1/\sqrt{2})$$

Inserting Eq. (34) into Eqs. (32) and (33), one obtains at $M = 1$:

$$D = \rho\frac{\delta^2}{\pi}\,a^2\,\frac{2^{5/2}}{3}\,x\bar{K}\beta^{-1/4}\left(1 + \frac{21}{20}\,\frac{2\bar{E} - \bar{K}}{\bar{K}}\,\beta^{1/2} + \ldots\right) \propto (-b)^{-1/4}x^{+3/4} \tag{35a}$$

and

$$c_D = \frac{\delta^2}{\pi}\,\frac{2^{7/2}}{3}\,\bar{K}\beta^{-1/4}\left(1 + \frac{21}{20}\,\frac{2\bar{E} - \bar{K}}{\bar{K}}\,\beta^{1/2} + \ldots\right) \propto (-b)^{-1/4}x^{-1/4} \tag{35b}$$

since $\beta = -2bx/a^2$. Since

$$c_D(x) = 1/x\textstyle\int_0^x c_p(x)\delta\, dx \tag{35c}$$

substitution of Eq. (35b) yields:

$$c_p = \frac{\delta}{\pi}\,2^{3/2}\bar{K}\beta^{-1/4}\left[1 + \frac{7}{4}\,\frac{2\bar{E} - \bar{K}}{\bar{K}}\,\beta^{1/2} + \ldots\right] \propto (-b)^{-1/4}x^{-1/4} \tag{36a}$$

and

$$p_{surf} - p_0 = \rho\,\frac{\delta}{\pi}\,a^2 2^{1/2}\bar{K}\beta^{-1/4}\left[1 + \frac{7}{4}\,\frac{2\bar{E} - \bar{K}}{\bar{K}}\,\beta^{1/2} + \ldots\right] \tag{36b}$$

At any M, the pressure coefficient can be obtained by evaluating Eq. (26). Carrying out the inner integrations and introducing dimensionless variables yields:

$$c_p = \frac{2\delta}{\pi M^2}\int^{z_1} dz\,\frac{M^2 - 1/2\ \beta^2 + 2Mz + 1/2a^2z^2}{\sqrt{z^2 - (1/2\beta - Mz - 1/2z^2)^2}} \tag{36c}$$

Since Eq. (36c) has the same form as Eq. (32a), it can also be reduced to standard form [Eq. (32b)] and be evaluated in the same manner.

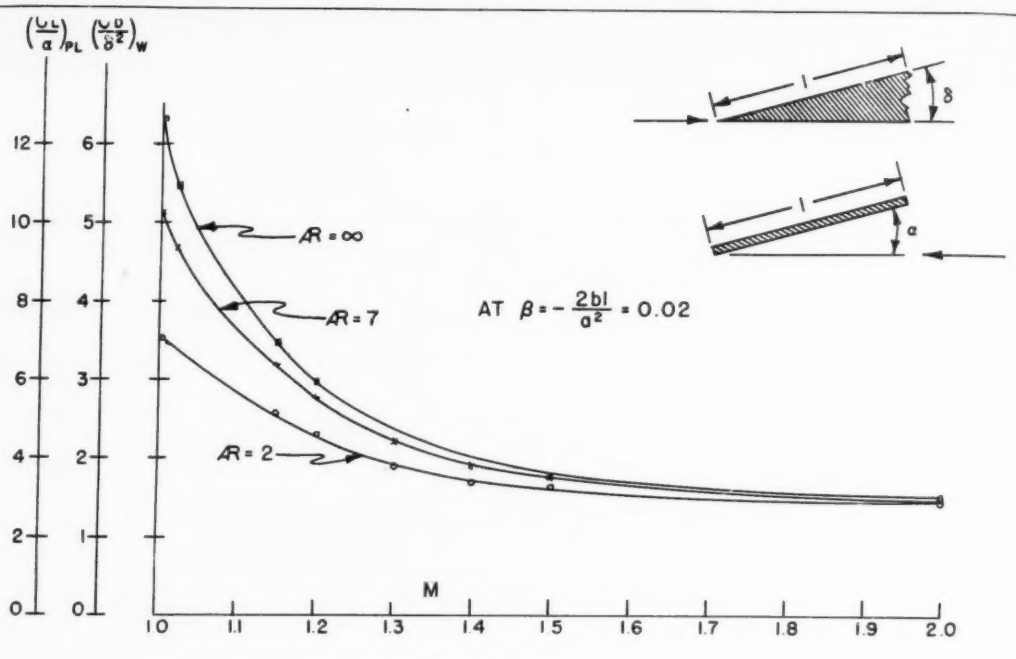
$\left(\frac{c_L}{\alpha}\right)_{PL}$ $\left(\frac{c_D}{\delta^2}\right)_W$
AR = ∞
AR = 7
AR = 2
AT $\beta = -\frac{2bl}{a^2} = 0.02$
M
1.0 1.1 1.2 1.3 1.4 1.5 1.6 1.7 1.8 1.9 2.0
FIG. 2
CD vs M — WEDGE CL vs M — FLAT PLATE

FIG. 9. c_D vs. M for finite wings of different A.R.'s.

(C) Physical Discussion of Results

(1) *The Theoretical Results at and near M = 1*

From Eq. (36a) it can be seen that at $M = 1$, the pressure becomes infinite, at the leading edge of the wedge profile as $x^{-1/4}$ for a given deceleration $(-b)$. Also, at any given station on the wedge surface, $x \neq 0$, p increases as $(-b)^{-1/4}$; for nearly constant speed (very small b), the representation becomes invalid.

It might be guessed from analogy to the stationary case that for subsonic velocities the pressure at the leading edge of a thin airfoil has a logarithmic infinity with x, and it can be seen from Eq. (16) that at supersonic velocities p remains finite. These features of $(p)_{(x=0)}$, for $M \gtrless 1$, can be *derived* from Eq. (26) after the inner integrals in Eq. (26) have been evaluated, and the outer integrals reduced to standard form.

From Eq. (35a), it can be seen that at $M = 1$, the drag of the wedge decreases with the length x of the wedge surface as $x^{3/4}$. From Eq. (18) it follows that, for supersonic velocities, the drag decreases, proportional to x. It can also be shown that for subsonic velocities, $D \sim x \, (\log x)$.

From Fig. 1 it can be seen by inspection that for any point P between L.E. and T.E., $0 < x < l$, the magnitude of the shaded area, changes continuously, as P moves through the x-axis, where $M = 1$ (i.e., where the sound speed lines are parallel to the tangent of the parabola). This is confirmed by investigating the expression (26) for φ_f—i.e., p, in which integrand and integration limits change continuously, by passing through the sound speed.

The singular point $x = 0$ is seen to be the only exception, as in the denominator of the line integral in Eq. (26), the term proportional $\bar{\tau}^2$ vanishes for $U = a$ and $x = 0$. Therefore, in the immediate vicinity of the leading edge of the wedge (or airfoil), the pressure distribution gradually changes its character, by passing through $M = 1$. This does not affect, however, the continuity of drag and lift, that as integrals over the p-distribution remain everywhere finite and change continuously by passing through the sound speed. But the slope of the c_D or c_L vs. M-curve experiences a discontinuity as shown in Figs. 3 and 7.

Eqs. (35b) or (33) and (18) have been used to plot in Fig. 3, c_D vs. M for a wedge profile of vertex angle δ, at several β-values. Since, in supersonic flow, the pressure distribution on the upper side of a wedge is the same as on the upper (or, except for the sign, on the lower) side of a flat plate of the same inclination, Fig. 3 represents at the same time the c_L vs. M-curve of a flat plate profile, at angle of attack $\alpha = \delta$, if the ordinate scale is changed. The curves in Fig. 3 expose the above-described features for c_D and c_L; for comparison the c_D or c_L vs. M-curve at constant speed ($\beta = 0$) is added.

Eqs. (36c) and (19) have been used to plot the pressure distribution along the surface of the wedge profile

(a) for a supersonic speed: $M = 1.3$, (b) for the sonic speed: $M = 1$, with $\beta = -2bx/a^2$ ranging from 0 . . . 0.03 (see Fig. 6). It is interesting to note how the pressure increases, near $M \sim 1$, at all stations of the surface, but particularly in the vicinity of the leading edge. These results should be regarded merely as qualitative indications.

Thus, these considerations have shown that the aerodynamic characteristics at supersonic speeds ($M - 1 > \sqrt{\beta}$) are hardly affected by β. But in the transonic range ($M - 1 < \sqrt{\beta}$), the theoretical values of c_p, c_D, and c_L, as computed by the linearized theory, depend strongly on the magnitude of the acceleration parameter. Since this theory is seen to become invalid in the limit of stationary motion at constant speed ($\beta = 0$), the results at small values of acceleration cannot be taken at face value. However, at high accelerations ($\beta \sim 0.02 \ldots 0.1$) these approximations become increasingly more valid, as shown in Section (C, 3). Thus, the spread of the c_D-curves, at various β, in the transonic range, may indicate that there the influence of acceleration is more essential than in the supersonic range.

(2) *The Drag of a Diamond Profile*

It remains to compute the drag of a diamond-shaped profile by adding the drag contributions originating from the two wedges of which the diamond is composed (see Fig. 5). This drag is given by:

$$D' = 2\int_0^l \Delta p\, f'(x)dx = -2\delta\rho\int_0^{l/2}\varphi_t\, dx + 2\delta\rho\int_{/,}^{l}\varphi_t\, dx$$

Dividing by $^1/_2\ \rho a^2 l$:

$$c_D = -(4\delta/la^2)\int_0^{l/2}\varphi_t\, dx + (4\delta/la^2)\int_{/2}^{l}\varphi_t\, dx \quad (37)$$

Now φ_t—i.e. c_p—can be obtained as the sum of the contributions to φ_t of two infinite wedges, wedge (I) starting at $x = 0$ and having vertex angle δ, and wedge (II) starting at $x = l/2$ and having vertex angle -2δ (see Fig. 5). For $0 < x < l/2$, only wedge (I) contributes.

Thus for $0 < x < l/2$: $\varphi_t = \varphi_t$, due to wedge (I), so that:

$$-\frac{4\delta}{la^2}\int_0^{l/2}\varphi_t\, dx = \frac{\delta^2}{\pi}\frac{2^{15/4}}{3}\bar{K}\beta^{-1/4} \times \left[1 + \left(\frac{21}{20\sqrt{2'}}\right)\left(\frac{2\bar{E} - \bar{K}}{\bar{K}}\right)\beta^{1/2} + \ldots\right] \quad (38)$$

here, as well as in the following $\beta = -2bl/a^2$, where l is the chord length of the diamond.

For $l/2 < x < l$, $\varphi_t = \varphi_t$, due to wedge (I) + φ_t, due to wedge (II), so that

$$\int_{l/2}^{l}\varphi_t\, dx = \int_{l/2}^{l}\varphi_t\, dx \text{ for wedge (I)} + \int_{l/2}^{l}\varphi_t\, dx \text{ for wedge (II)}$$
$$= \int_0^l(\varphi_t\, dx)\text{I} - \int_0^{l/2}(\varphi_t\, dx)_I + \int_{l/2}^{l}(\varphi_t\, dx)_{II}$$

Substituting for $(\varphi_t)_I$ and $(\varphi_t)_{II}$:

$$\frac{4\delta}{la^2}\int_{l/2}^{l}\varphi_t\, dx = \frac{\delta^2}{\pi}\frac{2^{15/4}}{3}(3 - 2^{3/4})\bar{K}\beta^{-1/4} \times \left[1 - (.214)\left(\frac{2\bar{E} - \bar{K}}{\bar{K}}\right)\beta^{1/2} + \ldots\right] \quad (39)$$

Adding Eqs. (38) and (39):

$$c_D = \frac{\delta^2}{\pi}\,10.4\,\bar{K}\beta^{-1/4}\left[1 + 2.76\left(\frac{2\bar{E} - \bar{K}}{\bar{K}}\right)\beta^{1/2} + \ldots\right] \quad (40)$$

Eqs. (40) and (21) have been used to plot c_D vs. M, at $\beta = 0.02$ and 0.1, for diamond profiles. Assuming that the greatest accelerations, which are nowadays available with rockets or otherwise, are of the order of $5.10^3 \ldots 10^4$ ft. per sec.,[2] the wings (e.g., $l \sim 3$ ft.) of such rockets will experience β-values of the indicated order. It is seen from Fig. 7 that also for diamond-shaped profiles, (c_D/δ^2) has a marked maximum at $M = 1$, but passes continuously through the transonic range, according to these considerations. It will be shown in another paper that in the subsonic range the drag falls off with decreasing M, until at very low speeds it reaches a value which is equal to the product of deceleration times "apparent mass."

Naturally the (c_L/α) vs. M-curve, plotted in Fig. 3, holds also for diamond profiles, as the lift coefficient of symmetrical airfoils does not depend on the profile form.

Fig. 8 shows how c_D varies with the acceleration parameter β, at $M = 1$.

(3) *Concluding Remarks*

Extension to Finite Aspect Ratios. A Validity Criterion.—At the end of these considerations, an attempt shall be made to find out to what extent these results may be expected to give a quantitative account of actual conditions. Before this is done, it may be appropriate to mention an extension of the present results to wings of finite aspect ratio and to discuss the results together.

The aerodynamic characteristics for rectangular wings of finite aspect ratio have been derived by the authors* by using the method of "retarded potentials" in an x-y-t-space. While the derivations of this investigation must be left for a separate paper, some analytical results have been plotted in Fig. 9, representing c_D vs. M for different aspect ratios, at an acceleration parameter $\beta = 0.02$. The maximum of the curves at $M = 1$ is seen to become less and less pronounced, as the aspect ratio decreases. This is further elucidated by Fig. 10, representing c_D vs. aspect ratio, at $M = 1$, for different β-values; it is seen that $c_D \to 0$ for A.R. $\to 0$, so long as $\beta \neq 0$. For $\beta = 0$, c_D becomes logarithmically infinite for all finite A.R. $\neq 0$.

* See a forthcoming report of the authors to O.N.R.

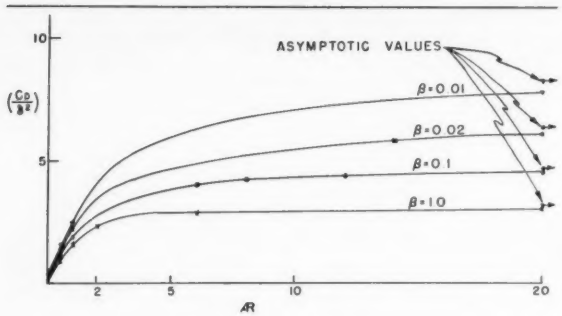

FIG. 3
C_D vs AR—WEDGE AT $M=1$

FIG. 10. c_D vs. A.R., at $M = 1$, for different β-values.

Since the results of the present investigation are obtained by a linearized approximation, they may be considered valid so long as the (velocity or) pressure-disturbance produced by the airfoil is small compared to the undisturbed (velocity or) pressure; in the present case the undisturbed quantities are (the sonic flight speed or) the dynamic pressure at the leading edge. In other words, it should be $(\Delta p/{}^1\!/_2\rho a^2) = c_p \ll 1$.

This criterion cannot be expected to be fulfilled at any station on the airfoil surface, separately. (At the leading edge, the pressure has been shown to grow beyond bound at $M = 1$, similarly as it does in the thin airfoil theory of the subsonic regime.) However, the criterion should be indicative, if an average of the pressure distribution over the chord length is taken or, in the three-dimensional case, an average over the plan form. Therefore, a more appropriate form of the criterion is

$$\bar{c}_p \ll 1$$

where $\bar{c}_p = (1/l)\int_0^l c_p(x)\,dx$ or $\bar{c}_p = (1/A)\int_A\int c_p\,dx\,dy$, respectively. But according to definition (35c), $\bar{c}_p = c_D/\delta$, which is shown in Fig. 9 for A.R. = 2, 7, and ∞.

For instance, if a very thin supersonic airfoil of 5 per cent thickness ratio is taken, the curves in Fig. 9 indicate at $M = 1$ for $\beta = 0.02$: $\bar{c}_p \sim 0.25$ for A.R. ∞; ~ 0.2 for A.R. 7; and ~ 0.14 for A.R. 2.

Thus, the above results might be considered as reasonably valid, even at $M = 1$. The smaller the aspect ratio is, the better is the approximation. Or, to put it more carefully: if quantitative results are desired, it might be worth while to develop a second order theory—e.g., along lines suggested by the paper of Lin, Reissner, and Tsien.[3]

Appendix (1)—Proof of Relation (12a)

If α is a sufficiently small quantity, then:

$$\frac{1}{\sqrt{(M+\alpha)^2-1}} = \sum_{k=0}^{\infty} \frac{\alpha^k}{k!}\frac{\partial^k}{\partial M^k}\left(\frac{1}{\sqrt{M^2-1}}\right) \quad (1)$$

On the other hand:

$$\frac{1}{\sqrt{(M+\alpha)^2-1}} = \frac{1}{\sqrt{M^2-1}} \times \left[1 - 2\left(-\frac{M}{\sqrt{M^2-1}}\right)\left(\frac{\alpha}{\sqrt{M^2-1}}\right) + \left(\frac{\alpha}{\sqrt{M^2-1}}\right)^2\right]^{-1/2} \quad (2)$$

By means of the formula

$$(1 - 2zh + h^2)^{-1/2} = \sum_{k=0}^{\infty} P_k(z)h^k$$

where Pk is the Legendre polynomial of degree k, Eq. (2) can be expanded as follows:

$$\frac{1}{\sqrt{(M+\alpha)^2-1}} = \sum_{k=0}^{\infty}\left(\frac{\alpha^k}{(M^2-1)^{(k+1)/2}}\right) \times P_k\left(-\frac{M}{\sqrt{M^2-1}}\right) \quad (3)$$

Comparing coefficients in Eqs. (1) and (3):

$$\frac{\partial^k}{\partial M^k}\left(\frac{1}{\sqrt{M^2-1}}\right) = \left(\frac{k!}{(M^2-1)^{(k+1)/2}}\right) \times P_k\left(-\frac{M}{\sqrt{M^2-1}}\right), \text{ q. e. d.}$$

Appendix (2)—Radius of Convergence of the Series in Powers of β, Eqs. (17) to (24)

If in Eq. (30) the new variable of integration y is introduced, defined by $y = ({}^1\!/_2\beta - Mz - {}^1\!/_2z^2)/z$, a straightforward calculation shows that

$$J = \frac{\pi}{2}M\beta - \frac{3\pi}{2}M + \int_{-1}^{+1} dy\,\frac{(My+2y^2)\sqrt{(M+y)^2+\beta}}{\sqrt{1-y^2}}$$

and

$$L = \pi M - 2\int_{-1}^{+1} dy\,\sqrt{(M+y)^2+\beta}\,\sqrt{1-y^2} + \beta\int_{-1}^{+1} dy\,\frac{\sqrt{1-y^2}}{\sqrt{(M+y)^2+\beta}}$$

If $|\beta| < (M-1)^2$, the expression $\sqrt{(M+y)^2+\beta}$ may be expanded in a power series in β valid throughout the range of integration. The power series for J and L and therefore the power series for the drag may then be obtained by means of term-by-term integration. Thus it is seen that the power series, as given in Section (A, 2), must converge for $|\beta| < (M-1)^2$.

Appendix (3)

Computation of the quantities appearing in Eq. (32) yields:

$$R_1 - R_2 = \left\{[(M-1)^2+\beta][(M+1)^2+\beta]\right\}^{-1/4} \times \left\{A_{1-2} + (\sqrt{M+1)^2+\beta} - (M+1)]H_{1-2} + [(M+1)^2 - 2M\sqrt{(M+1)^2+\beta} - \sqrt{[(M+1)^2+\beta][(M-1)^2+\beta]}C_{1-2}\right\}$$

$$S_1 - S_2 = 2\left\{[(M-1)^2+\beta][(M+1)^2+\beta]\right\}^{1/4} C_{1-2}$$

$$T_1 - T_2 = 2\left\{H_{1-2} - 2MC_{1-2}\right\}$$

where:

$$A_{1-2} = \frac{7M^2\beta - 2\beta^2}{6}, \quad H_{1-2} = \frac{-2M^3 + 10M\beta + 2M}{6}$$

$$C_{1-2} = \frac{-M^2 + 2\beta + 4}{6}$$

Furthermore:

$$k^2 = {}^1/_2 - \frac{(M^2-1)+\beta}{2\sqrt{[(M-1)^2+\beta][(M+1)^2+\beta]}}$$

$$n = \operatorname{cotg}\theta = \frac{2 + \sqrt{(M-1)^2+\beta} - \sqrt{(M+1)^2+\beta}}{2\sqrt{(M+1)^2+\beta}}$$

References

[1] Garrick, I. E., and Rubinow, S. I., *Theoretical Study of Air Forces on an Oscillating or Steady Thin Wing in a Supersonic Main Stream*, N.A.C.A. T.N. No. 1383, July, 1947.

[2] Gardner, C. S., Ludloff, H. F., and Reiche, F., *Drag of an Airfoil in Accelerated Supersonic Flight*, Journal of Applied Physics, Vol. 19, No. 12, December, 1948.

[3] Linn, C. C., Reissner, E., and Tsien, H. S., *On Two-Dimensional Non-Steady Motion of a Slender Body in a Compressible Fluid*, Journal of Mathematics and Physics, Vol. 27, No. 3, October, 1948.

[4] Robinson, A., and Young, A. D., *Note on the Application of the Linearized Theory for Compressible Flow to Transonic Speeds*, Cranfield College of Aeronautics, Report No. 2, January, 1947.

[5] Chang, C. C., *The Transient Reaction of an Airfoil due to Change in Angle of Attack at Supersonic Speed*, Journal of the Aeronautical Sciences, Vol. 15, No. 11, November, 1948.

[6] Goursat, E., and Hedricks, E. R., *Mathematical Analysis*, pp. 226–236; Ginn and Company, Boston, 1902.

Theoretical Lateral-Stability Derivatives for Wings at Supersonic Speeds

(*Continued from page 46*)

[3] Jones, Arthur L., and Alksne, Alberta, *The Damping Due to Roll of Triangular, Trapezoidal, and Related Plan Forms in Supersonic Flow*, N.A.C.A. T.N. No. 1548, 1948.

[4] Ribner, Herbert S., and Malvestuto, Frank S., Jr., *Stability Derivatives of Triangular Wings at Supersonic Speeds*, N.A.C.A. T.N. No. 1572, 1948.

[5] Jones, Arthur L., Spreiter, John R., and Alksne, Alberta, *The Rolling Moment Due to Sideslip of Triangular, Trapezoidal, and Related Plan Forms in Supersonic Flow*, N.A.C.A. T.N. No. 1700, 1948.

[6] Harmon, Sidney M., *Stability Derivatives of Thin Rectangular Wings at Supersonic Speeds. Wing Diagonals Ahead of Tip Mach Lines*, N.A.C.A. T.N. No. 1706, 1948.

[7] Malvestuto, Frank S., Jr., and Margolis, Kenneth, *Theoretical Stability Derivatives of Thin Sweptback Wings Tapered to a Point with Sweptback or Sweptforward Trailing Edges for a Limited Range of Supersonic Speeds*, N.A.C.A. T.N. No. 1761, 1949.

[8] Jones, Arthur L., and Alksne, Alberta, *The Yawing Moment Due to Sideslip of Triangular, Trapezoidal, and Related Plan Forms in Supersonic Flow*, N.A.C.A. T.N. No. 1850, 1949.

[9] Soulé, Hartley A., *Influence of Large Amounts of Wing Sweep on Stability and Control Problems of Aircraft*, N.A.C.A. T.N. No. 1088, 1946.

[10] Ribner, Herbert S., *The Stability Derivatives of Low-Aspect-Ratio Triangular Wings at Subsonic and Supersonic Speeds*, N.A.C.A. T.N. No. 1423, 1947.

[11] Tosti, Louis P., *Low-Speed Static Stability and Damping-in-Roll Characteristics of Some Swept and Unswept Low-Aspect-Ratio Wings*, N.A.C.A. T.N. No. 1468, 1947.

[12] Toll, Thomas A., and Queijo, M. J., *Approximate Relations and Charts for Low-Speed Stability Derivatives of Swept Wings*, N.A.C.A. T.N. No. 1581, 1948.

[13] Goodman, Alex, and Fisher, Lewis R., *Investigation at Low Speeds of the Effect of Aspect Ratio and Sweep on Rolling Stability Derivatives of Untapered Wings*, N.A.C.A. T.N. No. 1835, 1949.

[14] Bird, John D., *Some Theoretical Low-Speed Span Loading Characteristics of Swept Wings in Roll and Sideslip*, N.A.C.A. T.N. No. 1839, 1949.

[15] Fisher, Lewis R., *Approximate Corrections for the Effects of Compressibility on the Subsonic Stability Derivatives of Swept Wings*, N.A.C.A. T.N. No. 1854, 1949.

[16] Spreiter, John R., *Aerodynamic Properties of Cruciform-Wing and Body Combinations at Subsonic, Transonic, and Supersonic Speeds*, N.A.C.A. T.N. No. 1897, 1949.

[17] Lomax, Harvard, and Heaslet, Max. A., *Damping-in-roll Calculations for Slender Swept-Back Wings and Slender Wing-Body Combinations*, N.A.C.A. T.N. No. 1950, 1949.

Services of the Libraries of the Institute of the Aeronautical Sciences

The services of the Libraries are available to all members of the Institute, to Corporate Members, to advertisers in the AERONAUTICAL ENGINEERING REVIEW and AERONAUTICAL ENGINEERING CATALOG, and, under usual library limitations, to the public. Four specialized services are available.

The Paul Kollsman Lending Library

This lending library service makes available, *without charge*, the latest and more important aeronautical books.

Members may request the loan of any aeronautical or technical book they wish to borrow. Through an exchange agreement with the Engineering Societies Library, any book on general engineering may be borrowed from its great collection of over 160,000 volumes.

A photostating service is available at usual library rates.

Applications for membership in the library and further information will be sent on request.

The W. A. M. Burden Reference Library

This reference library contains over 12,000 aeronautical books, magazines, pamphlets, and reports gathered from world-wide sources and is one of the most complete aeronautical libraries in the world. Material from this library is not available for loan but may be used for reference purposes.

The Pacific Aeronautical Library

7660 Beverly Boulevard
Los Angeles 36, California

Established in cooperation with the aircraft companies the library serves. The leading aircraft companies in or near Los Angeles participate in its support and operation.

This service library for aeronautical research is available to the public for reading privileges. Source material includes aerodynamic and structural research reports, as well as books on drafting, production methods, history, and allied sciences. It furnishes books, periodicals, and pamphlet material to the participating aircraft companies to supplement their engineering libraries.

Technical Information Service

This service has experienced personnel under the supervision of trained aeronautical engineers to compile any information desired. The services range from listing specialized reference books to the preparation of exhaustive bibliographies, digesting of reports, and general surveys of any aeronautical subject. Some of the available services are:

Bibliographies on any aeronautical subject.
Reports on any aeronautical subject.
Digests of aeronautical books, papers, periodicals, and references.
Translations.
Engineering investigations of special aeronautical subjects.
Biographies of individuals engaged in aeronautics.
Photostats of any aeronautical or general engineering material.
Microfilms made on special order.
Photographs made from the Institute's photographic collection.
Drawings and tracings made.

In addition to the services mentioned any commission which comes within the scope of the Service will be accepted. Special arrangements may be made for work requiring several weeks or months.

Translators are available for accurate transcriptions of all foreign language data. Translations are carefully edited by trained engineers.

Reproductions of any material in the collections of the Institute may be ordered at standard photostat rates.

INSTITUTE OF THE AERONAUTICAL SCIENCES, INC.
2 EAST 64th STREET, NEW YORK 21, N.Y.

Readers' Forum

BRIEF REPORTS of investigations in the aeronautical sciences and discussions of papers published in the JOURNAL will be presented in this special department. The publication will be completed approximately 6 to 8 weeks after receipt of the material. No proof will be sent to the authors. The Editorial Committee does not hold itself responsible for the opinions expressed by the correspondents. Contributions should not exceed 800 words in length.

Supersonic Airfoils Simplified

James E. Broadwell
Department of Aeronautical Engineering, University of Michigan, Ann Arbor, Mich.
October 25, 1949

REFERENCE IS MADE to the simplified "Approach to Supersonic Airfoil Theory" of W. E. Strohmeyer and D. R. Gero in the August issue, as corrected in the October issue (JOURNAL OF THE AERONAUTICAL SCIENCES). The following simpler and still more direct approach has been found particularly well suited to undergraduate instruction because of the easy visualization of the geometrical concepts involved. The customary symbols are employed, as noted in the accompanying sketch.

It is assumed as usual that the general flow conditions at the given airfoil section are known and two-dimensional in character. The figure shows a simple example at $M = \sqrt{2}$; a thin, flat plate moving horizontally through the air at a small angle of attack α. Consider what has happened since the LE was one chord length back of where the TE is now. At that moment, pressure impulses traveled out from the LE' in all directions, relative to the air at a rate of V/M ft. per sec.; and, in the time required for the wing to go a distance $2c$, will have reached the circumference of a circle of radius $c\sqrt{2}$. Similar circles could be drawn from all other points through which the LE has passed, defining a zone limited by a common tangent line (the so-called Mach line) in this case at 45° to the direction of motion, as shown.

Consider the air now as in motion relative to the airfoil's lower surface. By construction, the pressure and deflection of air (because of its reaction on the airfoil surface) are confined to the region above and to the right of the line LE-A extended, because only within that zone is it possible for a disturbance to be transmitted. A particle of air striking directly under the LE will be deflected out of its original path through the angle α, but will have no immediate effect on particles still farther below. Particles of air which have gone before, however, have made it possible for all the air in the triangle LE-TE-A to be similarly deflected and, for negligible changes in density, it is uniformly so deflected. Furthermore, due to the weak oblique shock wave and small deflection, the longitudinal component of speed in this triangle is still approximately V.

The total section of air (normal to the direction of motion) acted upon over a unit of span is then TE-A or approximately c; the mass of air acted upon is ρVc slugs per sec., and the downward velocity imparted to it is $V\alpha$. The rate of change of momentum per sec., constituting the normal force for the lower surface (lbs. per ft. of span), is

$$F_l = \rho V^2 c\alpha = 2qc\alpha \tag{1}$$

The surface pressure per unit area is then F_l/c, and the gage pressure coefficient

$$p/q = F_l/cq = 2\alpha \tag{2}$$

Similar analysis holds for the upper surface, the pressure there being numerically equal but negative. Thus the section lift coefficient (substantially equal to the normal force coefficient):

$$C_l = (F_l - F_u/cq) = 4\alpha \tag{3}$$

It must be noted that Eqs. (2) and (3) are valid for the assumed $M = \sqrt{2}$ only. However, it is clear from the same principles that in any case the length of the line TE-A, and hence the reacting force, will be proportional to $\tan\mu$, which in this case happened to be unity. As $\tan\mu = 1/\sqrt{M^2 - 1}$, the final equations for pressure and lift (for $\alpha \ll \mu$) become:

$$p/q = (2\alpha/\sqrt{M^2 - 1}) \tag{4}$$

$$C_l = (4\alpha/\sqrt{M^2 - 1}) \tag{5}$$

In Eq. (4), α is considered negative when in a direction to produce negative p. The corresponding drag (neglecting surface friction) is then simply the rearward component of the normal force, or approximately in this case:

$$C_{dw} = C_l\alpha = (4\alpha^2/\sqrt{M^2 - 1}) \tag{6}$$

Here the subscript w indicates that it is wave drag, because the actual energy loss making up this element of the drag occurs in two oblique shock waves, one below the leading edge (practically coincident with the line LE-A) and a similar one above the trailing edge.

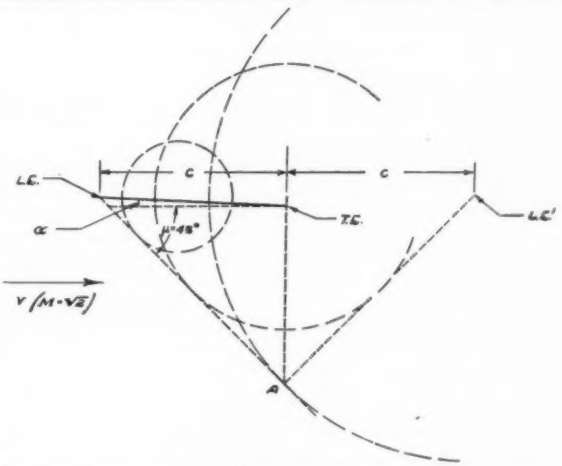

The same principles and the same result, expressed in Eq. (4) hold for *any* small increment of surface in two-dimensional flow. Hence, aerodynamic forces on finitely thick or curved surfaces complying with these general conditions can be found by simple summation or integration of the pressure times each increment of area involved. For a cambered airfoil of finite thickness with sharp LE and TE, C_l integrates to the same form as Eq. (5) if α is taken as the angle of attack of a straight line joining the LE and TE.

Corrections for sweep or tip loss are negligible for small LE sweep angle (up to about 10°) and for tips cut back at approximately the Mach angle. The theory becomes increasingly inaccurate at $M \to 1$, and in any case where the distance from the given airfoil section to the tip is less than $c/\sqrt{M^2 - 1}$. Subject to these and other minor qualifications, there is no induced angle in the sense employed in low-speed airfoil theory, and no direct

effect of aspect ratio. Thus wave drag pertains to thickness as well as to lift (angle-of-attack), and can be superimposed from results of separate computations. From test data thus far available, frictional drag appears to be of the same order of magnitude as under subsonic conditions.

Unsteady Flow Theory in Dynamic Stability

John W. Miles
Department of Engineering, University of California at Los Angeles
August 22, 1949

IN A PAPER delivered at a recent I.A.S. meeting,[1] I. C. Statler concluded that "unsteady flow effects are not important in the calculation of the dynamic stability and response of high-speed aircraft." With this broad conclusion, we cannot agree, and we wish to point out (what we regard as) certain fallacies in both the interpretation of the experimental data and the theoretical arguments presented in his paper. At the same time, we wish to modify some earlier predictions of our own.[2]

In calculating the dynamic stability derivatives, we may generally assume that the reduced frequency $k(=\omega c/2U)$ is less than 0.1. It follows that we may neglect terms of order k or higher in the aerodynamic forces in phase with displacements or accelerations, since they are to be compared with aerodynamic terms of order, zero, and the very large mechanical inertia terms, respectively. In the case of the aerodynamic forces in phase with the velocities, however, we must consider all terms of order k (*including terms of order* k log k), and it follows that the first-order effects of unsteady flow considerations will manifest themselves only in the damping terms. Moreover, in a system which is sufficiently underdamped to exhibit marked resonances, damping exerts only a second-order effect on the response of the system away from resonance, which will be governed by displacement or "spring" forces at lower frequencies and inertia forces at higher frequencies, whereas the magnitude of the resonant response is critically dependent on damping. Hence, the effects of discrepancies between the predictions of steady and unsteady flow theory as to the dynamic response of a system must be inferred from its behavior in the vicinity of resonance. Examination of Statler's results reveals that this is indeed the case, albeit he draws his conclusions from the behavior at the higher frequencies.

In two recent discussions in these columns, we have presented the first-order (in frequency) results for two-dimensional, thin airfoils in subsonic flow.[2, 3] (The first-order results for supersonic flow had been given earlier, for both the two- and three-dimensional cases.[4, 5]) These results indicate that the damping moment due to rotary motion (i.e., the *total* component of moment in phase with the angular velocity) is of order k log k for sufficiently small k, so that the pitch-damping derivative becomes infinite as log k when k approaches zero, indicating two-dimensional, unsteady flow considerations to be increasingly important (in determining the *damping per cycle*) as k is decreased, at least if strip theory is used, as in Statler's calculations. Moreover, the results of reference 3 indicate that this logarithmic term requires a compressibility correction factor of $(1 - M^2)^{-3/2}$ rather than the usual $(1 - M^2)^{-1/2}$. Unfortunately, as shown by Jones[6] and Reissner,[7] strip theory is completely inadequate for the treatment of unsteady flow effects at extremely low frequencies. Indeed, the reduction of Reissner's results for small k reveals that a term k log $(k\,AR)$, where AR is the aspect ratio, must be subtracted from the term k log k in the two-dimensional result, whence the term log k in the pitch-damping derivative is replaced by the considerably smaller (in magnitude) term log AR, and there is no singularity at $k = 0$. (There are, of course, additional aspect ratio corrections.) It follows that the numbers (predicting a large reduction in damping) cited by us in reference 3 are far from realistic and that Statler's use of strip theory cannot be a valid basis for any general conclusion. Nevertheless, an investigation of a conventional, subsonic configuration of a low aspect ratio tail aft of a straight wing based on the results of references 3 and 7, reveals that the only important unsteady flow effect appears in the "complex downwash lag" at the tail, in agreement with Statler's conclusion. (This investigation was carried out as a part of a more general study being conducted at the North American Aerophysics Laboratory.) However, this conclusion cannot be extended to such configurations as the canard or the flying wing or to any configuration in supersonic flow without further analysis, and, in particular, it appears that unsteady flow considerations will exercise a profound effect on the pitch damping of a flying wing in either subsonic or supersonic flow. Moreover, unsteady flow effects, particularly the complex sidewash correction, may be expected to exercise a pronounced effect on the lateral damping characteristics of a vertical fin, as implied by the tendency of many high-speed, jet aircraft (with fins designed on the basis of steady flow theory) to "snake." Thus, while we should agree with Statler's results for the particular configuration which he considered, we cannot agree with his conclusion that this happy state of affairs can be anticipated generally.

As previously pointed out,[2, 3] one of the errors in applying steady flow theory to unsteady flows is the failure of the former to include the term $\rho(\partial\phi/\partial t)$ in the Euler equation for the pressure. This same objection must be made to Statler's analysis of the oscillating fuselage. The potential given by the Munk theory[8] for a slender body of revolution is indeed valid for nonsteady flow, but the lift per unit length on a body of revolution is

$$\frac{\partial L(x,\,t)}{\partial x} = \rho U^2\left(\frac{\partial}{\partial x} + \frac{1}{U}\frac{\partial}{\partial t}\right)\left[\frac{S(x)w(x,\,t)}{U}\right] \tag{1}$$

where $w(x, t)$ is the instantaneous downwash (positive down) and $S(x)$ is the cross-sectional area at x. (We hope to discuss this situation more extensively in a future paper.) The operation of time differentiation on that part of $w(x, t)$ in phase with the displacement evidently gives rise to a damping force. If q is the angular velocity, l the length, and S_0 the base area, the damping derivative due to an oscillation about a point a aft of the nose, is found to be given by

$$\partial M/[\partial(ql/U)] = -2(\rho U^2/2)S_0 l\left(1 - \frac{a}{l}\right)^2 \tag{2}$$

The result obtained by Statler (which, incidentally, retains some terms not justified by slender body theory) is appropriate to flight along a curved flight path at constant angle of attack, but not to the case of oscillation about a straight flight path. Indeed, it is the confusion of these two situations which has been primarily responsible for the failure to account correctly for the effects of unsteady flow in the calculation of dynamic stability derivatives.

We do not wish to appear unduly critical of Statler's paper and remark that the errors we have discussed are extant in much of the antecedent work on the same subject. There has been a good deal of specious reasoning relative to nonstationary processes in moving reference frames; in many cases this may not have led to serious error, but it may be recalled that Zeno's sophistry with respect to time-dependent phenomena did not, in fact, prevent Achilles from catching the tortoise nor the arrow from catching Achilles.

References

[1] Statler, I. C., *Dynamic Stability at High Speeds from Unsteady Flow Theory*, New York, N.Y. (January 24–27, 1949); I.A.S. Preprint 187.

[2] Miles, J. W., *Quasi-Stationary Thin Airfoil Theory*, Journal of the Aeronautical Sciences, Vol. 16, No. 7, p. 440, July, 1949.

[3] Miles, J. W., *Quasi-Stationary Airfoil Theory in Compressible Flow*, Journal of the Aeronautical Sciences, Vol. 16, No. 8, p. 509, August, 1949.

[4] Miles, J. W., *The Aerodynamic Forces on an Oscillating Airfoil at Supersonic Speeds*, Journal of the Aeronautical Sciences, Vol. 14, No. 6, p. 356, Eqs. (A2), June, 1947.

[5] Miles, J. W., *On Harmonic Motion at Supersonic Speeds*, Journal of Aeronautical Sciences, Vol. 16, No. 6, pp. 378–379, June, 1949.

[6] Jones, R. T., *The Unsteady Lift of a Wing of Finite Aspect Ratio*, N.A.C.A. T.R. No. 681 (1940).

[7] Reissner, E., *Effect of Finite Span on the Airload Distributions for Oscillating Wings—I*, N.A.C.A. T.N. No. 1194 (1947).

[8] Munk, M., *The Aerodynamic Forces on Airship Hulls*, N.A.C.A. T.R. No. 184 (1924).

Stability of Sandwich Plates in Combined Shear and Compression

P. P. Bijlaard
Professor, Institute of Technology, Delft, Holland, on leave; Associate Professor, Cornell University, Ithaca, N.Y.
September 23, 1949

After he had written his Reader's Forum item published on pages 573–574 of the September issue of the JOURNAL OF THE AERONAUTICAL SCIENCES, two other papers on the same subject which substantiate his conclusions came to the writer's knowledge. In references 1 and 2 the shear buckling of infinitely long, simply supported sandwich plates is investigated by the energy method. Though this method gives somewhat too high critical stresses, these authors find a close agreement between their values and those of the present writer's method, which is either exact or conservative, so that both solutions are substantially accurate.

In reference 1 interaction curves for combined loading in shear and compression were derived from an earlier paper by van Vijngaarden. For shear and longitudinal compression they prove to be approximated by a parabola, which was known already to obtain for homogeneous plates.[3]

That the parabola also holds true for sandwich plates is demonstrated directly by the writer's method, and it can be shown to hold exactly for case (2). With a ratio $P_x/S = \gamma$ between the compression P_x in longitudinal (X-) direction of the plate and the shear S, both per unit width, the critical shear is

$$S_{cr.} = S_0 + (S_1^{-1} + S_2^{-1})^{-1} \qquad (1)$$

in which S_0 is the critical shear of the faces; S_1 obtains for a sandwich plate with infinite transverse shearing rigidity (case 1) and S_2 if only the shear modulus G_c of the core has a finite value (case 2). All these values refer to the same ratio $\gamma = P_x/S$. Values S_0 and S_1 follow from the theory of homogeneous plates. Value S_2 follows from the differential equation for case (2), being here[4]

$$[(h_c + t_f)^2 G_c/h_c]\nabla^2 w - P_{x2}\frac{\partial^2 w}{\partial x^2} + 2S_2\frac{\partial^2 w}{\partial x \partial y} = 0 \qquad (2)$$

With $w = Ye^{i\epsilon x}$ and $Y = e^{i\beta y}$ Eq. (2) yields

$$\beta_{1,2} = \epsilon\left[-\frac{h_c}{(h_c + t_f)^2}\frac{S_2}{G_c} \pm \left\{\left[\frac{h_c}{(h_c + t_f)^2}\frac{S_2}{G_c}\right]^2 + \frac{h_c}{(h_c + t_f)^2}\frac{P_{x2}}{G_c} - 1\right\}^{1/2}\right] \qquad (3)$$

while

$$Y = C_1 e^{i\beta_1 y} + C_2 e^{i\beta_2 y} \qquad (4)$$

The boundary conditions along the long sides $y = \pm b/2$ lead to the condition

$$(\beta_2 b/2) = (\beta_1 b/2) + n\pi \qquad (5)$$

With $\epsilon = \pi/L$, in which L is the half-wave length in X-direction, and with $n = 1$, Eq. (5) yields

$$\left[\frac{h_c}{(h_c + t_f)^2}\frac{S_2}{G_c}\right]^2 + \frac{h_c}{(h_c + t_f)^2}\frac{P_{x2}}{G_c} = 1 + \frac{L^2}{b^2} \qquad (6)$$

which, according to Eqs. (33). p. 86, and (15), p 189 of reference 5, may be written as

$$(S_2/S_{2cr.})^2 = 1 - (P_{x2}/P_{x2cr.}) \qquad (7)$$

in which $S_{2cr.}$ and $P_{x2cr.}$ obtain for shear alone or compression alone. Hence, for case (2) the parabolic interaction curve holds exactly, if buckling stresses for equal wave lengths are considered. The writer found that in the latter case this relation holds also sufficiently accurately for homogeneous plates (case 1). Hence, with Eq. (1) it may be easily shown that it holds also for the complete sandwich plate.

From Eq. (6) it follows that the critical shear $S_{cr.}$ may also be calculated directly for combined shear and longitudinal compression with Eqs. (5), (6), and (7) of the writer's Reader's Forum item in the September issue, if in these equations value

$$\alpha = -(\gamma/2) + [(\gamma^2/4) + 1 + (L^2/b^2)]^{1/2} \qquad (8)$$

In those Eqs. (5), (6), and (7) value η is the ratio between plastic and elastic buckling stress for the assumed wave length.

In the Reader's Forum item in the September issue on page 574, a typographical error occurs in the last formula of Eq. (7), where the middle division bar should vanish, so as to read:

$$r = (\pi^2 D_1/b^2 G_c)\ [h_c/(h_c + t_f)^2]$$

Furthermore, in the last sentence of that item, a line was omitted in typing. The writer wanted to say there that the expression $(D_f/D_1 + \varphi)$ in Eq. (6) is involved in the minimization of $P_{cr.}$ or $S_{cr.}$ by variation of the wave length, so that zero wave lengths, as found with vanishing D_f, do not occur here.

REFERENCES

[1] Plantema, F. J., and deKock, A. C., *The Elastic Overall Instability of Sandwich Plates with Simply-Supported Edges*, Report S. 346, Nationaal Luchtvaartlaboratorium, Amsterdam, December, 1948.

[2] Seide, P., *Shear Buckling of Infinitely Long Simply Supported Metalite Type Sandwich Plates*, N.A.C.A. T.N. No. 1910, July, 1949.

[3] Batdorf, S. B., and Stein, M., *Critical Combinations of Shear and Direct Stress for Simply Supported Rectangular Flat Plates*, N.A.C.A. T.N. No. 1223, March, 1947.

[4] Bijlaard, P. P., *Some Contributions to the Theory of Elastic and Plastic Stability*, Publ. Internat. Assoc. f. Bridge and Struct. Engineering, Zurich, Vol. 8, pp. 17–80, 1947.

[5] Bijlaard, P. P., *On the Elastic Stability of Sandwich Plates I–II*, Proc. Kon. Ned. Akad. v. Wet., Vol. 50, Nos. 1 and 2, 1947.

Errata—Note on the Velocity of Sound

Morris Morduchow
Polytechnic Institute of Brooklyn, Brooklyn, N.Y.
June 25, 1949

A list of errors in the article "Note on the Velocity of Sound," by Morris Morduchow (JOURNAL OF THE AERONAUTICAL SCIENCES, Vol. 16, No. 10, p. 635, October, 1949) follows:

Page 635, line 21, the sentence "The derivative $dp/d\rho$ is then zero everywhere except at the discontinuity where its value is indeterminate," should be replaced by the sentence "The derivative $dp/d\rho$ is then indeterminate everywhere including the discontinuity."

The following misprints may also be noted. On line 28, the word "of" should be omitted between the words "limit" and "the equations." On the top of p. 635, right column, the equation should read:

$$u\,du = (1/2)\gamma d(p/\rho)$$

On the Reduction of Unsteady Supersonic Flow Problems to Steady Flow Problems

John W. Miles
Department of Engineering, University of California at Los Angeles
September 26, 1949

WE CONSIDER a flow of supersonic velocity U, directed along the positive x-axis, over an airfoil whose projection on the plane $z = 0$ occupies the region S_1 and which has the prescribed normal velocity $w(x, y) \exp(i\omega t)$. The linearized, boundary value problem is then represented by the equations

$$[\nabla^2 - M^2[(\partial/\partial x) + ik]^2]\,\phi(x, y, z) = 0 \tag{1}$$

$$\phi_z(x, y, 0 \pm) = w(x, y), \qquad (x, y) \text{ in } S_1 \tag{2}$$

$$\phi(x, y, 0 \pm) = \pm\phi(x, y, 0 +) \exp[-ik(x - x_1)], \qquad (x, y) \text{ in } S_2 \tag{3}$$

$$\phi(x, y, 0) = 0, \qquad (x, y) \text{ in } S_3 \tag{4}$$

$$k = \omega b/U \tag{5}$$

where M is the Mach Number, k the reduced frequency, b the unit of length, $x = x_1(y)$ the trailing edge, S_2 the wake aft of the airfoil, including the trailing edge, and S_3 the remainder of the plane $z = 0$ (i.e., exclusive of S_1, S_2). The potential implicitly possesses the harmonic time dependence $\exp(i\omega t)$.

We now restrict our problem by assuming the trailing edge to be everywhere supersonic, so that the zone of action of the wake has no region in common with the zone of influence of the wing. The boundary condition (2) may then be suppressed. Introducing the transformation[1]

$$x' = x, \; y' = \beta y, \; z = \beta z, \; b' = \beta^{-1}b \tag{6}$$

$$(x', y', z') = \exp(i\kappa Mx)\,\phi(x, y, z) \tag{7}$$

$$w'(x', y') = \beta^{-1} \exp(i\kappa Mx) w(x, y) \tag{8}$$

$$\kappa = \beta^{-2}Mk \tag{9}$$

the boundary value problem of Eqs. (1) to (4) is reduced to

$$\Box^2\phi' = \phi'_{y'y'} + \phi'_{z'z'} - \phi'_{x'x'} = \kappa^2\phi' \tag{10}$$

$$\phi_{z'}'(x', y', 0 \pm) = w'(x', y'), \qquad (x'y') \text{ in } S_1' \tag{11}$$

$$\phi'(x', y', 0) = 0, \qquad (x', y') \text{ in } S_3' \tag{12}$$

where S_1' and S_3' differ from S_1 and S_3 only by the scale transformation of Eq. (6).

We now consider the simplified boundary value problem of Eqs. (10) to (12) and drop the primes on the coordinates. Magnaradze and Galin[2] have shown that, if $\psi(x, y, z)$ is a solution to the steady flow equation

$$\Box^2\phi = 0 \tag{13}$$

a solution to Eq. (10) is given by

$$\phi(x, y, z) = \psi(x, y, z) - \int_0^x \psi(\xi, y, z)\,(\partial/\partial\xi) \times J_0[\kappa(x^2 - \xi^2)^{1/2}]d\xi \tag{14}$$

where $x = 0$ is taken at the most forward point on the leading edge, and J_0 is Bessel's function of order zero. The derivation given by Galin is ingenious but does not clearly exhibit the restrictions on the result. However, having the result, we may verify it by direct substitution and state the sufficient (and, for all practical cases, necessary) conditions as:

(*a*) ϕ and its first derivatives with respect to x, y, z must be continuous in the open domain $z > 0$.

(*b*) $\phi(\bar{x}, y, z) = \phi_x(\bar{x}, y, z) = \phi y(\bar{x}, y, z) = \phi z(\bar{x}, y, z) = 0$, where $x = \bar{x}(y, z)$ is the upstream boundary of the zone of action of the airfoil (e.g., $\bar{x} = +(y^2 + z^2)^{1/2}$ for a delta wing with subsonic leading edges).

In view of the condition (*b*), we may rewrite Eq. (14) in the form

$$\phi(x, y, z) = \int_{\bar{x}(y, z)}^x J_0\,\kappa(x^2 - \xi^2)^{1/2}]d\psi(\xi, y, z) \tag{15}$$

In general, the conditions (*a*) and (*b*) will not be satisfied by the velocity potential, but this difficulty may be circumvented by recasting the boundary value problem in terms of the modified potential

$$\Phi(x, y, z) = \int_{\bar{x}(y, z)}^x \phi(\xi, y, z)d\xi \tag{16}$$

as done by Galin. In the case where the leading edge is everywhere subsonic, it does not appear that this would be necessary.

In order to apply the transformation (15), we require its inversion. Assuming the conditions (*a*) and (*b*), we obtain

$$\psi(x, y, z) = \int_{\bar{x}(y, z)}^x I_0[\kappa(x^2 - \xi^2)^{1/2}]d\phi(\xi, y, z) \tag{17}$$

where I_0 is Bessel's function of imaginary argument. This result may be established by direct substitution in Eqs. (10) and (13).

We may use Eq. (17) to transform the boundary condition (11), or, if Φ is introduced, the integral of Eq. (11), in accordance with Eq. (16). We then have the problem of finding a solution to Eq. (13) subject to a prescribed, normal (z) derivative over S_1 and vanishing over S_3. Since both the boundary conditions and the potential equation are those for steady flow, albeit the prescribed, normal velocity may exhibit a frequency dependence, our problem is reduced to one in steady flow. The restriction to a supersonic trailing edge is necessary for this reduction to an equivalent, steady flow problem, since the boundary condition (3) would *not* transform to the analogous steady flow boundary condition,

$$\psi(x, y, 0 \pm) = \pm\psi(x, y, 0 +) \text{ in } S_2$$

Galin[2] has applied the foregoing transformation to the oscillating, rectangular wing, but the results appear to be considerably more complex than those obtainable by other methods.[3] The principal difficulty in its application to the usual problems is the evaluation of the required integrals, although the results may be expanded in terms of Sonine's integrals.[4] Following this pattern we have checked the method by deriving the two-dimensional result. We note that a related method has been proposed by Germain and Bader in a paper not yet available to us.[5]

References

[1] Miles, J. W., *On Harmonic Motion at Supersonic Speeds*, Journal of the Aeronautical Sciences, Vol. 16, pp. 378–379, June, 1949.

[2] Galin, L. A., *A Wing of Rectangular Planform in Supersonic Flow* (translated from Russian), A.M.C.T.R. F-TS-1217-IA, Wright Field, Dayton, Ohio, May, 1949.

[3] Miles, J. W., *On the Oscillating Rectangular Airfoil at Supersonic Speeds*, Journal of the Aeronautical Sciences, Vol. 16, p. 381, June, 1949.

[4] Watson, G. N., *Bessel Functions* pp. 373–379; The Macmillan Company, New York (1945).

[5] Germain, P., and Bader, R. *A Study of Some Harmonic Oscillations by Means of a Correspondence with Homogeneous Motions* (in French), C. R. Acad. Sci. Paris, Vol. 228, pp. 1201–1202 (April 4, 1949); Appl. Mech. Rev., Vol. 2, p. 205 (September, 1949). Presumably the answer to the reviewer's criticism is the transformation of our Eq. (7) above.